Real-Time Optimization of Solid Oxide Fuel Cell Systems — Methodology and Implementation

Thèse N° 9276

Présentée le 17 mai 2019

à la Faculté des sciences et techniques de l'ingénieur
Laboratoire d'automatique 1
Programme doctoral en chimie et génie chimique

pour l'obtention du grade de Docteur ès Sciences

par

Tafarel DE AVILA FERREIRA

Acceptée sur proposition du jury

Prof. V. Hatzimanikatis, président du jury
Prof. D. Bonvin, Dr T. Faulwasser, directeurs de thèse
Prof. G. Pannocchia, rapporteur
Dr Y. S. Hajimolana, rapporteur
Dr J. Van Herle, rapporteur

2019

ÉCOLE POLYTECHNIQUE
FÉDÉRALE DE LAUSANNE

What I cannot create, I do not understand.
— Richard Feynman

À minha mãe …

Acknowledgements

This thesis represents part of my work as a PhD student at the Laboratoire d'Automatique at École Polytechnique Fédérale de Lausanne. Undertaking it has been a truly valuable and life-changing experience for me and it would not have been possible to do it without the support and guidance I received from numerous people who have contributed to creating a productive and pleasant work. Therefore, I wish to express my warmest gratitude to all those persons whose comments, suggestions, criticism, support and encouragement, both personal and academic, have had a considerable bearing on this work.

First and foremost, I would like to thank my advisor Prof. Dominique Bonvin for his continued support over the years and to express my sincere gratitude for allowing me to grow as a research scientist. In countless number of times he gave me confidence, encouragement and steered me in the right direction whenever he thought I needed it. I am thankful to him for making LA a fantastic place for sharing exciting research ideas. During my studies, I had the pleasure to collaborate with many post-docs in the lab. Thus, I thank my thesis co-director Dr. Timm Faulwasser, who has contributed to improve the overall quality of my work. I have learned a lot from very lively and productive discussions with him. Along the same line, I thank Dr. Alejandro Marchetti for his sharp and insightful feedback on certain segments of my work and for transmitting to me his vision about the field.

Special appreciation also goes to Predrag and Martand, with whom I shared many interesting discussions related to RTO and everything that surrounds it! Without them, this journey would have been much more difficult. I also thank Zacharie Wuillemin and Dr. Jan Van Herle for their insightful comments and feedback on my work regarding fuel cells, and for making possible to perform all experiments. I also thank SOLIDpower that allowed performing all experiments on the BlueGEN system. I would like to thank Prof. Gabriele Pannocchia, Dr. Jan Van Herle and Dr. Yashar Hajimolana, and Prof. Vassily Hatzimanikatis for accepting the invitation to be part of my thesis committee and for accepting to evaluate my thesis and its defense.

Moreover, I thank all the other professors at the Laboratoire d'Automatique, including Prof. Roland Longchamp, Prof. Colin Jones, Dr. Alireza Karimi, and Prof. Giancarlo Ferrari Trecate, for fostering a great working atmosphere in the lab. My sincere appreciation also goes to Christophe Salzmann for infinite patience and help, it would be incredibly difficult to perform the experiments without him. I thank the secretaries, Ruth, Eva, Francine, Margot and Nicole for making my life easier and always helping with great patience and professionalism. Thanks to Sandra and Phillipe for the help with students and for always being there for a friendly chat.

This professional adventure at LA has also enabled me to enrich my personal life and make great and long-lasting friendships. I thank all my labmates for a positive atmosphere and for making all difficult moments less stressful and more enjoyable. I am happy to have met Diogo, Shriniketh, Sohail, Ivan, Ehsan, Altug, Christoph, Georgios, Mahdieh, Sean, Milan, Luca, Harsh, Ioannis, Ye, Jean-Hubert, Francisco, Sanket, Faran, Petr, Michele, Pulkit, Mustafa and David. A special thanks to Harsh, my good friend, who supported me during my PhD and also worked together. A special mention goes to Predrag, Tomasz and Andrea with whom I shared so many enjoyable moments and immemorable trips that I will always appreciate!

Finally, I wish to thank my loving parents for providing me with unfailing support and continuous encouragement in all my life pursuits. My deepest thanks and appreciation goes to my beloved mother Regina, sister Marluci. This accomplishment would not have been possible without them.

Lausanne, December 2018 A.F. T.

Abstract

Optimization of industrial processes aims at minimizing operating cost or maximizing economic profit while respecting plant constraints. In process industry, real-time optimization (RTO) is often considered to ensure optimal plant operation and constraint satisfaction.

Solid-oxide fuel-cell (SOFC) devices oxidize fuels such as hydrogen and methane to produce electric energy through electrochemical reactions at very high efficiency. To reduce the emission of carbon dioxide and the high cost of non-renewable energies, fuel cells have become popular as an alternative energy source with a wide range of applications. The optimal operation of SOFC systems, while being subjected to changing operating conditions such as variations in the electrical power demand, remains a challenging problem in the field of control and optimization. In addition, these types of devices are characterized by slow dynamics and drifts such as degradation. This motivates the use of real-time optimization for optimizing and controlling the operation of SOFC systems.

The most popular RTO technique in industry is the so-called two-step approach. This approach consists in estimating the model parameters based on measurements by solving a parameter estimation problem, and computing the next operating point by solving an optimization problem using the updated model. However, this technique is highly dependent on model accuracy and tends to fail in the presence of structural plant-model mismatch. As an alternative, modifier adaptation has been developed to enforce convergence to the plant optimum even in presence of structural plant-model mismatch. Since plant optimality is often characterized by active constraints, it is possible to use a simpler version of modifier adaptation, called constraint adaptation (CA). This approach corrects the constraints in the model-based optimization problem by means of bias terms computed from the differences between the measured and predicted values of the constraints.

The active plant constraints—i.e. the intersection of the constraints where the plant optimum lies—for each mode of operation is typically known from experience. Therefore, as the optimum of SOFC systems typically lies on active plant constraints, we can apply constraint adaptation. One of the drawbacks of static RTO is the fact that it is necessary to wait until the plant reaches its steady state. Since this may be inappropriate for slow processes, we propose an RTO approach that can speed up the procedure by using transient measurements combined with a dynamic tendency model.

In this work, we apply constraint adaptation combined with transient measurements and a dynamic model to experimental SOFC systems. The proposed approach is applied to two SOFC systems: (i) an SOFC system with 6 cells that consists of both hardware and software components; (ii) a commercial SOFC system named BlueGEN. The results obtained are very promising. For both systems, the proposed approach can reach the power demand much faster than the time it takes for the process to settle to steady state. The optimizer is quick at finding and tracking the correct set of active constraints, thus avoiding large constraint violations. In addition, we study the effect of the RTO period on the convergence rate. Finally, we show that CA acts simultaneously as a controller and an optimizer that is able to efficiently detect and track the correct set of active constraints.

Résumé

L'optimisation des procédés industriels vise à minimiser les coûts d'exploitation ou à maximiser le profit économique tout en respectant les contraintes du procédé. Dans l'industrie des procédés, l'optimisation en temps réel (RTO) est souvent prise en compte pour optimiser le fonctionnement de l'installation et la satisfaction des contraintes.

Les dispositifs à piles à combustible à oxyde solide (SOFC) oxydent des combustibles tels que l'hydrogène et le méthane pour produire de l'énergie électrique par le biais de réactions électrochimiques à très haut rendement. Pour réduire les émissions de dioxyde de carbone et le coût élevé des énergies non renouvelables, les piles à combustible sont devenues populaires comme source d'énergie alternative offrant une vaste gamme d'applications. Le fonctionnement optimal des systèmes SOFC, tout en étant soumis à des conditions de fonctionnement changeantes telles que des variations de la demande en puissance électrique, reste un problème épineux dans le domaine du contrôle et de l'optimisation. De plus, ces types d'appareils se caractérisent par une dynamique lente et des changements au cours du temps telles que la dégradation. Cela motive l'utilisation de l'optimisation en temps réel pour optimiser et contrôler le fonctionnement des systèmes SOFC.

La technique RTO la plus populaire dans l'industrie est l'approche dite en deux étapes. Cette approche consiste à estimer les paramètres du modèle à partir de mesures en résolvant un problème d'estimation de paramètres et à calculer le point de fonctionnement en résolvant un problème d'optimisation à l'aide du modèle mis à jour. Cependant, cette technique dépend fortement de la précision du modèle et a tendance à échouer en présence d'une erreurs structurelles dans le modèle du procédé. Une variante, modifier adaptation a été développée pour imposer la convergence vers l'optimum du procédé, même en présence d'erreurs structurelles entre modèles de procédés. L'optimalité du procédé étant souvent caractérisée par des contraintes actives, il est possible d'utiliser une version plus simple de modifier adaptation, appelée constraint adaptation. Cette approche corrige les contraintes du problème d'optimisation basé sur un modèle au moyen de termes de biais calculés à partir des différences entre les valeurs mesurées et prédites des contraintes.

Les contraintes actives du procédé—i.e. l'intersection des contraintes où l'optimum du procédé se trouve—pour chaque mode de fonctionnement sont généralement bien connues par expérience. Par conséquent, comme l'optimum des systèmes SOFC repose généralement sur des contraintes actives, nous appliquons constraint adaptation. L'un des inconvénients de la RTO statique est le fait qu'il est nécessaire d'attendre que le système atteigne son état stationnaire. Comme cela peut être inapproprié pour les processus lents, nous proposons une approche RTO qui peut accélérer la procédure en utilisant des mesures transitoires combinées à un modèle de tendance dynamique.

Dans ce travail, nous appliquons expérimentalement aux systèmes SOFC l'adaptation de contraintes basée sur des mesures transitoires et un modèle dynamique. L'approche proposée est appliquée à deux systèmes SOFC expérimentaux : (i) un système SOFC à six cellules composé à la fois de composants matériels et logiciels ; (ii) un système SOFC commercial appelé BlueGEN. Les résultats obtenus sont très prometteurs. Pour les deux systèmes, l'approche proposée peut atteindre la demande d'énergie beaucoup plus rapidement que le temps nécessaire pour que le processus se stabilise. L'optimiseur recherche et suit rapidement l'ensemble correct de contraintes actives, évitant ainsi des violations importantes. De plus, nous étudions l'effet de la période de RTO sur le taux de convergence. Enfin, nous montrons que CA agit simultanément comme un contrôleur et un optimiseur capable de détecter et de suivre efficacement le bon ensemble de contraintes actives.

Contents

Acknowledgements **v**

Abstract (English/Français) **vii**

List of Figures **xiii**

List of Tables **xvi**

1 Introduction **1**

1.1 Motivation 1

1.1.1 Solid-Oxide Fuel-Cell Systems 1

1.1.2 Real-Time Optimization 2

1.2 State of the Art 5

1.2.1 Optimization of Solid-Oxide Fuel-Cell Systems 5

1.2.2 Real-Time Optimization 7

1.3 Contributions of the Thesis 14

1.3.1 Methodological Constributions to Modifier Adaptation 14

1.3.2 Optimization of Experimental SOFC Systems 14

1.4 Organization of the Thesis 16

2 Preliminaries **17**

2.1 Static Optimization Problem 17

2.2 Modifier-Adaptation Approaches 19

2.2.1 Constraint Adaptation 19

2.2.2 Modifier Adaptation 20

2.3 SOFC Model 24

2.3.1 SOFC Stack 24

2.3.2 Pre-Reformer 26

2.3.3 Afterburner 26

2.3.4 Heat Exchangers 27

3 Fast Real-Time Optimization Using Transient Measurements **31**

3.1 Introduction 31

3.2 Fast Constraint Adaptation 32

3.2.1 Use of Transient Measurements 32

3.2.2 Use of Transient Measurements and a Dynamic Model 33
3.2.3 Model Adequacy 34
3.3 Simulated Example: Solid-Oxide Fuel-Cell System 36
3.3.1 SOFC System Description 36
3.3.2 Formulation of the Optimization Problem 37
3.3.3 Simulation Results 38
3.4 Conclusions 45

4 Real-Time Optimization of a Small-Scale Experimental SOFC System 47
4.1 Introduction 47
4.2 SOFC System 48
4.2.1 Physical System 48
4.2.2 Software 49
4.3 Real-Time Optimization of the SOFC System 52
4.3.1 Dynamic Model 52
4.3.2 Experimental Results 52
4.4 Conclusions 58

5 Real-Time Optimization of a Commercial SOFC System 61
5.1 Introduction 61
5.2 BlueGEN System 62
5.2.1 System Description 63
5.2.2 Tendency Model 65
5.2.3 Operational Constraints 66
5.2.4 Formulation of the Optimization Problem 66
5.3 Real-Time Optimization Approach 67
5.4 Experimental Results with the BlueGEN System 68
5.4.1 Steady-State CA 68
5.4.2 Fast CA 69
5.4.3 Change in Active Constraints for Different Power Levels 71
5.4.4 Transient vs. Steady-State Performance 72
5.5 Discussion and Analysis of Experimental Results 73
5.5.1 Effect of Different Time Scales 73
5.5.2 Effect of Constraints on Operability and Performance 74
5.5.3 A Posteriori Assessment of Optimality 76
5.5.4 Operational Guidelines 77
5.6 Conclusions 77

6 Conclusions 79
6.1 Summary 80
6.2 Perspectives 81
6.2.1 Optimization of SOFC Systems 81
6.2.2 RTO Methodologies 83

Bibliography **91**

Curriculum Vitae **93**

List of Figures

1.1 Automation decision hierarchy 3
1.2 Qualitative comparison of the two-step approach and modifier adaptation. . . 13

2.1 RTO scheme via CA using steady-state plant measurements. 21

3.1 Estimation of $\widehat{G}_p\left(\mathbf{u}_j\right)$ from the measurement of $G_p^{dyn}(t_j)$ and estimation of $\Delta := G(\mathbf{u}_j) - G^{dyn}(t_j)$ from the model. 34
3.2 RTO scheme via CA using transient measurements and a dynamic model. . . . 35
3.3 SOFC system flowsheet. 36
3.4 *Simulation 1:* Efficiency, current, electrical power, methane flowrate, cell voltage, and air flowrate vs. time. 39
3.5 *Simulation 1*: Fuel utilization, air excess ratio, pre-reformer temperature, inlet air temperature, cathode and anode temperatures vs. time. 40
3.6 *Simulation 2*: Efficiency, current, electrical power, methane flowrate, cell voltage, and air flowrate vs. time. 41
3.7 *Simulation 2*: Fuel utilization, air excess ratio, pre-reformer temperature, inlet air temperature, cathode and anode temperatures vs. time. 42
3.8 *Simulation 3*: Efficiency, current, electrical power, methane flowrate, cell voltage, and air flowrate vs. time. 42
3.9 *Simulation 3*: Fuel utilization, air excess ratio, pre-reformer temperature, inlet air temperature, cathode and anode temperatures vs. time. 43
3.10 *Simulation 4*: Efficiency, current, electrical power, methane flowrate, cell voltage, and air flowrate vs. time. 43
3.11 *Simulation 4*: Fuel utilization, air excess ratio, pre-reformer temperature, inlet air temperature, cathode and anode temperatures vs. time. 44
3.12 *Simulation 5*: Efficiency, current, electrical power, methane flowrate, cell voltage, and air flowrate vs. time. 44
3.13 *Simulation 5*: Fuel utilization, air excess ratio, pre-reformer temperature, inlet air temperature, cathode and anode temperatures vs. time. 45

4.1 Available SOFC system flowsheet. 49
4.2 Tested SOFC system flowsheet. 50

4.3 Interface structure of the system optimization. Each box corresponds to a process, whose execution period is specified in the upper-hand corner. The largest rectangle comprises the inner-loop (loop performed in a higher frequency) blocks, while the *RTO* and the *Interface 1* blocks correspond to the outer-loop (loop performed in a lower frequency) blocks. Each arrow correspond to data exchange between processes: (1) RTO inputs and constraint measurements; (2) RTO inputs and constraint measurements, communication between inner- and outer-loops; (3) electrical heater setpoints and measurements; (4) all system temperature and cell voltage measurements, and inputs. 51
4.4 *Experiment 1*: Efficiency, current, electrical power, methane flowrate, cell voltage, and air flowrate vs. time. 54
4.5 *Experiment 1*: Fuel utilization, air excess ratio, pre-reformer temperature, inlet air temperature, cathode and anode temperatures vs. time. 54
4.6 *Experiment 2*: Efficiency, current, electrical power, methane flowrate, cell voltage, and air flowrate vs. time. 56
4.7 *Experiment 2*: Fuel utilization, air excess ratio, pre-reformer temperature, inlet air temperature, cathode and anode temperatures vs. time. 56
4.8 *Experiment 3*: Efficiency, current, electrical power, methane flowrate, cell voltage, and air flowrate vs. time. 57
4.9 *Experiment 3*: Fuel utilization, air excess ratio, pre-reformer temperature, inlet air temperature, cathode and anode temperatures vs. time. 57
4.10 Performance (in terms of efficiency and electric power) of CA_ss with $\tau_{RTO} = 30$ min and CA_dyn with $\tau_{RTO} = 3$ min. 58

5.1 Power balance of the BlueGEN system 63
5.2 BlueGEN system flowsheet. 64
5.3 Input-output representation of the BlueGEN system. 65
5.4 *Steady-state CA*: Efficiency, current, electrical power, methane flowrate, cell voltage, and air flowrate vs. time. 70
5.5 *Steady-state CA*: Fuel utilization, air-excess ratio, cathode outlet and inlet temperatures, and burner temperature vs. time. 71
5.6 *Fast CA*: Efficiency, current, electrical power, methane flowrate, cell voltage, and air flowrate vs. time. 73
5.7 *Fast CA*: Fuel utilization, air-excess ratio, cathode outlet and inlet temperatures, and burner temperature vs. time. 74
5.8 *Cycling experiment*: Efficiency, cathode outlet temperature, electrical power, cathode inlet temperature, cell potential, and burner temperature vs. time. . . 75

List of Tables

1.1 Classification of real-time optimization techniques 9

2.1 General overview of the SOFC model, with *n* heat exchanges in the SOFC system. 29

3.1 Parameters that differ between the *plant* and the *model* 38

4.1 Settling time to reach the power setpoint (±2%). 58

5.1 Operational constraints in the BlueGEN system. 67
5.2 Two CA schemes. 68
5.3 Range of DC efficiencies for each electrical power tested, where SS CA stands for standard steady-state constraint adaptation and Fast CA stands for constraint adaptation using transient measurements combined with a dynamic model. . 72

1 Introduction

1.1 Motivation

According to World Energy Outlook 2017, the global energy requirement will increase by 30% by 2040. Although the rate of increase is slowing down, this increase represents the amount of energy consumed by China and India today. The source of energy has significantly changed in the past twenty-five years. Nowadays, natural gas represents the main part of the global energy demand. The energy needs have changed dramatically with renewables representing a significant part of the energy consumption. In addition, measures to increase energy efficiency are very popular. Oil has been the rising force of energy end-use, representing 40% of the consumption rise in the last twenty-five years. For the next 20 years, the same share of growth is expected to be taken by electricity.

For many countries, renewables are expected to become by 2040 the most economical source of new generation, which represents about 65% of the global investment in power plants. Renewables are also used to provide heat and mobility and it is predicted to double by 2040.

Along the same lines, the Swiss government decided in 2011 to abandon plans to build new nuclear reactors and, in 2017, the Swiss voted in favor of establishing the Energy Strategy 2050 and forbidding the construction of new nuclear power plants [1].

1.1.1 Solid-Oxide Fuel-Cell Systems

In the view of new energy sources, fuel cells have been the focus of growing interest. Fuel cells convert energy with significantly lower carbon emissions compared to traditional systems. Fuel-cell devices convert chemical energy from hydrogen, methane and other fuels to electricity with very high efficiency. The importance of reducing carbon emissions is rapidly increasing, and a large number of countries are investing in fuel-cell and hydrogen technologies [2].

Fuel-cell systems appear to provide an effective option for enhancing sustainability, mainly due to their high efficiencies and absence of polluting emissions. The application of fuel-cell technologies in the energy field represents significant advances in terms of energy generation and environmental preservation. Solid-oxide fuel-cell (SOFC) systems combine both high efficiency and environmental-friendly features. The use of SOFCs for power generation at large scale has been reported in the US, Europe and Japan, and at small scale for military, residential, industrial and transportation purposes. However, there are still challenges regarding the commercialization of these devices, the cost issue and the system reliability [3]. Pollution reduction can be significantly reduced by fuel cells, specially SOFCs that emit virtually zero sulphur and nitrogen emissions, while the produced carbon dioxide is reduced by about 50% [4].

A significant number of barriers must be overcome before fuel cells become a worldwide-spread technology. The challenges range from issues with the cell itself, the stack interconnect, the seals, the high temperatures, the start-up time to reliable operation. In the field of control and optimization, the safe operation of SOFC systems at high efficiency, while being subjected to changing operating conditions remains a challenging problem [5, 6].

SOFC systems are operated continuously for years. Degradation plays an important role after a certain period of time, mainly due to the fact that slow drifts affect the optimal operating conditions. Furthermore, technical constraints that must be guaranteed for safe and reliable operation are difficult to be met. In addition, in the field of control and optimization, although a few studies present experimental results [7, 8], none of the reported investigations deals with a complete SOFC system. Hence, the question of how to continuously push the operation of an SOFC system towards maximal efficiency is of considerable interest.

1.1.2 Real-Time Optimization

Minimizing costs or maximizing profits are part of the operating situations that are important to process industry. The main challenges that industry face nowadays include production bottlenecks, energy consumption, product quality and product losses. Market competition and the need to limit energy requirements make process control and optimization very appealing. The engineering approach to tackle all these issues is to build a model of the process in order to determine optimal operating conditions that will both improve performance and satisfy process constraints. However, models are not perfect, and to rely only on them could lead to suboptimal operation or, even worse, constraint violation. In this context, real-time optimization (RTO) appears as a family of methods that combine numerical optimization and online process measurements to achieve optimal process operation, while explicitly accounting for plant-model mismatch and varying operating conditions.

Advances in the past 30 years has allowed RTO to utilize steady-state process models. First-principle models are mathematical models that comprise mass and energy balances, vapour-liquid equilibrium expressions, reaction kinetics, etc [9]. However, although relatively accurate models are available, important issues such as plant optimal operation and constraint satis-

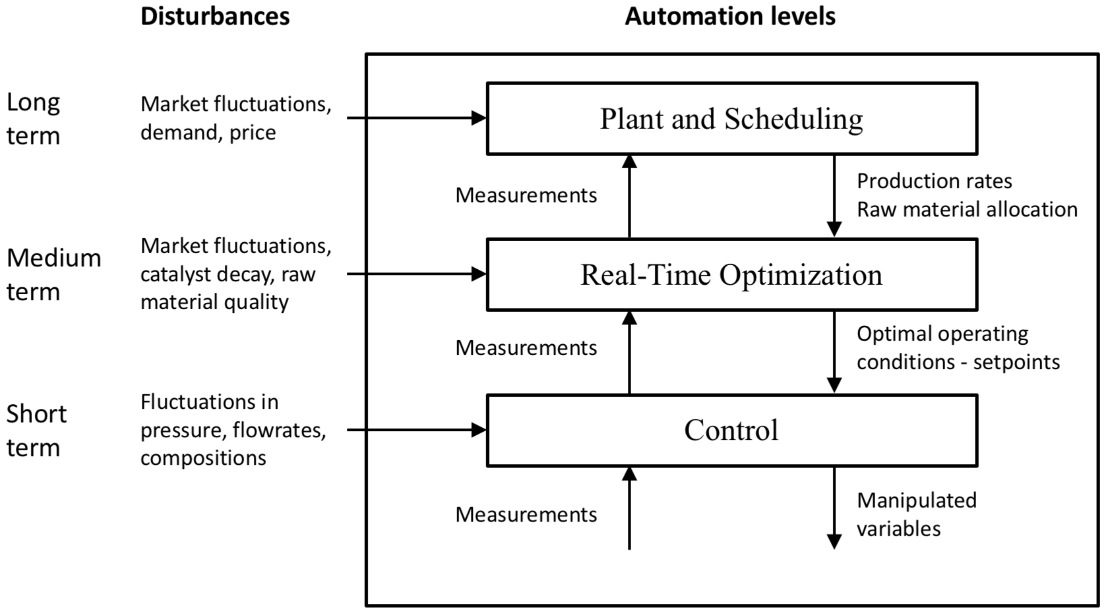
Disturbances
Automation levels
Long term
Market fluctuations, demand, price
Medium term
Market fluctuations, catalyst decay, raw material quality
Short term
Fluctuations in pressure, flowrates, compositions
Plant and Scheduling
Measurements
Production rates
Raw material allocation
Real-Time Optimization
Measurements
Optimal operating conditions - setpoints
Control
Measurements
Manipulated variables

Figure 1.1: Automation decision hierarchy [15].

faction need to be addressed. Typically, model predictive control (MPC) is used to move and maintain the plant at its optimum as optimal operation usually lies close or on constraints [10]. RTO is generally combined with low-level control to avoid constraint violation, which has become standard practice for steady-state optimization of processes that operate at nominal steady states—i.e. optimal steady states that are typically computed by a process model. Unfortunately, many companies still have difficulties in the acceptance of RTO, although several recent developments have proven this class of methods to be of major importance for industry [9].

A systematic approach is required to compute optimal policies for complex industrial processes. In the case of continuously operated processes, such as refineries and many bulk chemical plants, RTO systems are typically implemented as part of a multi-level automation decision hierarchy [11, 12]. At the upper level, planning and scheduling operations address long-term issues like production rate targets and raw materials allocation. Operating at the medium time scale of hours to days, the RTO level computes the optimal steady-state operating point in the form of setpoints that are passed to the lower-level process control system [9, 11]. In the case of batch and semi-batch processes, RTO algorithms can also be applied in a batch-to-batch fashion by parameterizing the time-varying input profiles and optimizing the operation of the next batch using measurements obtained from previous batches [13, 14]. Figure 1.1 depicts the decision hierarchy involving several automation levels.

RTO approaches have been developed with the aim of overcoming industrial problems with respect to:

- Constraint satisfaction [16, 17]
- Plant-model mismatch [18–20]
- Optimal operation [21–23]
- Discretization of the input profiles for batch optimization [24]
- Plant gradient estimation [19, 25, 26]
- Convergence speed [27]

Among the aforementioned problems, convergence speed appears to be critical. The number of RTO iterations, or the number of changes of operating points, needed to drive the plant to a fixed point defines the convergence speed. RTO is capable of tracking the plant optimum in case of low-frequency disturbances, which means that the convergence speed depends on the plant settling time. The time that an RTO scheme takes to converge is affected by the settling time of the system and the number of RTO iterations it takes to converge. This implies that systems with large settling times may take several hours, or even days, to converge to their optimum. The convergence time can be mathematically written as:

$$\text{Convergence time} = \#\text{Iterations} \times \text{Settling time} \tag{1.1.1}$$

Note that the number of iterations depends on the RTO method, whereas the settling time is related to the dynamics of the plant.

The standard RTO approach in industry is the so-called two-step approach [11, 28, 29]. This RTO method first uses plant measurements to update the model parameters via the solution to a nonlinear regression problem; then, the second step computes the plant inputs by solving an optimization problem considering the updated model. This method, however, cannot guarantee constraint satisfaction as the approach relies on a model that is typically uncertain. This may have safety, economic and environmentally harmful consequences. This also implies that industrial processes often do not operate at optimal conditions. Since structural plant-model mismatch is often present, the solution obtained by the two-step approach may not satisfy the plant optimality conditions [30]. In addition, many processes such as fuel-cell systems are affected by slow drifts (due to degradation, fouling, etc.), which makes achieving optimal efficiency and keeping the operation at high performance difficult. Moreover, the convergence speed is also an issue that is not tackled by the two-step approach. The number of iterations that this RTO approach takes to converge depends on the size of the problem and the nature of plant-model mismatch.

The family of RTO schemes known as modifier adaptation circumvents the main disadvantages of the two-step approach. Modifier adaptation (MA) can enforce convergence to plant optimality even in the presence of structural plant-model mismatch [19]. Although MA is proven to guarantee plant optimality upon convergence, a wide number of practical challenges still need to be overcome before it becomes accepted in industry.

A practical problem related to MA is the requirement to estimate plant gradients—i.e. plant sensitivities with respect to each input. However, estimating these gradients may be impractical for processes with several inputs. Finite differences is the most commonly used approach to estimate plant gradients. This method, however, requires perturbing each plant input individually at the current plant operating point, and measuring each corresponding plant output. As this procedure is required to be done at every RTO iteration, the convergence speed is directly affected for plants that possess large settling times. Alternatively, transient measurements are used for steady-state optimization via modifier adaptation in [27]. It is shown therein that the plant optimum can be reached in a single transient operation if plant gradients are accurately estimated.

Many processes have their optimal operation at the intersection of constraints [9, 10]. If plant optimality is expected to be fully determined by active constraints, one can use constraint adaptation (CA) instead, that is, a simpler version of modifier adaptation that does not require the estimation of plant gradients [17, 22]. Similarly to MA, the convergence speed of CA depends on the process settling time. However, optimality can only be guaranteed if the model-adequacy conditions—i.e conditions that enable a process model to be suitable for RTO—are fulfilled and the set of active constraints of the plant is known.

If the system has two time scales, of which one is considered fast and the other slow, it is possible to implement CA without having to wait for steady state [7]. However, this type of time-scale separation is not always present in complex systems since the system outputs may be affected by components with different dynamics. Hence, steady-state CA may fail if the output measurements obtained during transient operation are inadequate for adapting the steady-state model. Considering the above, it is still unclear how one can speed up RTO using transient measurements of a process characterized by multiple time scales. This thesis tackles this issue, which consists in answering the following question: how to estimate quickly—i.e. ahead of time—the steady state of a process that possesses multiple time scales?

1.2 State of the Art

1.2.1 Optimization of Solid-Oxide Fuel-Cell Systems

In 1937, two Swiss chemists, Emil Baur and Hans Preis, reported a series of experiments on fuel cells with solid electrolytes in the form of ceramic materials [31]. Although this first study on fuel cells was performed 80 years ago, it is only in the past 20 years that fuel cells, in particular SOFCs, have been intensively studied worldwide [32].

There are many types of fuel cells such as proton-exchange membrane, direct methanol, alkaline, phosphoric acid, microbial fuel cells, and solid-oxide fuel cells. The latter are distinguished by their high temperatures and efficiencies, and are typically used to generate power and provide heat to small businesses, private households or public buildings [33, 34].

The optimization of SOFC systems has received increasing attention in the past 15 years [35]. Yet, most of the literature on control and optimization of fuel-cell systems deals with proton-exchange membrane cells [36–38]. These studies used heuristic approaches to maximize system efficiency. Although the proposed approaches increase process performance, tackling these types of problems in a systematic way requires a rigorous optimization approach.

In [39], the authors optimize a 200 kW SOFC co-generation power plant. The study aims at minimizing the total system cost and maximizing system efficiency. The results show that optimal performance depends highly on the internal reforming rate, air temperature in the stack, cell voltage, and fuel utilization in the stack. In [40], a hybrid SOFC—an SOFC system with gas turbine and steam turbine—with electrical power ranging from 1.5 MW to 10 MW is studied. Similarly to the previous study, the authors also aim at reducing process costs and increasing efficiency. However, in addition to fuel utilization, they use the steam-to-carbon ratio, the operating pressure and the fuel cost as manipulated variables. The objective in [41] is to guarantee safe operation while attaining maximal system efficiency of a complete SOFC system. Therein, the manipulated variables are the air flow, the bypass air, and the fuel flowrates. Many other studies in the optimization of SOFC field with different objectives such as maximizing life time, exergy efficiency, or minimizing CO_2 emissions or thermal gradients have been reported [42–45]. In addition to the aforementioned manipulated variables, the air temperature, the reformer temperature, the operating pressures, the gas recycling, and the nitrogen flowrate have also been used in other studies [39, 40, 46–48]. Notably, a vast number of optimization approaches for SOFC systems have been proposed. Although very significant, all the aforementioned works are simulation studies.

Experimental studies concerning SOFC dynamics are rare [49]. While only few experiments on the optimization of SOFC configuration can be found in the literature [50, 51], even fewer are available on the optimization of SOFC operating conditions [7]. The latter reference presents an experiment where RTO is applied to a single SOFC stack. This experiment aims at optimizing the operating condition by maximizing the electrical efficiency while respecting operating constraints related to system safety and lifetime. Model predictive control is widely used to control this type of system. Most of the works on control of SOFCs are either purely theoretical or they merely use offline data for model validation [52–54]. Only a few experimental studies can be found on MPC applied to SOFCs [55, 56]. Note that MPC typically aims at controlling the system at some operating conditions, that is, not considering improving performance by maximizing efficiency or reducing costs.

SOFC systems are affected by disturbances as well as changes in the power demand. As a result, the optimal steady-state operating point changes with time. This motivates the use of RTO for optimizing and controlling the operation of SOFC systems [57].

As models may become impractical for online implementation, it is common to use simplified models for this purpose. In this context, RTO methods conveniently make use of plant measurements and appropriate model adaptation strategies to steer the plant to its optimum despite the absence of an accurate model [14].

One of the main difficulties in applying steady-state RTO algorithms is that their implementation is slow, in particular for systems that have long settling times and several inputs. Indeed, since the models are typically updated based on steady-state data, one has to wait for steady state each time the model is updated and the RTO problem executed. In order to overcome this difficulty, it has been proposed to use transient measurements in the context of RTO in [7]. The RTO experiment was performed on a short 6-cell SOFC stack. The authors claim that it is possible to speed up convergence when time-scale separation is present. The system has two time scales, namely, the nearly instantaneous electrochemical scale ($\ll 1$ s) and the thermal scale on the order of 30 min. It is assumed that the power response is mainly governed by the electrochemical scale and the temperature dynamics is considered as a slow parametric drift. This allowed implementing RTO without having to wait for steady state, with a RTO period of 10 s, which increased the convergence speed significantly. However, this type of time-scale separation is not always present in SOFC systems because the outputs might be affected by components with different dynamics, for instance, a pre-reformer or heat exchangers. Hence, steady-state RTO may fail if the output measurements obtained during transient operation are not representative of the corresponding steady-state values.

In addition to the aforementioned difficulties, since SOFC systems are operated continuously for long periods of time, certain technical constraints must be guaranteed for safe and reliable operation. However, slow drifts due to degradation or thermal inertia make achieving optimal efficiency levels difficult.

1.2.2 Real-Time Optimization

Process industries produce industrial goods by continuous operation (e.g. oil refining, fertilizers, SOFC systems) at near steady state and by discontinuous (batch) operation (e.g. fermentation for beverage products, pharmaceutical production, waste-water treatment). Process optimization is a field of study that aims at improving the performances of process plants, while enforcing constraint satisfaction. With the advent of computers and new technologies, the use of more complex mathematical models for optimization has become possible [58–60]. Due to plant-model mismatch and disturbances that typically affect the process, the direct use of model-based optimization may lead to suboptimal performance or unsafe operation.

For the aforementioned reasons, RTO has emerged as an alternative optimization technique that uses both process models and plant measurements. RTO algorithms differ in the way the available measurements are utilized to update the model used for optimization. RTO techniques can also be classified as 'model-based' or 'model-free' approaches. This distinction is related to whether or not a mathematical model of the process is used for on-line computations [61]. In the case of 'model-based' approaches, the process model must satisfy certain conditions in order to be considered suitable for RTO.

Model-Adequacy Conditions

An important concept in 'model-based' approaches is that of model adequacy. In practice, process models that provide a good accuracy and fast computation are selected. As typically these models are not perfect, certain conditions related to their adequacy must be specified. Model-adequacy conditions are related to whether a process model is suitable for use in a RTO scheme. A model is considered to be adequate if it is capable of producing a fix point for the used RTO scheme at the plant optimum. In other words, for the RTO approach to be able to compute the optimal plant inputs from the plant measurements, there must exist a set of parameters (model parameters or optimization parameters, depending on the chosen RTO approach) such that the real-time optimizer can generate the plant optimum. These conditions may vary depending on the RTO approach.

In RTO, the necessary conditions of optimality are used frequently. They are typically used either to enforce or verify plant optimality. Next, we briefly describe the concept of necessary conditions of optimality. This concept will be mathematically formalized in the next chapter.

Necessary Conditions of Optimality

The necessary conditions of optimality (NCO) are typically used to verify whether a process or a plant is operating at its optimum. These conditions are known as the first-order Karush-Kuhn-Tucker (KKT) conditions. They are mainly divided in two parts: (i) the constraint part, and (ii) the gradient (or sensitivity) part. These sensitivities are gradients of the constraint or cost functions with respect to the inputs. NCO are quite important as they are utilized in RTO approaches to guarantee that the problem is at a feasible point—i.e. respecting all constraints—and to push the reduced gradients to zero. Reduced gradients are either the gradients of the cost function (when no constraint is active) or a linear combination between the gradients of the cost function and active constraints.

'Model-Based' Approaches

Although the name 'model-based' techniques suggests that only process models are utilized, this class of techniques uses plant measurements combined with process models to perform the optimization. This class of RTO techniques uses process models repetitively between iterations, and the measurements are used to bridge the gap between the uncertain model and the plant outputs. The best known 'model-based' RTO techniques are the two-step approach [11, 28, 29], integrated system optimization and parameter estimation (ISOPE) method [18, 21, 25, 62], modifier adaptation [19, 22], bias update [16], constraint adaptation [17] and identification for optimization [24]. The classification of RTO techniques depending on the type of approach is given in Table 1.1. Next, we describe each 'model-based' RTO approach in more detail:

Table 1.1: Classification of real-time optimization techniques [14].

RTO approach	
'Model-based'	**'Model-free'**
1. Two-step approach [11, 28, 29]	8. Active-constraint tracking [65]
2. Bias update [16]	9. Self-optimizing control [66, 67]
3. Constraint adaptation [17]	10. Extremum seeking [23, 26]
4. Identification for optimization [24]	11. NCO tracking [20, 68]
5. ISOPE [18, 21, 25, 62]	12. SCFO [69, 70]
6. Modifier adaptation [19, 22]	
7. Iterative set-point optimization [71]	

1. The most commonly applied model-based RTO scheme is the two-step approach, which is typically used in industrial softwares [11, 28, 29]. The first step is a parameter estimation problem, wherein the model parameters are updated to best fit the measurements. The second step solves the optimization problem using the updated model to compute the next operating point. This technique has gained popularity due to the intuitive idea behind it [29]. However, it is well known that, in the presence of structural plant-model mismatch, the two-step approach does not usually converge to plant optimality [19, 63, 64]. It turns out that an RTO algorithm will not converge to the plant optimum unless the necessary conditions of optimality (NCO) of the model-based optimization problem match those of the plant. As the NCO are mainly characterized by gradients, in the presence of structural plant-model mismatch, the two-step approach may fail at finding a set of model parameters that would make plant and model gradients match.

2. Bias update is a RTO method that adds bias terms to constraint functions and process model equations—i.e. mass and energy balances, thermodynamic relationships, etc [16]. These bias terms correspond to the differences between the actual and predicted plant outputs. This method is specific to the case where there are as many active constraints as inputs at the plant optimum. This approach is of considerable industrial relevance and it is commonly used in model predictive control formulations [16]. The main weakness of the bias-update approach is the fact that this method only guarantees feasibility. However, optimality can be guaranteed if the correct set of plant active constraints is known and the model-adequacy conditions are fulfilled. It is argued in [16] that the set of active constraints for each mode of operation is known from experience. In the case of newly designed plants, the set of active constraints could be identified from the results of flexibility studies.

3. Constraint adaptation (CA) [17] is a variant of the bias-update technique. Note that CA updates only the constraint functions, whereas bias update adds modifiers to the process model equations in addition to the constraint functions. CA assumes that the plant optimum lies at the intersection of active constraints. Therefore, if the process model used is adequate, the model gradients are sufficiently accurate to push the plant to the correct set of active constraints and, thereby, to plant optimality. The main

feature of CA is the fact that it guarantees feasibility upon convergence. However, this approach may lead to suboptimal performance when plant optimality is not completely determined by active constraints.

4. Identification for optimization is a RTO method that shares some features of the two-step approach as it consists in solving two problems: parameter identification and cost optimization [24]. This method proposes to modify the objective function of the identification step by including the cost and constraint functions of the optimization problem. Appropriate weighting for the cost and constraint functions are included in the identification objective. The authors in [24] claim that this way of optimizing is relevant as the method becomes less dependent on the model, thus allowing using inaccurate or incomplete process models.

5. Integrated system optimization and parameter estimation (ISOPE) is another RTO technique that falls into the class of model-based approaches [18, 21, 25, 62]. This technique utilizes correction terms, that is, a gradient-modification term, in order to correct the cost function of the optimization problem. This way, the algorithm satisfies the plant NCO upon convergence. In addition, ISOPE uses process measurements to estimate the model parameters.

6. Modifier adaptation (MA) is a RTO approach, which, in contrast to ISOPE, does not estimate model parameters. Instead, MA uses affine correction terms to adapt the cost and constraint functions of the optimization problem [19, 22]. In MA, modifiers—i.e. the differences between the plant and model gradients of the cost and constraint functions, and the differences between the plant and model constraints—are updated iteratively in order to locally match the plant NCOs. The main advantage of MA is that an operating point satisfying the Karush-Kuhn-Tucker (KKT) optimality conditions of the plant is reached upon convergence. The main disadvantage of MA is the fact that plant gradients are required for its implementation. Typically, these gradients are estimated via finite differences. As finite differences require plant perturbations, this approach may be time consuming in the case of many inputs and slow processes. However, in order to overcome this difficulty, a few approaches such as dual MA [72] and dual ISOPE [62] have been proposed.

7. Iterative set-point optimization [71] is an optimization method derived from ISOPE. This method also shares features with MA. Similarly to ISOPE, this method adapts the objective function by adding zeroth- and first-order terms to the output variables, not the objective function directly, whereas the constraint functions are adapted as in MA. Note that here the zeroth-order terms correspond to the differences between the plant and model outputs or constraints, and the first-order terms correspond to the difference between the plant and model gradients of outputs and constraint functions. Therefore, iterative set-point optimization also satisfies the KKT conditions of the plant upon convergence. This method estimates plant gradients by taking into account the past operation points instead of perturbing the plant to obtain additional information.

’Model-Free’ Approaches

’Model-free’ RTO techniques update the input profiles from the measurements directly, that is, the updated inputs are computed without the use of a process model. Although this class of RTO techniques has in its name ’model-free’, in some cases, the process model can be used. However, the process model is only used offline; it is not used for numerical optimization online as in the ’model-based’ approaches. In the past 20 years, model-free techniques have been developed that include active-constraint tracking [65], self-optimizing control [66, 67], extremum-seeking control [23, 26], NCO tracking [20, 68], sufficient conditions for feasibility and optimality [69, 70]. Next, we describe each ’model-free’ RTO approach in more detail:

8. Active-constraint tracking is a technique that uses direct input adaptation [65]. It is a RTO approach that utilizes feedback control to adjust the inputs by identifying certain characteristics that are invariant, namely, the necessary conditions of optimality, in order to guarantee optimality despite uncertainty. As the concept of invariants are used to obtain the gradients, no parameter is estimated and model is used for implementation. More specifically, the invariants correspond to the active constraints and cost gradients with respect to inputs. The algorithm is implemented as follows: (i) the active constraints are determined offline by the simplified model, (ii) an experiment is performed with the optimal inputs and the invariants computed based on the measurements obtained, (iii) the inputs are updated, and Steps (ii) and (iii) are repeated until convergence.
9. Self-optimizing control adjusts the manipulated variables so that the process operates with reasonable loss [66, 67]. Typically, optimal setpoints provided by the optimization layer are input to the feedback control layer. The controlled variables are kept constant and the loss with respect to the cost function is evaluated. It is said that a self-optimizing control is obtained if this loss is acceptable. The losses are evaluated by comparing the sensitivities of the model and measured outputs. Many scenarios are evaluated and the worst-case loss for a given set of noise and disturbances is selected.
10. Extremum-seeking control is a RTO technique that uses limited knowledge of the process in order to find a local optimum of cost function [23, 26]. This method, which implements a gradient-descent approach, estimates a local gradient of the steady-state input-output map. A sinusoidal perturbation is added to the inputs, and the measured outputs are filtered. This allows estimating the gradients of the objective function with respect to the inputs. The amplitudes of the oscillations in the outputs are scaled by the local gradient at the point of operation. This means that, when the cost gradient is pushed to zero, the effects of the input oscillations are less significant. An integrator is used to update the model parameters so that a point of zero gradient can be reached.
11. NCO tracking is a RTO method that uses measurements to compensate the adverse effect of uncertainty by using direct input adaptation [20, 68]. The direct input adaptation is performed so as to enforce the NCO. Appropriate control laws are design to update the NCOs that include the plant active constraints and the sensitivities. NCO tracking has

two parts: (i) a nominal process model is used to identify the active constraints at the optimum, and (ii) appropriate measurements are used to enforce the NCO by feedback control. Note that the gradients in NCO tracking are pushed to zero using a controller with integral action.

12. Sufficient conditions for feasibility and optimality (SCFO) is a solver that guarantees (i) convergence to the plant optimum, (ii) constraint satisfaction at every iterate, and (iii) monotonic cost improvement [69, 70]. This algorithm performs the optimization in two steps. In the first step, the solver computes a descent direction for the cost function and a new feasible operating point. This first step computes a direction that will minimize the cost and move away from the constraints. The gradients of cost and constraint functions are taken into account to compute this direction. In the second step, the solver computes the step size by assuming that Lipschitz constants are available for the plant. This second step can be seen as a filtering step, where additional constraints are included in the optimization problem by considering the Lipschitz constants for each constraint. These constraints represent polytopes that correspond to the robust feasible areas where the next optimal operating point will lie.

Comparison of Two-Step Approach and Modifier Adaptation

Now, we turn back to ’model-based’ approaches again. Two RTO approaches deserve special attention, namely, the two-step approach and modifier adaptation. The two-step approach due to its wide industrial application and modifier adaptation because it represents the transition from the use of output measurements to the use of estimated necessary conditions of optimality. Figure 1.2 depicts a qualitative comparison of these RTO approaches in terms of implementation aspects.

Output Modifier Adaptation

A few modifications of MA have been proposed. An alternative modification for MA, labeled output MA, is proposed in [19, 73, 74]. Instead of using affine corrections to update the cost and constraint functions, this approach considers affine corrections to update the model outputs. Note that this approach is applicable to the case where the cost and constraint functions are known functions of the input and output variables. This RTO scheme was initially proposed by [19], where it is claimed that the performance of this RTO approach is case dependent, that is, the potential advantages over standard MA are process dependent. The definition of the modifiers represents the main difference between standard and output MA. While one approach updates the model outputs and uses the modified model to solve the optimization problem, the other corrects the constraint and cost functions directly in the optimization problem. Note that output MA possesses the same features as standard MA regarding KKT matching upon convergence. Later on, this approach was shown to have some advantages when the cost and constraint modifiers are inaccurate, and this inaccuracy can be

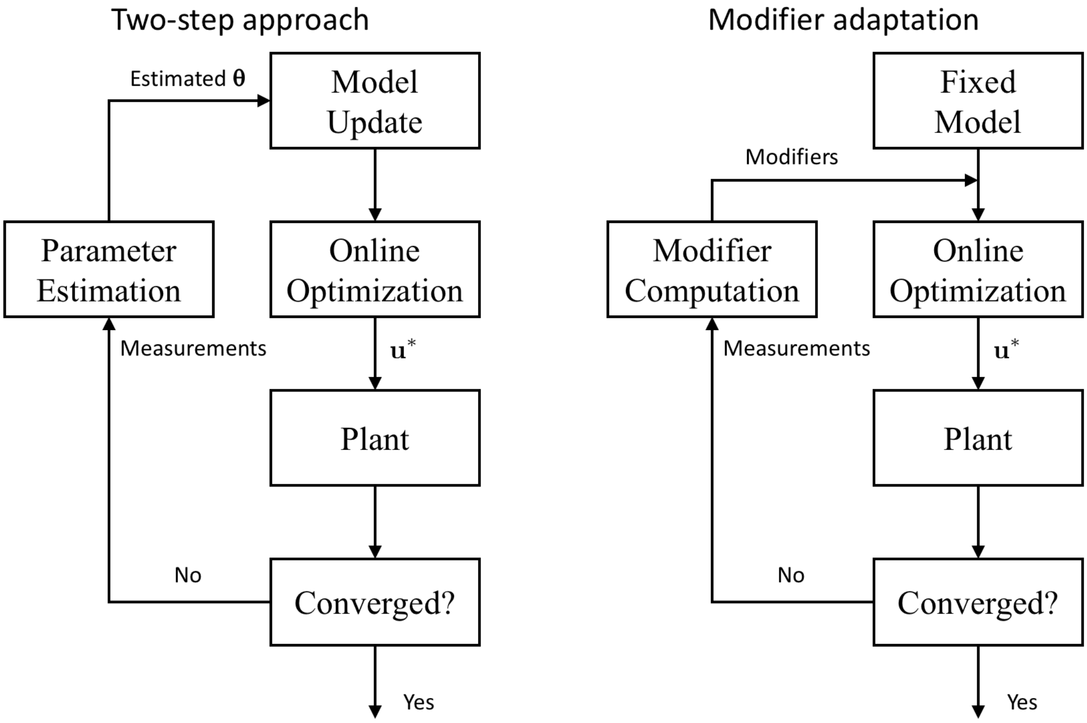
Two-step approach
Estimated θ
Model Update
Parameter Estimation
Online Optimization
Measurements
u*
Plant
No
Converged?
Yes
Modifier adaptation
Fixed Model
Modifiers
Modifier Computation
Online Optimization
Measurements
u*
Plant
No
Converged?
Yes

Figure 1.2: Qualitative comparison of the two-step approach and modifier adaptation.

compensated by using output modifiers instead [73, 74]. Up to now, no theoretical analyses has shown advantages of this method over standard MA.

Use of Transient Measurements for Static Optimization

Transient measurements have been proposed in the context of steady-state RTO of dynamic processes [7, 27, 75]. This approach uses transient measurements to either estimate steady-state plant gradients for MA or compute the zeroth-order modifiers for CA. The main advantage of these methods is that they allow the plant to converge to its optimum in a single transient operation. This is particularly interesting for plants that have large settling times. In [27], the authors estimate plant gradients via neighbouring extremals, which means that the proposed approach works well for the case of parametric plant-model mismatch. The basic idea consists in applying static MA during transient as if the plant were at steady state. The RTO period—i.e. the time between two consecutive RTO iterations—is treated as a tuning parameter of the optimization problem. However, this approach may fail in cases where the plant dynamics exhibit behaviors such as inverse response.

CA combined with transient measurements has been applied to a single solid-oxide fuel-cell stack in [7]. Similarly to the previous approach, transient measurements are collected to compute the zeroth-order modifiers. The authors mention that the tested system is characterized by two time scales: one slow and another fast, with a time-scale difference factor of about

200. This way, while the fast dynamics have already settled, the slow dynamics are treated as slow process drifts that are simply considered as another source of plant-model mismatch. However, the authors highlight the fact that the proposed approach works well for system where time scale-separation is present.

1.3 Contributions of the Thesis

The main contribution of this thesis is twofold: a novel RTO approach and its experimental application to a commercial solid-oxide fuel-cell system, namely, BlueGEN. This work led to the additional contributions that are described next.

1.3.1 Methodological Constributions to Modifier Adaptation

Fast RTO

We propose a novel RTO technique based on the constraint-adaptation approach. The proposed approach aims at dealing with an open challenge in RTO, namely, improve the convergence speed. As SOFC systems are characterized by large settling times, standard RTO approaches applied to these types of systems may result in slow convergence. To circumvent this problem, we reduce significantly the RTO period—i.e. the time that it takes to perform a RTO iteration. This means that static RTO is performed during transient operation. This approach tends to work well in systems characterized by a time-scale separation—i.e. systems that possess both slow and fast dynamics. However, this type of time-scale separation is rarely seen in complete SOFC systems because the dynamics are affected by the presence of various units and recycles. As a consequence, static RTO may fail if the measurements collected during transient operation are not representative of the plant steady state. To this end, we propose to apply constraint adaptation using transient measurements combined with a dynamic model. This way, we can speed up convergence of CA by executing the static RTO problem more frequently, without having to wait for the plant to settle to a new steady state between successive RTO iterations. Furthermore, optimality can be reached in a single transition to steady state. In addition, we study the impact of RTO tuning parameters such as the RTO filter and the RTO period. The advantages of the proposed approach include a simple way of using transient measurements to predict plant steady-state values, and an illustration that the use of dynamic models helps reach plant optimality. This approach has been applied to both a small-scale experimental SOFC system and to the commercial BlueGEN system [33].

1.3.2 Optimization of Experimental SOFC Systems

Small-scale experimental SOFC system

This work investigates the RTO implementation on a SOFC system that consists of a reformer and a SOFC stack, which are combined to a virtual afterburner and a virtual heat exchanger.

Since the system has multiple time scales, we deal with the slow dynamics by using dynamic models and transient measurements in the context of static RTO. We then perform experiments on the SOFC system to validate the proposed methodology. In addition, we study how the RTO period affects the convergence speed of the proposed RTO approach. Note that the experimental setup in this experiment considers a SOFC stack without the physical presence of the afterburner and the heat exchangers (the effects of these elements are simulated and implemented via electrical heaters). To the best of the author's knowledge, there exist no experimental results regarding the real-time optimization of solid-oxide fuel-cell systems as per 2012. The main contributions of this experimental validation are twofold: (i) the implementation of 'hardware-in-the-loop' operation—i.e. operation of a system that consists of both hardware and software components—of a 6-cells SOFC system, and (ii) the implementation of a fast RTO approach aiming to speed up convergence and improve the performance of the system. In addition, despite the fact that SOFC systems have slow dynamics, we show experimentally that the proposed approach is able to deal with external disturbances such as changes in the electrical power demand, thereby moving to the desired setpoint faster than with standard RTO approaches.

Commercial SOFC System

We investigate further the experimental application of CA using transient measurements together with a dynamic model. The system studied is a commercial micro-CHP consisting of a 70-cell SOFC stack, a pre-reformer, an afterburner and several heat exchangers. This complete SOFC system corresponds to the commercial BlueGEN system [33]. To the best of the author's knowledge, no investigation has reported experimental results concerning the application of RTO approaches to a complete commercial SOFC system. We propose to improve the operational efficiency of BlueGEN online—i.e. while the system is being operated—by means of real-time optimization. We apply CA using transient measurements to the BlueGEN system. In contrast to the previously mentioned small-scale experimental SOFC system, the BlueGEN system is much larger and the afterburner and multiple heat exchangers are physically present. The outcome of the experimental case study shows that the RTO scheme can drive the system toward optimal efficiency regardless of the requested power demand and the constraints imposed on the system. The contributions of this investigation include: (i) the experimental implementation of a fast RTO approach to a complete SOFC system, (ii) an a posteriori analysis that supports the fact that optimality has indeed been reached, and (iii) demonstration that the set of active constraints that determine plant optimality changes with the power demand. However, the main contribution of this study is the fact that the proposed RTO approach can drive the SOFC system to optimality and remain there despite the presence of slow drifts such as thermal inertia of the SOFC components and slower dynamics associated with the thermal recycle. This contribution is quite important as it shows the capability of the proposed RTO approach to deal with degradation that typically affects SOFC systems in long-term operations.

1.4 Organization of the Thesis

Chapter 2 presents a number of preliminary results on which the remaining parts of this thesis are built. This includes the MA approach and the SOFC model.

Chapter 3 contains the methodology proposed to speed up RTO implementation and to deal with multiple time-scale systems, namely, fast RTO. The basic principle is explained, and the effect of measurement noise, RTO filter and RTO period is illustrated by means of a simulated SOFC system.

Chapter 4 presents experimental results of fast RTO applied to a small system which consists of actual and virtual elements that interact dynamically. The effectiveness of fast RTO in terms of speeding up convergence is demonstrated. In addition, we perform an experimental verification of the effect of the RTO period in fast RTO.

Chapter 5 contains the experimental implementation of fast RTO to a commercial SOFC system. We show that fast RTO is effective at driving the SOFC system to optimality and maintain it there despite changing power loads and the presence of disturbances such as slow drifts. The system operability with respect to constraints is analyzed, and a qualitative assessment of optimal performance is provided. We show that the proposed approach is capable of operating at optimal efficiency despite the fact that the system is continuously in transient mode.

Chapter 6 concludes the thesis, and gives a number of perspectives for future work.

2 Preliminaries

RTO methods are typically applied to industrial processes with the aim of finding the optimal steady-state operating conditions. In this thesis, we propose and analyze an RTO approach that is able to optimize a process quickly. Next, we first review static RTO methodology, more specifically, MA approaches. Variations to static RTO approaches will be extended, used, analyzed and applied to SOFC systems.

Steady-state optimization provides a framework for computing optimal operating conditions for a continuous process. In Section 2.1, some attributes of optimal operation are described. A process model never perfectly represents a real plant. In this context, numerical optimization will fail at finding the optimal plant operating conditions. Hence, MA approaches, which use plant measurements in combination with a process model to cope with plant-model mismatch, is described in Section 2.2. Finally, a process model that comprises all components of a complete SOFC system is described in Section 2.3.

2.1 Static Optimization Problem

The optimization of plant operation at steady state can be stated as the following NLP problem:

$$\min_{\mathbf{u}} \quad \Phi_p(\mathbf{u}) := \phi\big(\mathbf{u}, \mathbf{y}_p(\mathbf{u})\big) \tag{2.1.1a}$$

$$\text{s.t.} \quad \mathbf{H}_p(\mathbf{u}) := \mathbf{h}\big(\mathbf{u}, \mathbf{y}_p(\mathbf{u})\big) = \mathbf{0}, \tag{2.1.1b}$$

$$\mathbf{G}_p(\mathbf{u}) := \mathbf{g}\big(\mathbf{u}, \mathbf{y}_p(\mathbf{u})\big) \leq \mathbf{0}, \tag{2.1.1c}$$

$$\mathbf{u}^{\mathrm{L}} \leq \mathbf{u} \leq \mathbf{u}^{\mathrm{U}}, \tag{2.1.1d}$$

where $\mathbf{u} \in \mathbb{R}^{n_u}$ are the inputs or decision variables; $\phi : \mathbb{R}^{n_u} \times \mathbb{R}^{n_y} \to \mathbb{R}$ denotes the objective function to be minimized; $\mathbf{h} : \mathbb{R}^{n_u} \times \mathbb{R}^{n_y} \to \mathbb{R}^{n_h}$ represents the set of equality constraints involving the inputs and outputs; $\mathbf{g} : \mathbb{R}^{n_u} \times \mathbb{R}^{n_y} \to \mathbb{R}^{n_g}$ is the set of inequality constraints involving the inputs and outputs; and $\mathbf{u}^{\mathrm{L}}$ and $\mathbf{u}^{\mathrm{U}}$ are the lower and upper bounds on the inputs. Note that the subscript $(\cdot)_p$ is used to indicate quantities related to the plant. In this thesis, the 'inputs' represent the degrees of freedom used to optimize the process, which could be flowrates, electrical current, or even setpoints for a low-level controllers.

Problem (2.1.1) has its optimum characterized by the necessary conditions of optimality. As equality constraints can be expressed as inequality constraints, one can include both the equality and inequality equations in Problem (2.1.1) as elements of the constraint vector $\mathbf{g}$:

$$\min_{\mathbf{u}} \quad \varphi_p(\mathbf{u}) := \phi\big(\mathbf{u}, \mathbf{y}_p(\mathbf{u})\big) \tag{2.1.2a}$$

$$\text{s.t.} \quad \mathcal{G}_p(\mathbf{u}) := \mathbf{g}\big(\mathbf{u}, \mathbf{y}_p(\mathbf{u})\big) \leq \mathbf{0}, \tag{2.1.2b}$$

$$\mathbf{u}^{\mathrm{L}} \leq \mathbf{u} \leq \mathbf{u}^{\mathrm{U}}. \tag{2.1.2c}$$

With the formulation in (2.1.2) and assuming that $\mathbf{u}_p^*$ is a regular point for the constraints, i.e. the active constraints are linearly independent, then, there exist unique values for the vector of Lagrangian multipliers $\boldsymbol{\mu}$ such that the following first-order Karush-Kuhn-Tucker (KKT) conditions hold at $\mathbf{u}_p^*$:

$$\mathcal{G}_p(\mathbf{u}_p^*) \leq \mathbf{0}, \ \ \mathbf{u}^{\mathrm{L}} \leq \mathbf{u}_p^* \leq \mathbf{u}^{\mathrm{U}}, \tag{2.1.3a}$$

$$\nabla_{\mathbf{u}} \mathbf{L}_p(\mathbf{u}_p) = \nabla_{\mathbf{u}} \boldsymbol{\varphi}_p(\mathbf{u}_p^*) + \boldsymbol{\mu}^T \nabla_{\mathbf{u}} \mathcal{G}_p(\mathbf{u}_p^*) + \boldsymbol{\zeta}^{UT} - \boldsymbol{\zeta}^{LT} = \mathbf{0}, \tag{2.1.3b}$$

$$\boldsymbol{\mu}^T \mathcal{G}_p(\mathbf{u}_p^*) = 0, \ \ \boldsymbol{\zeta}^{UT}(\mathbf{u}_p^* - \mathbf{u}^U) = 0, \ \ \boldsymbol{\zeta}^{LT}(\mathbf{u}^L - \mathbf{u}_p^*) = 0, \tag{2.1.3c}$$

$$\boldsymbol{\mu} \geq \mathbf{0}, \ \ \boldsymbol{\zeta}^{UT} \geq \mathbf{0}, \ \ \boldsymbol{\zeta}^{LT} \geq \mathbf{0}, \tag{2.1.3d}$$

where the Lagrangian function is defined as: $L_p(\mathbf{u}_p) = \varphi_p(\mathbf{u}_p) + \boldsymbol{\mu}^T \mathcal{G}_p(\mathbf{u}_p) + \boldsymbol{\zeta}^{UT}(\mathbf{u}_p - \mathbf{u}^U) + \boldsymbol{\zeta}^{LT}(\mathbf{u}^L - \mathbf{u}_p)$.

The necessary conditions of optimality (2.1.3) are referred to as the primal feasibility conditions (2.1.3a), stationarity conditions (2.1.3b), complementary slackness conditions (2.1.3c), and dual feasibility conditions (2.1.3d). Together, these conditions are called the KKT conditions. Note that they are necessary but not sufficient conditions of optimality. These necessary conditions must hold at any local minimum, which is also a regular point of the constraints.

2.2 Modifier-Adaptation Approaches

In practice, the steady-state input-output map $\mathbf{y}_p(\mathbf{u})$ of the plant is *not precisely known*, and one relies on an approximation given by a nonlinear steady-state model of the form:

$$\mathbf{f}(\mathbf{x},\mathbf{u},\boldsymbol{\theta}) = \mathbf{0}, \tag{2.2.1a}$$

$$\mathbf{y} = \mathbf{F}(\mathbf{x},\mathbf{u},\boldsymbol{\theta}), \tag{2.2.1b}$$

where $\mathbf{x} \in \mathbb{R}^{n_x}$ are the state variables, and $\boldsymbol{\theta} \in \mathbb{R}^{n_\theta}$ the model parameters. For given $\mathbf{u}$ and $\boldsymbol{\theta}$, the solution to (2.2.1a) can be expressed as the steady-state mapping $\mathbf{x} = \boldsymbol{\xi}(\mathbf{u},\boldsymbol{\theta})$, and the input-output mapping predicted by the model can be written as $\mathbf{y}(\mathbf{u},\boldsymbol{\theta}) = \mathbf{F}(\boldsymbol{\xi}(\mathbf{u},\boldsymbol{\theta}),\mathbf{u},\boldsymbol{\theta})$.

Using model (2.2.1), the following *model-based* optimization problem can be formulated:

$$\min_{\mathbf{u}} \quad \Phi(\mathbf{u}) := \phi\big(\mathbf{u},\mathbf{y}(\mathbf{u},\boldsymbol{\theta})\big) \tag{2.2.2a}$$

$$\text{s.t.} \quad \mathbf{H}(\mathbf{u}) := \mathbf{h}\big(\mathbf{u},\mathbf{y}(\mathbf{u},\boldsymbol{\theta})\big) = \mathbf{0}, \tag{2.2.2b}$$

$$\mathbf{G}(\mathbf{u}) := \mathbf{g}\big(\mathbf{u},\mathbf{y}(\mathbf{u},\boldsymbol{\theta})\big) \leq \mathbf{0}, \tag{2.2.2c}$$

$$\mathbf{u}^{\mathrm{L}} \leq \mathbf{u} \leq \mathbf{u}^{\mathrm{U}}. \tag{2.2.2d}$$

Since the optimization of a real process is typically affected by plant-model mismatch and disturbances, the solutions to Problems (2.1.1) and (2.2.2) are usually different. The objective of real-time optimization is to reach plant optimality by iteratively adapting the available model using plant measurements. Modifier adaptation has been developed to enforce convergence to the plant optimum even in the presence of structural plant-model mismatch [19]. As mentioned previously, if the plant optimum lies on active constraints, it is possible to use a simpler version of MA, called constraint adaptation, that corrects the constraints in the model-based optimization problem by means of only bias terms computed from the differences between the measured and predicted values of the constraints [7, 17, 57]. Next, we review the constraint-adaptation approach.

2.2.1 Constraint Adaptation

The idea behind constraint adaptation is to use measurements to correct the constraint values predicted by the model [17]. When plant optimality is governed by active constraints, constraint adaptation can be used to find and track the active constraints. At the k^{th} RTO iteration, the inputs $\mathbf{u}_k$ are applied to the plant and, after waiting for steady state, the plant constraints $\mathbf{H}_p$ and $\mathbf{G}_p$ are measured to compute the following constraint modifiers (or biases):

$$\boldsymbol{\epsilon}_k^{\mathbf{H}} := \mathbf{H}_p(\mathbf{u}_k) - \mathbf{H}(\mathbf{u}_k), \tag{2.2.3a}$$

$$\boldsymbol{\epsilon}_k^{\mathbf{G}} := \mathbf{G}_p(\mathbf{u}_k) - \mathbf{G}(\mathbf{u}_k), \tag{2.2.3b}$$

where $\boldsymbol{\epsilon}_k^{\mathbf{H}}$ are the equality constraint modifiers and $\boldsymbol{\epsilon}_k^{\mathbf{G}}$ the inequality constraint modifiers. Based on these modifiers, the following modified optimization problem is solved to determine the next optimal inputs $\mathbf{u}_{k+1}^{\star}$:

$$\mathbf{u}_{k+1}^{\star} = \arg\min_{\mathbf{u}} \quad \Phi(\mathbf{u}) \tag{2.2.4a}$$

$$\text{s.t.} \quad \mathbf{H}(\mathbf{u}) + \boldsymbol{\epsilon}_k^{\mathbf{H}} = \mathbf{0}, \tag{2.2.4b}$$

$$\mathbf{G}(\mathbf{u}) + \boldsymbol{\epsilon}_k^{\mathbf{G}} \leq \mathbf{0}, \tag{2.2.4c}$$

$$\mathbf{u}^{\mathrm{L}} \leq \mathbf{u} \leq \mathbf{u}^{\mathrm{U}}. \tag{2.2.4d}$$

An important property of the constraint-adaptation scheme is that the iterates are guaranteed to reach a feasible operating point upon convergence. In practice, constraint adaptation is implemented with exponential filtering of the modifiers or of the inputs, which (i) prevents large modifications of the operating point between consecutive RTO iterations, (ii) reduces the impact of measurement noise, and (iii) provides additional handles (the filter gains) for enforcing convergence. If exponential filtering of the inputs is used, the next operating point is obtained as follows:

$$\mathbf{u}_{k+1} = \mathbf{K}\mathbf{u}_{k+1}^{\star} + (\mathbf{I} - \mathbf{K})\mathbf{u}_k, \tag{2.2.5}$$

where the filter matrix $\mathbf{K}$ is often chosen as a diagonal matrix with the diagonal elements in the interval $(0,1]$. Figure 2.1 depicts the RTO scheme via constraint adaptation using steady-state plant measurements.

2.2.2 Modifier Adaptation

The idea behind MA is to add first-order correction terms to the cost and constraint functions in the optimization problem [19, 22]. At the kth iteration, with the inputs $\mathbf{u}_{\mathbf{k}}$ applied to the plant, the modified cost and constraint functions are constructed as follows:

$$\Phi_{\mathrm{m},k}(\mathbf{u}) := \Phi(\mathbf{u}) + \boldsymbol{\epsilon}_k^{\Phi} + \left(\boldsymbol{\lambda}_k^{\Phi}\right)^{\mathsf{T}} (\mathbf{u} - \mathbf{u}_k), \tag{2.2.6}$$

$$\mathbf{G}_{\mathrm{m},k}(\mathbf{u}) := \mathbf{G}(\mathbf{u}) + \boldsymbol{\epsilon}_k^{\mathbf{G}} + \left(\boldsymbol{\lambda}_k^{\mathbf{G}}\right)^{\mathsf{T}} (\mathbf{u} - \mathbf{u}_k), \tag{2.2.7}$$

$$\mathbf{H}_{\mathrm{m},k}(\mathbf{u}) := \mathbf{H}(\mathbf{u}) + \boldsymbol{\epsilon}_k^{\mathbf{H}} + \left(\boldsymbol{\lambda}_k^{\mathbf{H}}\right)^{\mathsf{T}} (\mathbf{u} - \mathbf{u}_k), \tag{2.2.8}$$

where $\boldsymbol{\lambda}_k^{\Phi} \in \mathbb{R}^{n_u}$, $\boldsymbol{\lambda}_k^{\mathbf{G}} \in \mathbb{R}^{n_u \times n_g}$, and $\boldsymbol{\lambda}_k^{\mathbf{H}} \in \mathbb{R}^{n_u \times n_h}$ are the first-order gradient modifiers for the cost and the inequality and equality constraint functions, respectively. These modifiers are defined as the following plant-model differences at $\mathbf{u}_k$:

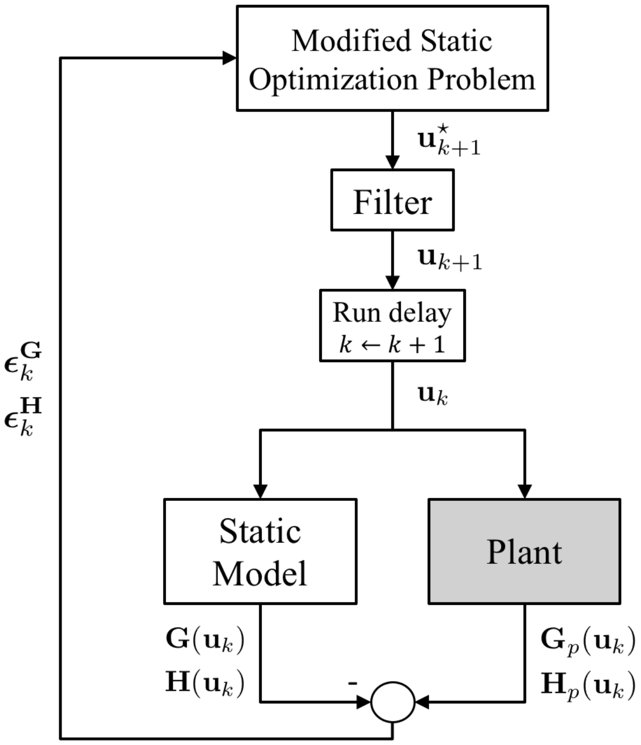
Modified Static Optimization Problem
$\mathbf{u}_{k+1}^{\star}$
Filter
$\mathbf{u}_{k+1}$
Run delay
$k \leftarrow k+1$
$\mathbf{u}_k$
$\epsilon_k^{\mathbf{G}}$
$\epsilon_k^{\mathbf{H}}$
Static Model
Plant
$\mathbf{G}(\mathbf{u}_k)$
$\mathbf{H}(\mathbf{u}_k)$
-
$\mathbf{G}_p(\mathbf{u}_k)$
$\mathbf{H}_p(\mathbf{u}_k)$

Figure 2.1: RTO scheme via CA using steady-state plant measurements.

$$(\boldsymbol{\lambda}_k^{\Phi})^{\mathsf{T}} := \left.\frac{d\Phi_p}{d\mathbf{u}}\right|_{\mathbf{u}_k} - \left.\frac{d\Phi}{d\mathbf{u}}\right|_{\mathbf{u}_k}, \tag{2.2.9}$$

$$(\boldsymbol{\lambda}_k^{\mathbf{G}})^{\mathsf{T}} := \left.\frac{d\mathbf{G}_p}{d\mathbf{u}}\right|_{\mathbf{u}_k} - \left.\frac{d\mathbf{G}}{d\mathbf{u}}\right|_{\mathbf{u}_k}, \tag{2.2.10}$$

$$(\boldsymbol{\lambda}_k^{\mathbf{H}})^{\mathsf{T}} := \left.\frac{d\mathbf{H}_p}{d\mathbf{u}}\right|_{\mathbf{u}_k} - \left.\frac{d\mathbf{H}}{d\mathbf{u}}\right|_{\mathbf{u}_k}. \tag{2.2.11}$$

The plant gradients $\frac{d\Phi_p}{d\mathbf{u}}$, $\frac{d\mathbf{G}_p}{d\mathbf{u}}$ and $\frac{d\mathbf{H}_p}{d\mathbf{u}}$ are assumed to be available at $\mathbf{u}_k$. Since ϕ, $\mathbf{g}$ and $\mathbf{h}$ are known functions of $\mathbf{u}$ and $\mathbf{y}$, these plant gradients can be inferred from the measured plant outputs $\mathbf{y}_p(\mathbf{u}_k)$ and the estimated plant output gradients $\left.\frac{d\mathbf{y}_p}{d\mathbf{u}}\right|_{\mathbf{u}_k}$:

$$\left.\frac{d\Phi_p}{d\mathbf{u}}\right|_{\mathbf{u}_k} = \left.\frac{\partial\phi}{\partial\mathbf{u}}\right|_{\mathbf{u}_k,\mathbf{y}_p(\mathbf{u}_k)} + \left.\frac{\partial\phi}{\partial\mathbf{y}}\right|_{\mathbf{u}_k,\mathbf{y}_p(\mathbf{u}_k)} \left.\frac{d\mathbf{y}_p}{d\mathbf{u}}\right|_{\mathbf{u}_k},$$

$$\left.\frac{d\mathbf{G}_p}{d\mathbf{u}}\right|_{\mathbf{u}_k} = \left.\frac{\partial\mathbf{g}}{\partial\mathbf{u}}\right|_{\mathbf{u}_k,\mathbf{y}_p(\mathbf{u}_k)} + \left.\frac{\partial\mathbf{g}}{\partial\mathbf{y}}\right|_{\mathbf{u}_k,\mathbf{y}_p(\mathbf{u}_k)} \left.\frac{d\mathbf{y}_p}{d\mathbf{u}}\right|_{\mathbf{u}_k}.$$

$$\left.\frac{d\mathbf{H}_p}{d\mathbf{u}}\right|_{\mathbf{u}_k} = \left.\frac{\partial\mathbf{h}}{\partial\mathbf{u}}\right|_{\mathbf{u}_k,\mathbf{y}_p(\mathbf{u}_k)} + \left.\frac{\partial\mathbf{h}}{\partial\mathbf{y}}\right|_{\mathbf{u}_k,\mathbf{y}_p(\mathbf{u}_k)} \left.\frac{d\mathbf{y}_p}{d\mathbf{u}}\right|_{\mathbf{u}_k}.$$

The next optimal inputs $\mathbf{u}_{k+1}^{\star}$ are computed by solving the following modified optimization problem:[1]

$$\begin{aligned}
\mathbf{u}_{k+1}^{\star} := \arg\min_{\mathbf{u}} \quad & \Phi_{\mathrm{m},k}(\mathbf{u}) \\
\text{s.t.} \quad & \mathbf{G}_{\mathrm{m},k}(\mathbf{u}) \leq \mathbf{0}, \\
& \mathbf{H}_{\mathrm{m},k}(\mathbf{u}) = \mathbf{0}, \\
& \mathbf{u}^{\mathrm{L}} \leq \mathbf{u} \leq \mathbf{u}^{\mathrm{U}}.
\end{aligned} \tag{2.2.12}$$

The next operating point is then determined upon applying a first-order filter to the inputs as per (2.2.5). In its simplest form, the MA algorithm is implemented as follows:

Algorithm 1 (Modifier Adaptation [19])

Initialization. *Provide the initial point* $\mathbf{u}_0$ *and select the input filter matrix* $\mathbf{K}$.

For $k = 0 \to \infty$

1. *Apply the inputs* $\mathbf{u}_k$ *to the plant, wait for steady state, measure* $\mathbf{y}_p(\mathbf{u}_k)$ *and evaluate* $\Phi_p(\mathbf{u}_k) := \phi\big(\mathbf{u}_k, \mathbf{y}_p(\mathbf{u}_k)\big)$ *and* $\mathbf{G}_p(\mathbf{u}_k) := \mathbf{g}\big(\mathbf{u}_k, \mathbf{y}_p(\mathbf{u}_k)\big)$.
2. *Compute estimates of* $\frac{d\Phi_p}{d\mathbf{u}}$ *and* $\frac{d\mathbf{G}_p}{d\mathbf{u}}$ *at* $\mathbf{u}_k$. *These estimates require data from perturbed operating points in the neighborhood of* $\mathbf{u}_k$.
3. *Evaluate the modifiers* (2.2.9)-(2.2.11).
4. *Compute* $\mathbf{u}_{k+1}$ *by solving Problem* (2.2.12) *and applying Filter* (2.2.5).

end

The strength of MA lies in its ability to reach a KKT point of the *plant* upon convergence, as stated in the following theorem.

Theorem 1 (MA convergence ⇒ KKT matching [19]) *If the input sequence* $\{\mathbf{u}_k\}$ *generated by Algorithm 1 is convergent and its limit value* $\mathbf{u}_\infty := \lim_{k\to\infty} \mathbf{u}_k$ *is a KKT point of the modified optimization Problem* (2.2.12), *then* $\mathbf{u}_\infty$ *is also a KKT point of the plant Problem* (2.1.1).

---

[1] Note that the modified cost function is often defined as $\Phi_{\mathrm{MA},k}(\mathbf{u}) := \Phi(\mathbf{u}) + (\boldsymbol{\lambda}_k^{\Phi})^{\mathsf{T}}(\mathbf{u} - \mathbf{u}_k)$ or $\Phi_{\mathrm{MA},k}(\mathbf{u}) := \Phi(\mathbf{u}) + (\boldsymbol{\lambda}_k^{\Phi})^{\mathsf{T}}\mathbf{u}$, since the addition of the constant terms $\boldsymbol{\epsilon}_k^{\Phi}$ and $-(\boldsymbol{\lambda}_k^{\Phi})^{\mathsf{T}}\mathbf{u}_k$ to the cost function does not affect the solution $\mathbf{u}_{k+1}^{\star}$.

Remark 1 (First-order matching) *KKT matching in Theorem 1 relies on the fact that the modified constraints match the values and the gradients of the plant contraints at* $\mathbf{u}_k$*, and the modified cost function matches the gradient of the plant cost function at* $\mathbf{u}_k$*, that is,*

$$\mathbf{G}_{\mathrm{m},k}(\mathbf{u}_k) = \mathbf{G}_p(\mathbf{u}_k), \tag{2.2.13}$$

$$\left.\frac{d\mathbf{G}_{\mathrm{m},k}}{d\mathbf{u}}\right|_{\mathbf{u}_k} = \left.\frac{d\mathbf{G}_p}{d\mathbf{u}}\right|_{\mathbf{u}_k}, \tag{2.2.14}$$

$$\left.\frac{d\Phi_{\mathrm{m},k}}{d\mathbf{u}}\right|_{\mathbf{u}_k} = \left.\frac{d\Phi_p}{d\mathbf{u}}\right|_{\mathbf{u}_k}. \tag{2.2.15}$$

The KKT-matching theorem states that the solution to the MA algorithm is at KKT point of the plant. However, other conditions must be guaranteed in order to enforce the convergence.

One of these conditions is model adequacy. In the context of the MA framework, a model is called adequate if there exist values of zeroth- and first-order modifiers such that a fixed point of the MA algorithm coincides with the plant optimum $\mathbf{u}_p^*$ [76]. A requirement that the process model must satisfy in order to enable convergence of MA approaches is discussed in [19] and summarized next.

Theorem 2 (Model adequacy [19]) *Let* $\mathbf{u}_p^*$ *be a the unique plant optimum that is assumed to be a regular point for the constraints. If the process model is such that the reduced Hessian of the cost function* Φ *is positive definite at* $\mathbf{u}_p^*$*,*

$$\nabla_r^2 \Phi(\mathbf{u}_p^*) \prec 0 \quad \textit{(positive definite)}, \tag{2.2.16}$$

then the process model is said to be adequate for the MA scheme.

Owing to the fact that the model adequacy condition is satisfied when the process model is convex, a method of model convexification via convex approximations in order to automatically satisfy Theorem 2 has been proposed in [77].

MA approaches have the ability to converge to a plant KKT point upon convergence. The next question is whether there exist convergence conditions for MA. In an attempt to answer this question necessary and sufficient conditions for the convergence of MA have been proposed in [19]. Later on, a method that upper bounds the cost and constraint functions has been proposed in [78]. This approach enforces feasible-side convergence of MA by adding quadratic terms to the model cost and constraint functions. The use of second-order modifiers for MA schemes, and how, in the presence of reliable measurements, first- and second-order data can be used to approximate SQP-like model-free RTO schemes has been discussed in [79]. The combination of trust-region methods with the MA framework in order to enforce global convergence has been studied in [80]. However, convergence properties are still subject of study as, unfortunately, only impractical conditions have been proposed so far.

2.3 SOFC Model

Here we describe the SOFC model that is used to implement the proposed RTO methodologies in this thesis. This section provides a description of each component of a SOFC system. Hence, modeling of an SOFC stack, a pre-reformer, an afterburner, and heat exchangers are considered.

2.3.1 SOFC Stack

The stack model includes three parts, the internal reforming, the stack voltage, and the mass and energy balances. These are briefly described next and given in more details in [81] and [82].

Internal Reforming. We consider that all methane that is not converted in the pre-reformer is reformed in the stack. For simplicity, we assume that the methane is converted instantaneously. Hence, the internal-reforming equations are of algebraic nature. The overall endothermic reaction that takes place in the stack is:

$$\mathrm{CH_4 + 2H_2O \rightarrow CO_2 + 4H_2} \quad \Delta\mathrm{H_R} = 164.95\ \mathrm{kJ.mol^{-1}}. \tag{2.3.1}$$

Stack Voltage. The electrochemical model expresses the cell potential as a function of the flowrates and the electrical current. To compute the effective potential in the fuel cell, we compute the maximum potential that the cell produces, U_N, and subtract its losses. These losses (or overpotentials) include:

- (i) the ohmic loss caused by the ionic resistance of the electrolyte and current collectors, η_{el};
- (ii) the activation overpotential attributed to charge-transfer kinetics, $\eta_{act,cath}$;
- (iii) the diffusion overpotential caused by concentration gradients between the electrode surface and the bulk flow, $\eta_{diff,an}$ and $\eta_{diff,cath}$;
- (iv) the overpotential losses due to the dissociation of the oxygen molecules into ions on the cathode surface, η_{diss};
- (v) the ohmic losses, η_{MIC}.

Hence, the effective cell potential U_{cell} can be written as follows:

$$U_{cell} = U_N - \eta_{el} - \eta_{act,cath} - \eta_{diff,an} - \eta_{diff,cath} - \eta_{diss} - \eta_{MIC}. \tag{2.3.2}$$

The electrical power, P_{el}, and the efficiency, η, are expressed in terms of the cell potential as:

$$P_{el} = U_{cell} N_{cell} I, \tag{2.3.3}$$

$$\eta = \frac{P_{el}}{q_{CH_4} LHV_{CH_4}}, \tag{2.3.4}$$

where N_{cell}, and LHV_{CH_4} are parameters that represent the number of cells in the stack, and the lower heating value of the methane, respectively. The electric current is represented by I and q_{CH_4} is the methane flowrate that enters the SOFC system. The air-excess ratio is defined by:

$$\lambda_{air} = \frac{0.21}{2} \frac{q_{air}}{q_{CH_4}}. \tag{2.3.5}$$

The fuel utilization is given by:

$$\nu = \frac{N_c}{8F} \frac{I}{q_{CH_4}}, \tag{2.3.6}$$

where F is the Faraday constant.

Mass and Energy Balances. Following the lumped-model approach, the fuel cell is divided into four smaller thermal bodies over which the temperature is assumed to be uniform:

- the electrolyte at temperature T_e,
- the metal interconnect at temperature T_i,
- the fuel channel at temperature T_{an},
- the air channel at temperature T_{cath}.

Based on these thermal bodies, we can perform an overall material and energy balance around the fuel-cell stack as in [81]. According to these authors, one can separate the fuel cell in four parts, which allows expressing the model equations as functions of the temperatures of the fuel and air at the inlet and outlet. These temperatures can be measured and compared to experimental data. In addition, the electrolyte temperature needs to be estimated since, usually, it cannot be measured. Hence, these result in four differential equations that represent the energy balance around each thermal body.

2.3.2 Pre-Reformer

Natural gas is primarily composed of methane. Using methane as a fuel is advantageous due to its thermodynamics, its wide availability, and the available distribution network. In this perspective, fuel cells represent a high-efficiency alternative for electricity and heat production compared to the direct combustion of methane. The aim of the methane-steam reforming process is to convert methane and steam into syngas, which is then fed to the anode of the fuel cell. This is done through two main chemical reactions [82], namely, steam reforming and water gas shifting:

$$\mathrm{CH_4 + H_2O \rightarrow CO + 3H_2} \quad \Delta \mathrm{H_R} = 206.1\ \mathrm{kJ.mol^{-1}}. \tag{2.3.7}$$

$$\mathrm{CO + H_2O \rightarrow CO_2 + H_2} \quad \Delta \mathrm{H_R} = -41.15\ \mathrm{kJ.mol^{-1}}. \tag{2.3.8}$$

The remaining methane is converted in the stack. It is important to mention that, while the second reaction is exothermic, the first one is highly endothermic, which results in an overall *endothermic* process. In a SOFC system, a pre-reformer is needed since direct injection of methane and steam inside the fuel cell would induce cold spots inside the stack.

Energy Balance. As the process is mainly endothermic, the temperature of the reformer tends to decrease. The energy flows entering and leaving the system include two components:

- the enthalpy of the streams entering the reformer,
- the enthalpy of the streams leaving the reformer.

An energy balance of the reformer gives the following ODE:

$$\rho_r V_r C_{p,r} \frac{dT_{ref}}{dt} = \sum_j q_{r,j} H_{r,j}(T_{r,j}) - \sum_l q_{r,l} H_{r,l}(T_{ref}), \tag{2.3.9}$$

where T_{ref} is the temperature of the pre-reformer, H_r is the molar enthalpy of each component that enters or leaves the pre-reformer, $T_{r,j}$ represents the temperature of the *jth* component that enters the pre-reformer, q_r is the molar flowrate associated with the components that enter or leave the pre-reformer, the subscript j denotes the components that enter the pre-reformer, while the subscript l stands for the components that leave the pre-reformer. The model parameters ρ_r, V_r and $C_{p,r}$ represent the density, the volume and the heat capacity of the reformer, respectively.

2.3.3 Afterburner

When the anodic flow leaves the fuel cell, it still contains fuel. The outgoing flow contains small amounts of H_2 and CO that can be oxidized. The remaining fuel is burned with the excess of air in order to create a hot flow that is used to heat up the inlet flow of air and to provide heat to the pre-reformer. This heat recovery allows increasing the system efficiency,

The afterburner oxidizes the anodic flow using the cathodic flow through the following combustion equations:

$$\begin{aligned} \mathrm{H_2} + \tfrac{1}{2}\mathrm{O_2} &\rightarrow \mathrm{H_2O}, && (2.3.10)\\ \mathrm{CO} + \tfrac{1}{2}\mathrm{O_2} &\rightarrow \mathrm{CO_2}. && (2.3.11) \end{aligned}$$

It is assumed that the combustion is complete.

Energy Balance. We can write an energy balance of the afterburner. Upon assuming that the afterburner operates at constant pressure under ideal gas mixing, the outlet temperature is equal to the temperature inside the burning chamber. Hence, the energy balance reads:

$$\begin{aligned} \rho_b V_b C_{p,b} \frac{dT_{burner}}{dt} = \sum_j q_{b,j} H_{b,j}(T_{b,j}) - \sum_l q_{b,l} H_{b,l}(T_{burner}) - \\ q_{H_2} \Delta H_{r,H_2} - q_{CO} \Delta H_{r,CO}, \end{aligned} \qquad (2.3.12)$$

where $\Delta H_{r,i}$ represents the molar reaction enthalpy of a component that is oxidized, and H_b is the molar enthalpy of each component that enters or leaves the afterburner. The afterburner temperature is represented by T_{burner}. The temperature of jth component that enters the afterburner is represented by $T_{b,j}$, q_b is the molar flowrate associated with the components that enter or leave the afterburner. The subscripts j and l denote the components entering and leaving the afterburner, respectively. The parameters ρ_b, V_b and $C_{p,b}$ represent the density, the volume and the heat capacity of the afterburner.

2.3.4 Heat Exchangers

A heat exchanger is used to transfer heat from a hot flow to a cold flow. This can be used here to pre-heat the air inlet by using the heat available in the hot exhaust of the afterburner. A plate heat exchanger is considered due to its flexibility and efficiency. It consists of a series of corrugated and gasketed metal plates pressed together as proposed in [83]. The gaskets allow distributing the flows to the channels located between two plates. It is assumed that the considered heat exchanger can be modeled as a big plate, the equivalent area of which depends on its layout.

Energy Balances. For the hot flow, one can write:

$$\rho_h V_{ch} C_{p,h} \frac{dT_h}{dt} = \frac{A(T_m - T_h)}{R_{h,tot}} + \sum_j q_{h,j} H_{h,j}(T_{h,j}) - \sum_l q_{h,l} H_{h,l}(T_h), \qquad (2.3.13)$$

where T_h represents the temperature of the gases on the hot side and T_m is the metallic plate temperature. The molar enthalpy of each component that enters or leaves the hot side of the heat exchanger is denoted by H_h. The temperature of the *jth* component that enters the hot side of the heat exchanger is represented by $T_{h,j}$, q_h is the molar flowrate associated with the components that enter or leave the hot side of the heat exchanger. As before, the subscript j denotes the components entering the hot side of the heat exchanger, while the subscript l stands for the components leaving the hot side. The variables ρ_h and $C_{p,h}$ are parameters that represent the average density and the heat capacity of the gases on the hot side. $R_{h,tot}$ represents the overall thermal resistance of the hot side, A stands for the heat exchange area. The volume of the channel is assumed to be the same on both sides and given by V_{ch}.

The enthalpies related to the inlet and outlet flows are taken into account at their respective temperatures. Furthermore, this tendency model assumes that the composition remains the same between inlet and outlet.

The energy balance for the cold side reads:

$$\rho_c V_{ch} C_{p,c} \frac{dT_c}{dt} = \frac{A(T_c - T_m)}{R_{c,tot}} + \sum_j q_{c,j} H_{c,j}(T_{c,j}) - \sum_l q_{c,l} H_{c,l}(T_c), \tag{2.3.14}$$

where T_c represents the temperature of the gases on the cold side. The temperature of the *jth* component that enters the cold side of the heat exchanger is denoted by $T_{c,j}$. The molar enthalpy of each component that enters or leaves the cold side of the heat exchanger is represented by H_c. The molar flowrate associated with the components that enter or leave the cold side of the heat exchanger is denoted by q_c. As before, the subscript j denotes the components entering the cold side of the heat exchanger, while the subscript l stands for the components leaving the cold side. The parameters ρ_c, V_{ch} and $C_{p,d}$ represent the density, the volume and the heat capacity of the gases on the cold side, respectively. The overall thermal resistance of the cold side is represented by $R_{c,tot}$.

Finally, the energy balance for the metallic plate is affected by the thermal flow that goes from the hot side to the cold side. The heat-exchange dynamics are mostly determined by the metallic plate as it has the largest time constant. The energy balance for the metallic plate can be written as:

$$\rho_m V_{plate} C_{p,m} \frac{dT_m}{dt} = \frac{A(T_c - T_m)}{R_{c,tot}} - \frac{A(T_m - T_h)}{R_{h,tot}}, \tag{2.3.15}$$

where ρ_m, V_{plate} and $C_{p,m}$ are parameters that represent the density, the volume and the heat capacity of the metallic plate, respectively.

Table 2.1 summarizes the SOFC model order used for simulation and RTO implementation. For RTO, we use the algebraic version with all time derivatives set to zero.

Table 2.1: General overview of the SOFC model, with n heat exchanges in the SOFC system.

Component	Variables	Order
SOFC stack	$T_e, T_i, T_{an}, T_{cath}$	4
Pre-reformer	T_{ref}	1
Afterburner	T_{burner}	1
Heat exchanger	T_m, T_c, T_h	3n
	Overall model	6+3n

3 Fast Real-Time Optimization Using Transient Measurements

This chapter discusses the use of transient measurements in the context of steady-state RTO. It is based on the following publications [8, 84].

T. de Avila Ferreira, Z. Wuillemin, A. G. Marchetti, C. Salzmann, J. Van Herle, and D. Bonvin. Real-time optimization of an experimental SOFC system. *J. Power Sources*, *Submitted*, 2018.

T. de Avila Ferreira, G. François, A. G. Marchetti, and D. Bonvin. Use of transient measurements for static real-time optimization. *IFAC-PapersOnLine*, 50(1):5737–5742, 2017.

3.1 Introduction

Modifier adaptation is a real-time optimization method characterized by its ability to enforce plant optimality upon convergence despite the presence of model uncertainty. MA uses steady-state measurements and solves a static optimization problem. Hence, after every input change, one typically waits for the plant to reach steady state before measurements are taken again, which may make convergence to plant optimality rather slow.

Recently, an approach that uses transient measurements for steady-state MA has been proposed. This way, plant optimality can be reached in a single transient operation. Here, in the context of constraint adaptation (CA), we propose to improve this approach by using a dynamic model to process transient measurements for the estimation of zeroth-order modifiers. The approach is illustrated through the simulated example of a SOFC system. It is shown that the approach is rather independent of the choice of the RTO period. The time needed to reach plant optimality is of the order of the plant settling time, whereas several transitions to steady state would have been necessary using the standard MA scheme.

Since, MA typically requires several iterations to steady state before converging to plant optimality, it is of great interest to combine the MA properties with the ability of implicit schemes to converge to the plant optimum in a single iteration to steady state. A first step in that direction was made recently in [27], who proposed to implement steady-state MA in the transient phase, thereby attempting to reach optimality in a single transient operation to steady state. For this, the steady-state optimization problem is solved repeatedly online, with the *steady-state* modifiers being estimated from *transient* measurements. The latter are used as if they were steady-state measurements. The approach is consistent since transient measurements tend to steady-state measurements when the plant reaches steady state. The nice MA property of reaching a KKT point of the plant upon convergence is preserved, provided the gradient estimates converge to their true values. However, the main disadvantage of this approach is that, during transient operation, the steady-state gradient estimates might be rather inaccurate, which might lead to oscillatory behavior and even prevent convergence.

This chapter proposes to use dynamic models to process transient measurements and predict the corresponding steady-state constraint and output values. The main contribution of the proposed approach includes: (i) a simply way of using transient measurements to predict plant steady-state values, and (ii) an illustration that the use of dynamic models helps reach plant optimality.

This chapter is organized as follows. Section 3.2 describes the use of transient measurements to estimate steady-state values with the use of dynamic models. The implementation aspects are illustrated via a simulated SOFC system in Section 3.3, while Section 3.4 concludes this chapter.

3.2 Fast Constraint Adaptation

The objective of constraint adaptation using transient measurements is to speed up convergence of constraint adaptation by executing the steady-state RTO problem more frequently, without having to wait for the plant to settle to a new steady state between successive RTO iterations.

3.2.1 Use of Transient Measurements

Consider the *jth* iteration during transient operation. At time t_j with the inputs $\mathbf{u}_j$, the values of the plant constraints *at steady state* are estimated (not measured) and compared to the model predictions. Then, the next optimal inputs $\mathbf{u}^*_{j+1}$ are computed, filtered and applied to the plant until the next RTO execution at time $t_{j+1} = t_j + \tau_{RTO}$, where τ_{RTO} is the RTO period. The optimization problem for computing $\mathbf{u}^*_{j+1}$ can be written as:

$$\mathbf{u}^*_{j+1} = \arg\min_{\mathbf{u}} \quad \Phi(\mathbf{u}) \tag{3.2.1a}$$

$$\text{s.t.} \quad \mathbf{H}(\mathbf{u}) + \hat{\boldsymbol{\epsilon}}^{\mathbf{H}}_j = \mathbf{0}, \tag{3.2.1b}$$

$$\mathbf{G}(\mathbf{u}) + \hat{\boldsymbol{\epsilon}}^{\mathbf{G}}_j \le \mathbf{0}, \tag{3.2.1c}$$

$$\mathbf{u}^{\mathrm{L}} \le \mathbf{u} \le \mathbf{u}^{\mathrm{U}}, \tag{3.2.1d}$$

where $\hat{\boldsymbol{\epsilon}}_j^{\mathbf{H}}$ and $\hat{\boldsymbol{\epsilon}}_j^{\mathbf{G}}$ represent the *steady-state* constraint modifiers estimated at time t_j as follows:

$$\hat{\boldsymbol{\epsilon}}_j^{\mathbf{H}} := \widehat{\mathbf{H}}_p(\mathbf{u}_j) - \mathbf{H}(\mathbf{u}_j), \tag{3.2.2a}$$

$$\hat{\boldsymbol{\epsilon}}_j^{\mathbf{G}} := \widehat{\mathbf{G}}_p(\mathbf{u}_j) - \mathbf{G}(\mathbf{u}_j), \tag{3.2.2b}$$

with $\widehat{\mathbf{H}}_p(\mathbf{u}_j)$ and $\widehat{\mathbf{G}}_p(\mathbf{u}_j)$ representing the estimates of the plant constraints *at steady state* corresponding to the current inputs $\mathbf{u}_j$. We propose to use exponential filtering of the inputs:

$$\mathbf{u}_{j+1} = \mathbf{K}\mathbf{u}^*_{j+1} + (\mathbf{I} - \mathbf{K})\mathbf{u}_j. \tag{3.2.3}$$

There are different ways of estimating $\widehat{\mathbf{H}}_p(\mathbf{u}_j)$ and $\widehat{\mathbf{G}}_p\left(\mathbf{u}_j\right)$, two of which are described next.

Let us denote by $\mathbf{y}_p^{dyn}(t_j)$ the measured plant outputs at time t_j. The corresponding measured constraints are $\mathbf{H}_p^{dyn}(t_j) := \mathbf{h}\big(\mathbf{u}_j, \mathbf{y}_p^{dyn}(t_j)\big)$ and $\mathbf{G}_p^{dyn}(t_j) := \mathbf{g}\big(\mathbf{u}_j, \mathbf{y}_p^{dyn}(t_j)\big)$. The superscript $(.)^{dyn}$ is introduced to distinguish these dynamic quantities from the steady-state plant mappings $\mathbf{y}_p$, $\mathbf{H}_p$ and $\mathbf{G}_p$. In [27], the authors proposed to simply use the *dynamic* measurements at time t_j as estimates of the *steady-state* values corresponding to the current inputs $\mathbf{u}_j$, that is,

$$\widehat{\mathbf{H}}_p\left(\mathbf{u}_j\right) := \mathbf{H}_p^{dyn}\left(t_j\right), \tag{3.2.4a}$$

$$\widehat{\mathbf{G}}_p\left(\mathbf{u}_j\right) := \mathbf{G}_p^{dyn}\left(t_j\right). \tag{3.2.4b}$$

3.2.2 Use of Transient Measurements and a Dynamic Model

We assume the availability of a dynamic model that is consistent with the steady-state model (2.2.1) used for optimization:[1]

$$\dot{\mathbf{x}}(t) = \mathbf{f}\left(\mathbf{x}(t),\, \mathbf{u}(t), \boldsymbol{\theta}\right), \qquad \mathbf{x}(0) = \mathbf{x}_0, \tag{3.2.5a}$$

$$\mathbf{y}(t) = \mathbf{F}\left(\mathbf{x}(t),\, \mathbf{u}(t), \boldsymbol{\theta}\right). \tag{3.2.5b}$$

The dynamic model predicts the constrained variables during transient operation as $\mathbf{H}^{dyn}(t_j) := \mathbf{h}\big(\mathbf{u}_j, \mathbf{y}(t_j)\big)$ and $\mathbf{G}^{dyn}(t_j) := \mathbf{g}\big(\mathbf{u}_j, \mathbf{y}(t_j)\big)$.

Instead of taking the current measured values of the plant constraints as steady-state estimates, as was done in (3.2.4), this method proposes to account for dynamic effects (at least those predicted by the model) by estimating the plant steady-state quantities as the transient measurements at time t_j corrected by the offsets between the values predicted by the model

---

[1] Consistency with the steady-state model implies here that the dynamic model and steady-state model predict the same steady-state values.

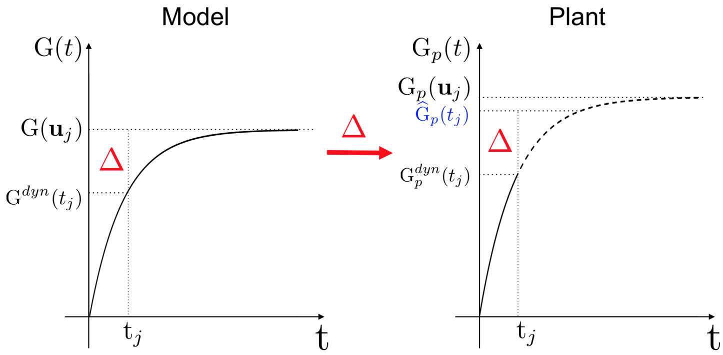

Figure 3.1: Estimation of $\widehat{G}_p\left(\mathbf{u}_j\right)$ from the measurement of $G_p^{dyn}(t_j)$ and estimation of $\Delta := G(\mathbf{u}_j) - G^{dyn}(t_j)$ from the model.

at steady state and at time t_j:

$$\widehat{\mathbf{H}}_p\left(\mathbf{u}_j\right) = \mathbf{H}_p^{dyn}\left(t_j\right) + \left(\mathbf{H}(\mathbf{u}_j) - \mathbf{H}^{dyn}(t_j)\right), \tag{3.2.6a}$$

$$\widehat{\mathbf{G}}_p\left(\mathbf{u}_j\right) = \mathbf{G}_p^{dyn}\left(t_j\right) + \left(\mathbf{G}(\mathbf{u}_j) - \mathbf{G}^{dyn}(t_j)\right). \tag{3.2.6b}$$

The basic idea is illustrated in Figure 3.1. It follows that the constraint modifiers can be evaluated as the differences between the dynamic constraint measurements and the corresponding values predicted by the dynamic model:

$$\hat{\boldsymbol{\epsilon}}_j^{\mathbf{H}} = \mathbf{H}_p^{dyn}(t_j) - \mathbf{H}^{dyn}(t_j), \tag{3.2.7a}$$

$$\hat{\boldsymbol{\epsilon}}_j^{\mathbf{G}} = \mathbf{G}_p^{dyn}(t_j) - \mathbf{G}^{dyn}(t_j). \tag{3.2.7b}$$

Figure 3.2 depicts the RTO scheme via constraint adaptation using transient measurements and a dynamic model.

If the dynamic and steady-state models are consistent, the advantage of the method presented in this subsection over the one in [27] is a dynamic adjustment that accounts for the modeled dynamic effects, which vanish when steady state is reached upon convergence.

3.2.3 Model Adequacy

Model-adequacy conditions for the bias update scheme for the case where the plant optimum is fully determined by active constraints have been proposed in [16]. Here, we adapt those conditions for CA. The process model is said to be adequate if zeroth-order modifiers can be found such that a fixed point of the CA scheme corresponds to a (local) plant optimum $\mathbf{u}_p^*$.

For simplicity of notation, we consider the case without equality constraints and with the input bounds included in the inequality constraints $\mathbf{G}$. Let $\mathscr{A}(\mathbf{u}_p^*)$ be the set of active inequality

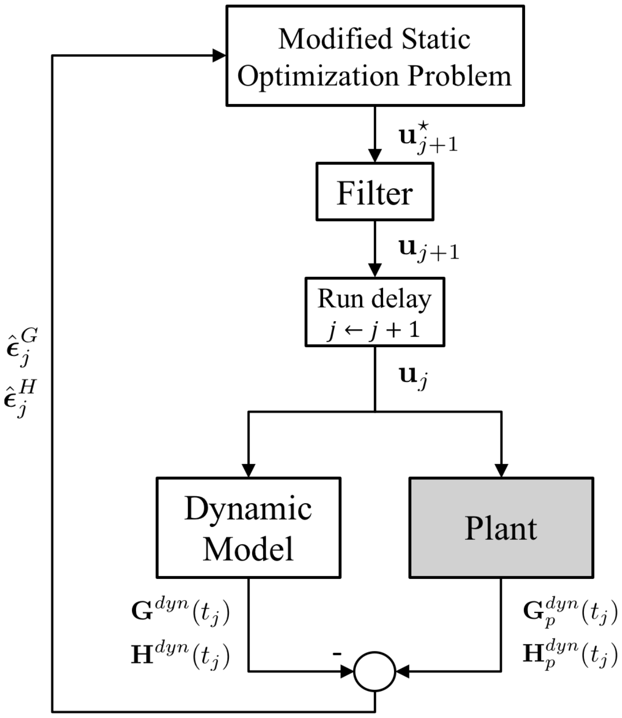
Modified Static Optimization Problem
$\mathbf{u}^{\star}_{j+1}$
Filter
$\mathbf{u}_{j+1}$
Run delay
$j \leftarrow j+1$
$\mathbf{u}_j$
$\hat{\boldsymbol{\epsilon}}^G_j$
$\hat{\boldsymbol{\epsilon}}^H_j$
Dynamic Model
Plant
$\mathbf{G}^{dyn}(t_j)$
$\mathbf{H}^{dyn}(t_j)$
-
$\mathbf{G}^{dyn}_p(t_j)$
$\mathbf{H}^{dyn}_p(t_j)$

Figure 3.2: RTO scheme via CA using transient measurements and a dynamic model.

constraints at the plant optimum, with card($\mathscr{A}$) = n_u. CA ensures that the modified constraints match the plant constraints, that is,

$$G_i(\mathbf{u}^*_p, \bar{\boldsymbol{\theta}}) + \epsilon^{G_i} = 0, \quad i \in \mathscr{A}(\mathbf{u}^*_p) \tag{3.2.8a}$$

$$G_i(\mathbf{u}^*_p, \bar{\boldsymbol{\theta}}) + \epsilon^{G_i} < 0, \quad i \notin \mathscr{A}(\mathbf{u}^*_p), \tag{3.2.8b}$$

where the constraint modifiers ϵ^{G_i} are evaluated at $\mathbf{u}^*_p$. The process model is considered to be adequate for reaching the plant optimum in the CA scheme if there exists $\mu_i \geq 0$ such that

$$\nabla\Phi(\mathbf{u}^*_p, \bar{\boldsymbol{\theta}}) + \sum_i \mu_i \nabla G^a_i(\mathbf{u}^*_p, \bar{\boldsymbol{\theta}}) = \mathbf{0}, \quad i \in \mathscr{A}(\mathbf{u}^*_p), \tag{3.2.9a}$$

where $\mathbf{G}^a$ denotes the active inequality constraints at the plant optimum and μ_i are the corresponding Lagrange multipliers of the CA problem. Note that these conditions ensure that the gradient errors in the cost and constraint functions predicted by the model do not change the set of active constraints.

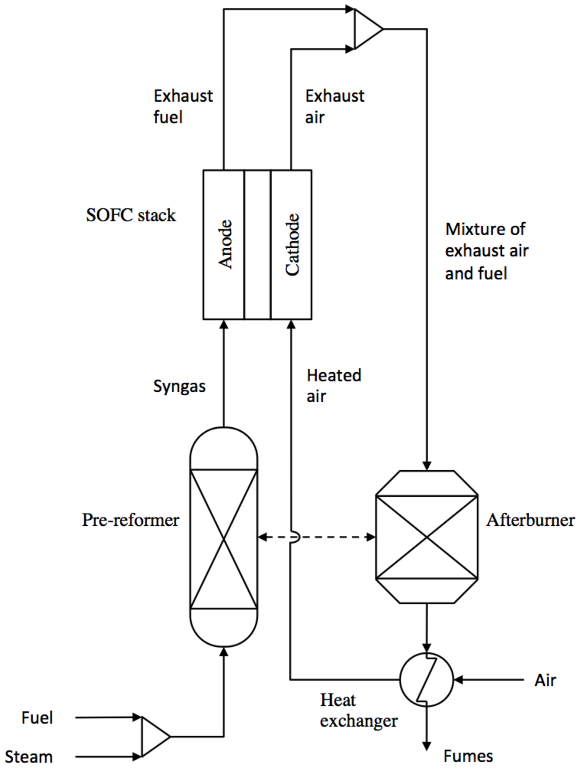
Exhaust fuel
Exhaust air
SOFC stack
Anode
Cathode
Mixture of exhaust air and fuel
Syngas
Heated air
Pre-reformer
Afterburner
Air
Heat exchanger
Fuel
Steam
Fumes

Figure 3.3: SOFC system flowsheet.

3.3 Simulated Example: Solid-Oxide Fuel-Cell System

3.3.1 SOFC System Description

Figure 3.3 depicts the layout of the SOFC model considered. The electric current, and the air and fuel flows are the manipulated variables. It is assumed that the temperature of all streams and the electrical potential of the stack can be measured. The electrical power, the system efficiency, the fuel utilization, and the air-excess ratio are computed based on the manipulated and output variables.

A complete fuel-cell system generally consists of a fuel-cell stack, a pre-reformer, a burner and heat exchangers. The model of this system is described in Section 2.3. The solid lines in Figure 3.3 represent exchange of mass between the SOFC components, whereas the dashed line represents heat transfer. The purpose of the pre-reformer is to convert the available fuel to syngas, which is rich in hydrogen. The syngas in combination with air produces electricity through an electrochemical reaction inside the stack. The unreacted fuel and air are fed to the afterburner, which oxidizes the exhaust fuel. The afterbuner outlet is then used to heat the inlet air stream. This way, costs related to heating are minimized as no external heat source is needed.

3.3.2 Formulation of the Optimization Problem

The optimization of a SOFC system aims at operating at maximal efficiency for any allowed power demand. In addition, the system must operate in a safe way.

The static optimization problem can be written mathematically as follows:

$$\begin{aligned}
\max_{\mathbf{u}} \quad & \eta(\mathbf{u}) = \frac{P_{el}}{q_{CH_4}\ LHV_{CH_4}} \\
\text{s.t.} \quad & P_{el}(\mathbf{u}) = P_{el}^{S}\ [W] \\
& U_{cell}(\mathbf{u}) \geq 0.7\ [V] \\
& \nu(\mathbf{u}) \leq 0.8 \\
& \lambda_{air}(\mathbf{u}) \geq 4 \\
& 0.144 \leq q_{CH_4} \leq 0.422\ [L.min^{-1}] \\
& 15 \leq q_{air} \leq 50\ [L.min^{-1}] \\
& 0 \leq I \leq 50\ [A],
\end{aligned} \tag{3.3.1}$$

where η is the efficiency of the SOFC system, P_{el} represents the power demand, P_{el}^{S} is the setpoint for the power demand, U_{cell} denotes the cell voltage, ν is the fuel utilization, λ_{air} represents the air excess ratio, LHV_{CH_4} is the lower heating value of the fuel, I is the electrical current, and q_{CH_4} and q_{air} denote the fuel and air feedrates, respectively. Three inputs are used to operate this SOFC system, namely, the current, and the fuel and air feedrates, that is, $\mathbf{u} = [I,\ q_{CH_4},\ q_{air}]^{\mathrm{T}}$.

To avoid any damage due to fuel starvation and re-oxidation of the anode, a conservative bound of 0.8 (80%) is set on the fuel utilization. Additionally, a lower bound of 0.7 V is set to protect the stack from accelerated degradation. Moreover, to prevent the system from steep thermal gradients, we enforce the air-excess ratio to be larger than 4. Also, a lower bound of 0.144 L/min is set on the fuel feedrate, and an upper bound of 50 A is placed on the current to avoid excessive heating. Finally, an equality constraint is set in order to meet the power demand.

The optimization problem (3.3.1) can be cast into the generic NLP formulation given in (2.2.2). To have this generic formulation, one defines the scalar cost function Φ and the constraints H and $\mathbf{G}$ as follows:

$$\Phi = -\eta, \tag{3.3.2}$$

$$H = P_{el} - P_{el}^{S}, \tag{3.3.3}$$

Table 3.1: Parameters that differ between the *plant* and the *model*

Parameter	Plant	Model
$E_{act,cath}$ $[J.mol^{-1}]$	153260.5	150000.0
k_0 $[\Omega^{-1}.m^{-2}]$	4.103096×10^{11}	4.5×10^{11}
$E_{diss,cath}$ $[J.mol^{-1}]$	1.543785	1.54
R_0 $[\Omega.m^2]$	9.225228×10^{-14}	10×10^{-14}

$$\mathbf{G} = \begin{bmatrix} 0.7 - U_{cell} \\ v - 0.8 \\ 4 - \lambda_{air} \end{bmatrix}. \tag{3.3.4}$$

3.3.3 Simulation Results

This section describes the application of CA to the dynamic SOFC model described in Subsection 2.3. In order to investigate the effect of plant-model mismatch, we consider as *Plant* a model with a specific set of parameters and as *Model* a model with a different set of parameters. Both sets of parameters are given in Table 3.1.

We solve Problem (3.3.1) using both the CA approach using steady-state measurements, described in Subsection 2.2.1, and the CA approach using transient measurements and a dynamic model described in Subsection 3.2.1. The static model used for CA corresponds to the dynamic model of Subsection 2.3 with all time derivatives set to zero.

To evaluate the performance of the two algorithms, the setpoint of the electrical power P_{el}^S is changed every 2.5 h. The electrical power profile applied is the following:

$$P_{el}^S(t) = \begin{cases} 100\ [W], & \text{t} \leq 2.5\text{ h} \\ 120\ [W], & 2.5\text{ h} < \text{t} \leq 5\text{ h} \\ 100\ [W], & \text{t} > 5\text{ h}. \end{cases} \tag{3.3.5}$$

Here, the filter matrix $\mathbf{K}$ is a diagonal matrix defined as $\mathbf{K} = K_f\,\mathbf{I}$, where K_f is a scalar, and $\mathbf{I} \in \mathbb{R}^{n_u \times n_u}$ is the identity matrix. The following simulations are performed to investigate the effects of the filter gain, the RTO period, and measurement noise:

- **Simulation 1:** *CA_ss, $K_f = 0.6$, no noise.*
- **Simulation 2:** *CA_dyn, $K_f = 0.6$, $\tau_{RTO} = 10$ min, no noise.*
- **Simulation 3:** *CA_dyn, $K_f = 0.6$, $\tau_{RTO} = 3$ min, no noise.*
- **Simulation 4:** *CA_dyn, $K_f = 0.3$, $\tau_{RTO} = 10$ min, no noise.*

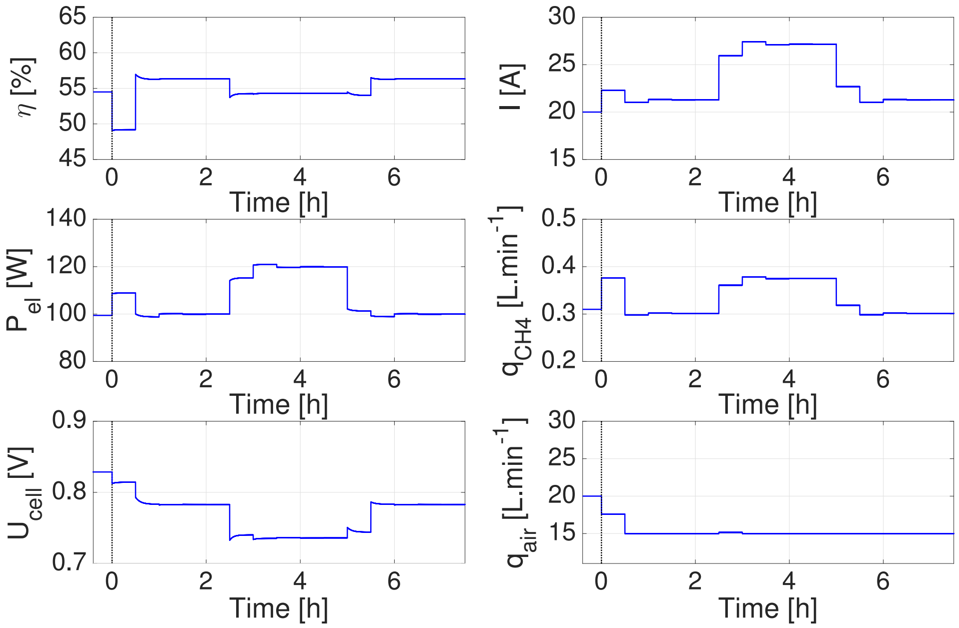

Figure 3.4: *Simulation 1:* Efficiency, current, electrical power, methane flowrate, cell voltage, and air flowrate vs. time.

- **Simulation 5:** *CA_dyn, K_f = 0.6, τ_{RTO} = 3 min, measurement noise.*

CA using Steady-State Measurements

We apply CA_ss as per Section 2.2.1 and Figure 2.1. The plant is initially at steady state at some conservative operating point. The plant and the model are subjected to the same inputs, and the corresponding outputs are used to compute the modifiers according to (2.2.3). The inputs for the next RTO period are computed by solving the modified RTO Problem (2.2.4). These optimal inputs are filtered as per (2.2.5) with $K_f = 0.6$ and then fed to the plant and the model. This procedure is repeated every 30 min until convergence. The performance of CA_ss is described next.

Simulation 1, CA_ss, K_f = 0.6, no noise: Figures 3.4 and 3.5 show the performance of CA_ss. The plant converges to plant optimality in a single iteration (30 min), either from a conservative initial point or following a step change in electric power.

CA using Transient Measurements and a Dynamic Model

We apply next CA_dyn as per Section 3.2.1 and Figure 3.2. We investigate the effects of both the RTO period (τ_{RTO} = 3 and 10 min) and the amount of filtering (K_f = 0.3 and 0.6). The

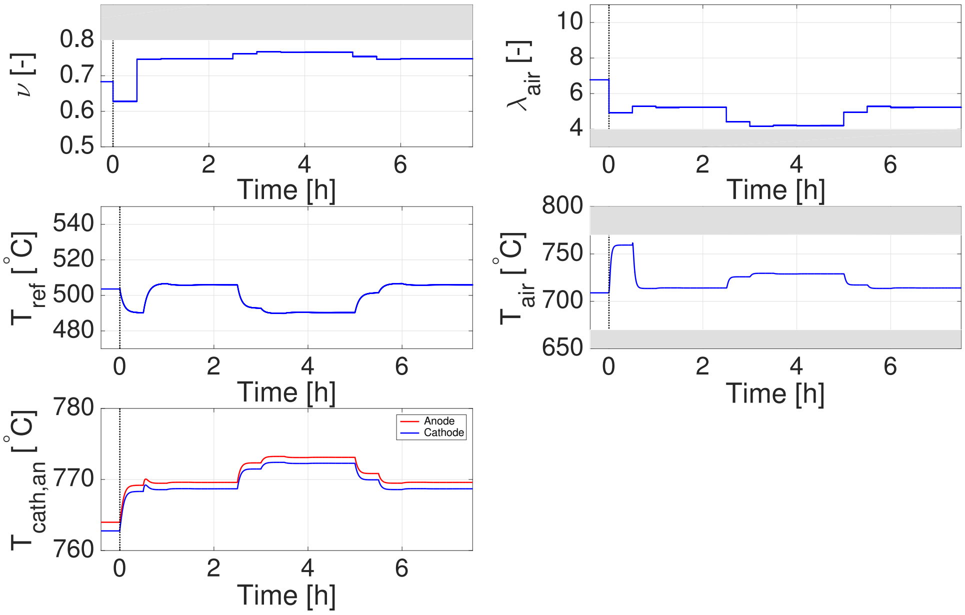

Figure 3.5: *Simulation 1*: Fuel utilization, air excess ratio, pre-reformer temperature, inlet air temperature, cathode and anode temperatures vs. time.

measurements are taken during the transient phase as the SOFC system does not reach steady state for any of the investigated cases.

The plant is initially at steady state at a conservative operating point. The plant and the model are subjected to the same inputs, the dynamic SOFC model is integrated, and the corresponding outputs are used to compute the modifiers according to (3.2.7). The inputs for the next RTO period are computed by solving the modified RTO Problem (3.2.1). These optimal inputs are filtered as per (3.2.3) and then fed to the plant and the model. This procedure is repeated every τ_{RTO} min until convergence. The effects of the RTO period, the amount of filtering, an the noise measurement on the performance of CA_dyn are described next.

Effect of RTO Period

Simulation 2, CA_dyn, K_f = 0.6, τ_{RTO} = 10 min, no noise: Figures 3.6 and 3.7 depict the performance of CA_dyn with a RTO period of 10 min. The plant takes 1 to 2 iterations (10 to 20 min) to converge to a new steady state, which is considerably faster than in *Simulation 1*.

Simulation 3, CA_trans_dyn, K_f = 0.6, τ_{RTO} = 3 min, no noise: Figures 3.8 and 3.9 show the performance of CA_dyn with a RTO period of 3 min. The plant also takes 1 to 2 iterations (3 to 6 min) to converge to a new steady state. The convergence speed is increased significantly compared to *Simulations 1* and *2*. One can see that, by reducing the RTO period, the plant

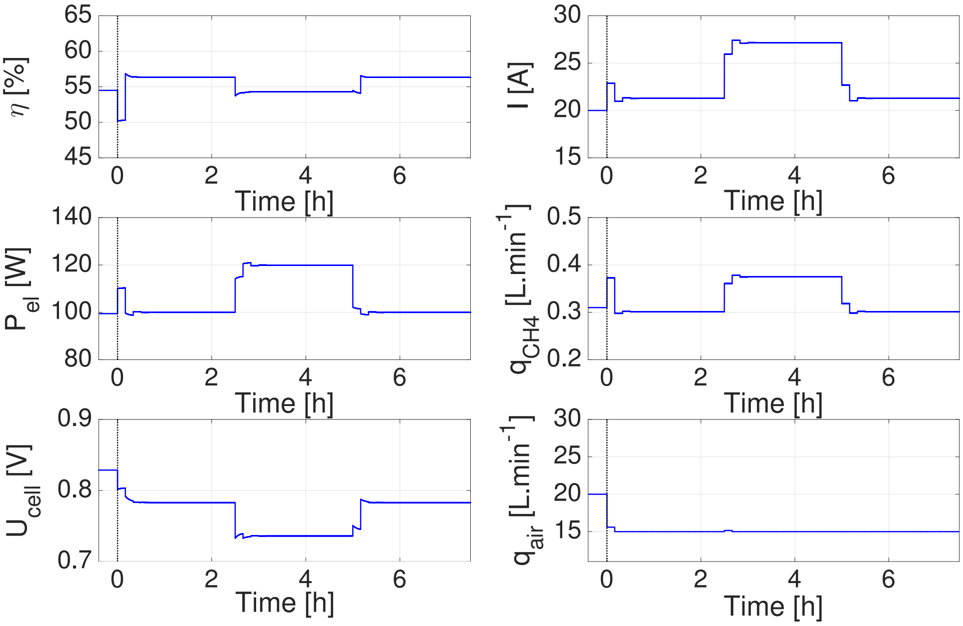

Figure 3.6: *Simulation 2*: Efficiency, current, electrical power, methane flowrate, cell voltage, and air flowrate vs. time.

reaches optimality faster.

Effect of Filtering

Simulation 4, CA_dyn, K_f = 0.3, τ_{RTO} = 10 min, no noise: Figures 3.10 and 3.11 show the performance of CA_dyn for a larger amount of filtering (K_f=0.3). The plant reaches optimality in a single iteration (10 min). One can see that the filter gain does not play an important role for CA_dyn. We have also verified that, for smaller RTO periods, the same behavior is observed.

Effect of Noise

Simulation 5, CA_dyn, K_f = 0.6, τ_{RTO} = 3 min, measurement noise: Figures 3.12 and 3.13 depict the performance of CA_dyn for noisy measurements. We assume that the cell voltage as well as all measured temperatures are subjected to noise with zero mean and standard deviations $\sigma_{U_{cell}} = 0.0025$ and $\sigma_T = 0.125$, respectively. Note that the efficiency η and the electrical power P_{el} are functions of the cell voltage. Hence, these output variables are also subjected to noise. Despite the noise introduced in the measurements, the plant shows similar performance to noise-free simulations and reaches optimality in a single iteration (3 min).

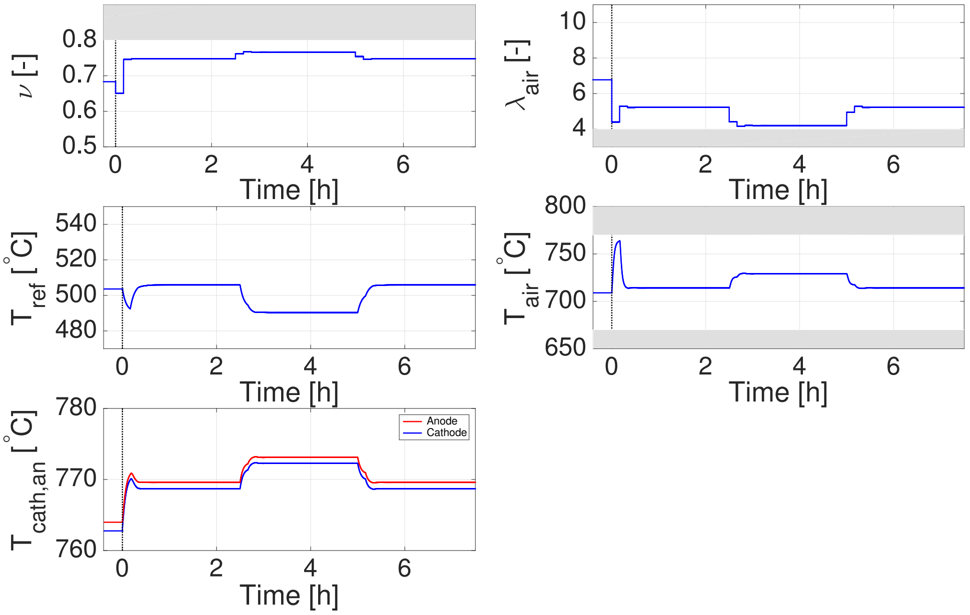

Figure 3.7: *Simulation 2*: Fuel utilization, air excess ratio, pre-reformer temperature, inlet air temperature, cathode and anode temperatures vs. time.

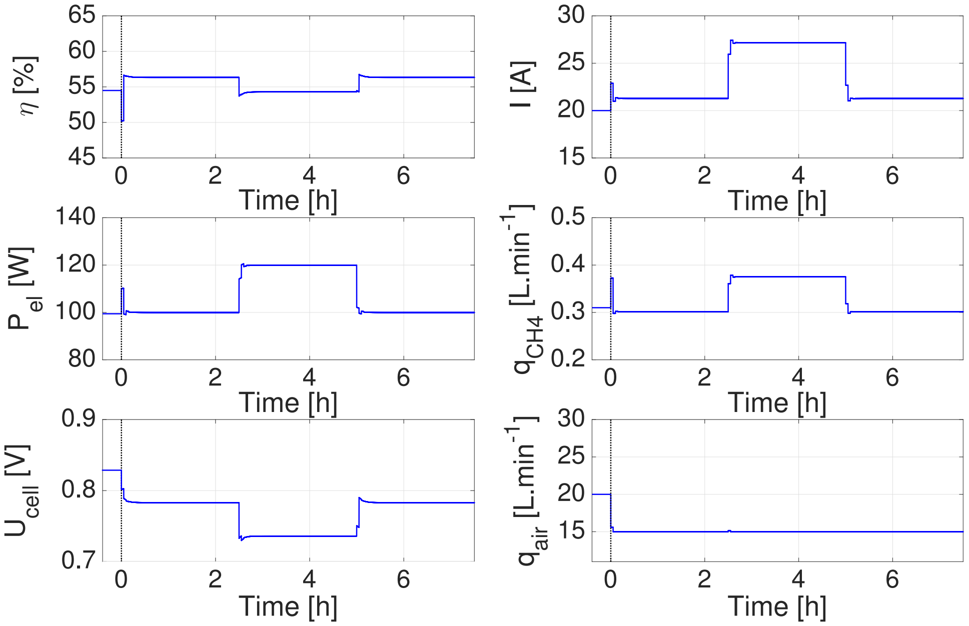

Figure 3.8: *Simulation 3*: Efficiency, current, electrical power, methane flowrate, cell voltage, and air flowrate vs. time.

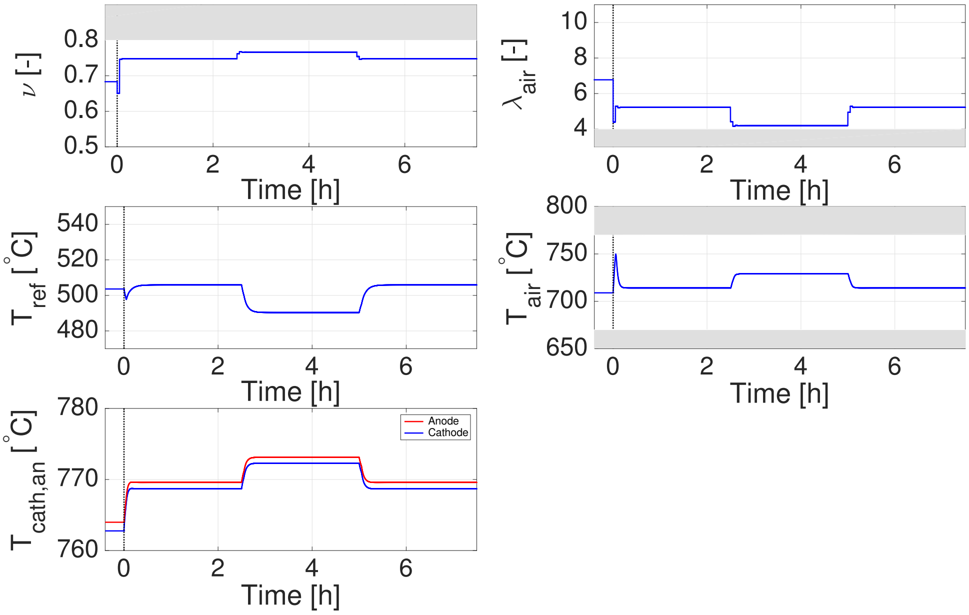

Figure 3.9: *Simulation 3*: Fuel utilization, air excess ratio, pre-reformer temperature, inlet air temperature, cathode and anode temperatures vs. time.

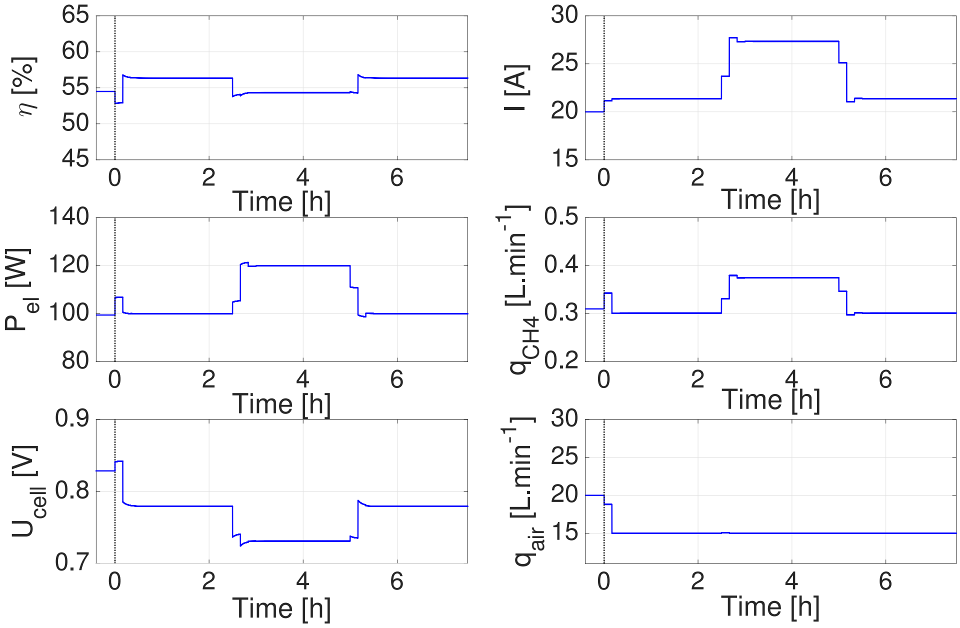

Figure 3.10: *Simulation 4*: Efficiency, current, electrical power, methane flowrate, cell voltage, and air flowrate vs. time.

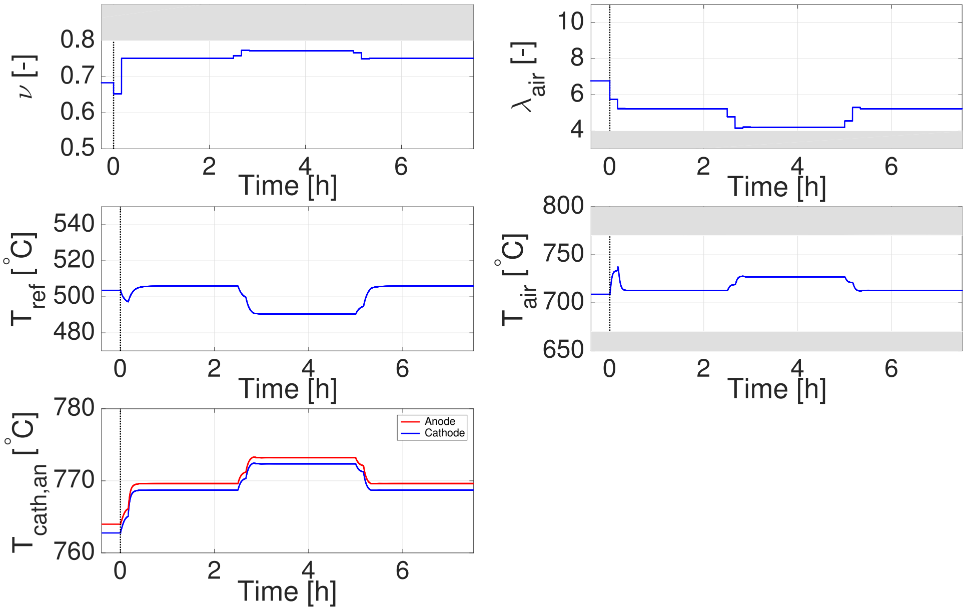

Figure 3.11: *Simulation 4*: Fuel utilization, air excess ratio, pre-reformer temperature, inlet air temperature, cathode and anode temperatures vs. time.

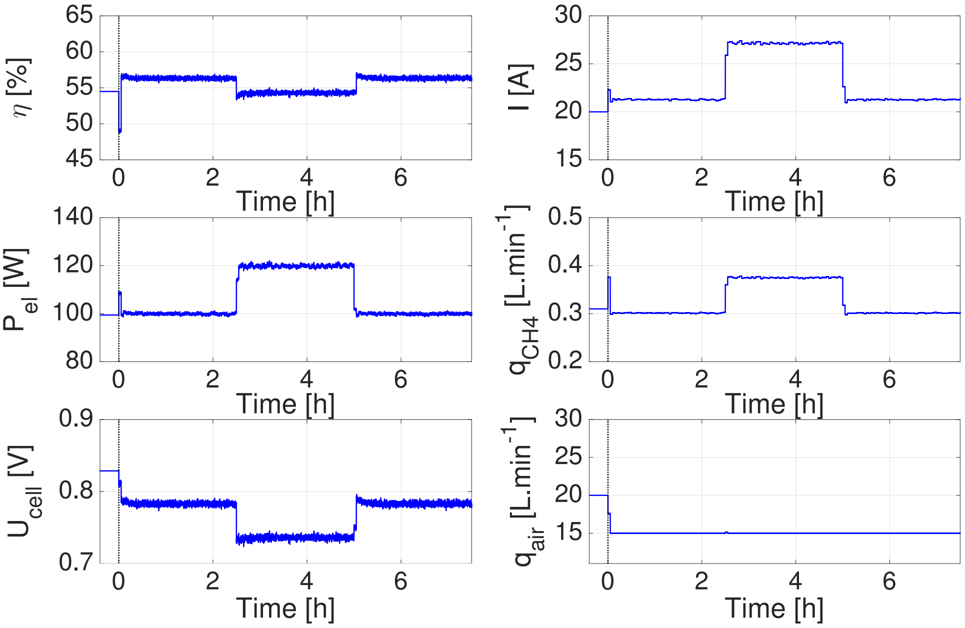

Figure 3.12: *Simulation 5*: Efficiency, current, electrical power, methane flowrate, cell voltage, and air flowrate vs. time.

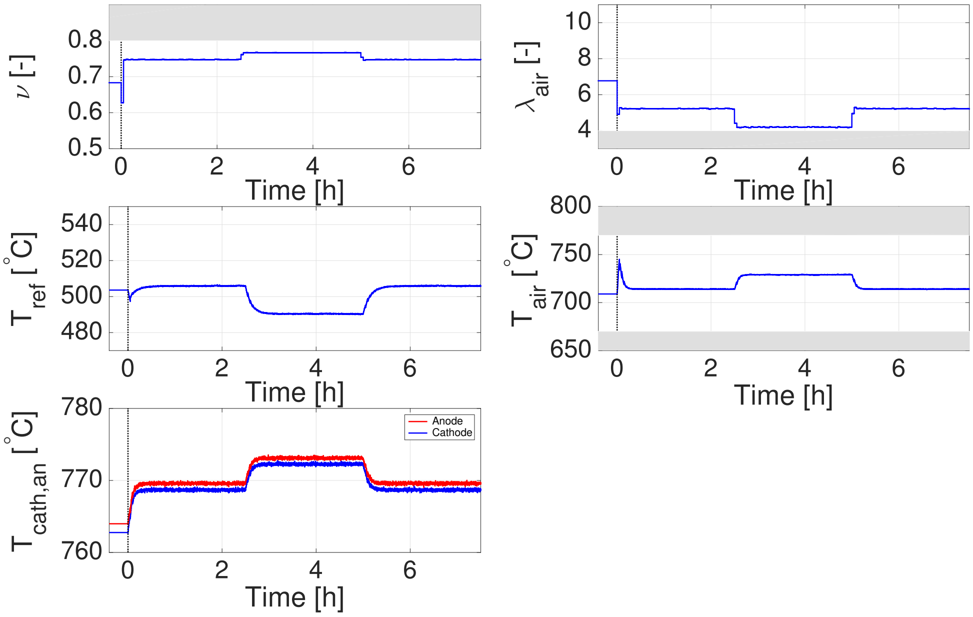

Figure 3.13: *Simulation 5*: Fuel utilization, air excess ratio, pre-reformer temperature, inlet air temperature, cathode and anode temperatures vs. time.

3.4 Conclusions

This chapter has described a RTO methodology that enables faster convergence to plant optimality. The approach has been illustrated by means of the real-time optimization of a small scale SOFC system. The proposed approach is based on constraint adaptation that uses either steady-state measurements or transient measurements together with a dynamic model.

The improvement consists in processing these transient measurements through dynamic models, thereby improving the estimation of plant constraints at steady state. This way, static CA can be implemented during transient operation, with the objective of reaching optimality in a single transition to steady state. In a way, this is similar to what is done with *implicit* RTO methods, such as extremum-seeking control [26], self-optimizing control [66] and NCO-tracking [20]. However, CA that uses transient information has the advantage of being an *explicit* RTO method, which repeatedly solves the optimization problem and is therefore able to deal with changing active constraints.

The use of a dynamic model to process transient measurements is key for implementing a high-frequency RTO scheme, thereby leading to fast convergence. In addition, the use of a dynamic model significantly reduces the adverse effect of having different time scales in the plant. Finally, we showed that the use of CA with small RTO periods does not only act as an optimizer but, in this case, also as a controller.

4 Real-Time Optimization of a Small-Scale Experimental SOFC System

This chapter discusses the experimental implementation of the fast RTO approach proposed in Chapter 3 to a small-scale experimental SOFC system. It is based on the following publication [8].

T. de Avila Ferreira, Z. Wuillemin, A. G. Marchetti, C. Salzmann, J. Van Herle, and D. Bonvin. Real-time optimization of an experimental SOFC system. *J. Power Sources*, *Submitted*, 2018.

4.1 Introduction

To the best of the author's knowledge, as recently as 2012, no experimental results regarding real-time optimization of solid-oxide fuel-cell systems had been reported. Hence, as part of a collaborative project between Group of Energy Materials – EPFL, Automatic Control Laboratory – EPFL and SOLIDpower SA, we decided to validate experimentally the RTO methodology presented in Chapter 3. For this reason, we built an interface that would allow exchanging data between the optimization algorithm implemented in MATLAB and the SOFC system controlled via LabVIEW. The SOFC system was located at EPFL Valais in Sion, Switzerland. All experiments were performed remotely from EPFL Lausanne, Switzerland. The results are presented in this chapter.

The only experimental work regarding the operational optimization of an SOFC system is reported in [80]. However, as mentioned previously, this experiment lacks answering the following questions: (i) Can RTO speed up systems that have multiple time scales? (ii) In the context of fast RTO, what is the influence of tuning parameters such as the RTO period? With the objective of bridging the large gap between simulation work and experimental applications in the context of control and optimization of SOFC systems, this chapter presents RTO experiments of a SOFC system with the aim of answering the aforementioned questions.

The chapter is structured as follows: Section 4.2 describes the experimental setup, namely, hardware and software. Section 4.3 describes the experimental implementation of fast RTO, where the effect of the RTO period and the use of a dynamic model is analyzed. Section 4.4

concludes the chapter. It is worth mentioning that all figures in this chapter show experimental data.

4.2 SOFC System

4.2.1 Physical System

The available experimental system includes a pre-reformer, a stack, as well as two electrical heaters used to heat up the air inlet stream and the pre-reformer.

The SOFC stack used in this study is a short-stack developed by SOLIDpower. It consists of six planar anode-supported cells with an active area of 80 cm^2, pressed between gas-diffusion layers and metallic interconnector plates. The anodes are made of standard nickel/yttrium-stabilized-zirconia (Ni-YSZ) cermet, and the thin electrolyte is made of dense YSZ and a CGO (ceria-gadolinia) barrier layer. The cathodes consist of screen-printed $(\text{La, Sr})(\text{Co, Fe})\text{O}_3$, which allows operating at temperatures between 650°C and 850°C. The stack is placed in a high-temperature furnace at 750°C and is connected to a testing station that provides controlled flowrates of air and pre-heated fuel. Additionally, an active load is used to set the delivered current. The syngas coming from the pre-reformer enters the anode chamber at about 450°C. The heated air enters the cathode chamber at about 700°C. The pre-reformer is fed with natural gas and steam at about 400°C. Several options are available for fuel processing. In this study, the fuel is reformed partially in the pre-reformer, with the remaining part of the fuel being reformed in the stack so as to keep the temperature within the operating range. The pre-reformer is a shell-and-tube reactor, whose model is described in [83]. The water pump, fuel, and air blowers, as well as the pre-reformer and air heaters are electrically driven. The control of the testing station is ensured by a LabVIEW interface.

Figure 4.1 represents the available SOFC system. The electric current, the air and fuel flows, as well as the pre-reformer and air electrical heater temperatures are the manipulated variables. These variables are controlled by a PI controller. The temperature of all streams and the electrical potential of the stack are the measured outputs of this system. The electrical power, system efficiency, fuel utilization, and air-excess ratio are computed based on the manipulated and output variables.

A complete fuel-cell system generally consists of a fuel-cell stack, a pre-reformer, an after-burner heat exchangers. In this work, we propose to combine the aforementioned available SOFC system with mathematical models of the afterburner and heat exchangers. This results in an *SOFC system* that combines hardware and software parts. This specific manner of operating a system is named 'hardware-in-the-loop' operation. Figure 4.2 depicts the layout of the experimental SOFC system. The available and virtual parts of the SOFC system are highlighted by dotted lines. The solid arrows represent mass flows, whereas the dashed arrows represent signals.

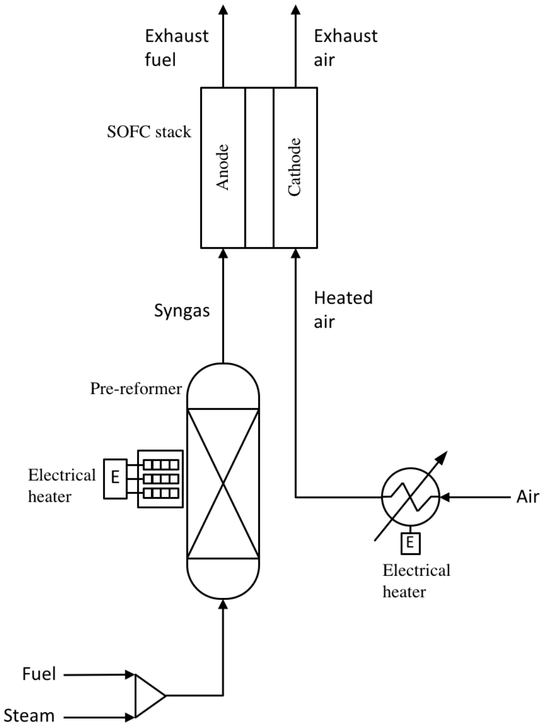

Figure 4.1: Available SOFC system flowsheet.

4.2.2 Software

The available SOFC system is controlled via LabVIEW, while the dynamic SOFC model is implemented in MATLAB. Hence, we developed an interface in LabView and implemented the data communication as proposed in [85]. The cathode and anode temperatures are read from the available SOFC system and sent to the model, where they are used as initial conditions for the afterburner dynamic model. This model also needs to know the composition of the anode and cathode streams. However, since there is no sensor to measure gas compositions, the compositions inside the stack are estimated using the fuel-cell model. The computed afterburner temperature is sent to the virtual heat exchanger (dynamic heat-exchanger model) that computes the temperature of the air stream. This temperature is used as setpoint (Setpoint 2) for the available electrical heater. The afterburner temperature is also sent to a pre-reformer dynamic model to compute its expected reformer temperature. This computed temperature is then sent as setpoint (Setpoint 1) to the electrical heater that heats up the available pre-reformer. In other words, the pre-reformer and air heat exchanger temperatures are determined by the virtual system (dynamic models) connected to the available SOFC system. Hence, although these temperatures are manipulated variables, they cannot serve as decision variables in the optimization problem. The sampling time used to perform the communication between software and hardware is 5 s. Figure 4.3 shows a simplification of structure to establish an interface between the RTO algorithm and the SOFC hardware.

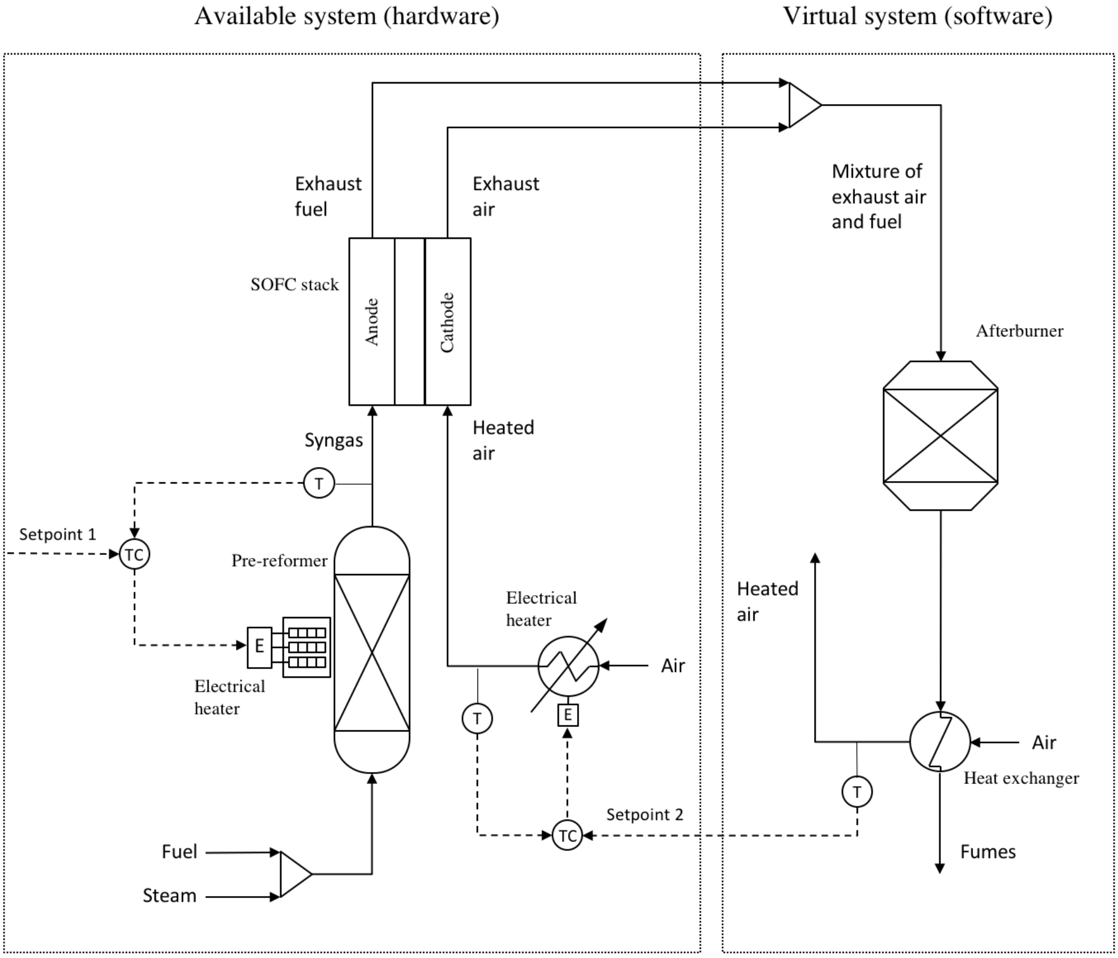
Available system (hardware)
Virtual system (software)
Exhaust fuel
Exhaust air
Mixture of exhaust air and fuel
SOFC stack
Anode
Cathode
Afterburner
Syngas
Heated air
T
Setpoint 1
TC
Pre-reformer
Electrical heater
E
Electrical heater
Air
E
T
Heated air
Air
T
Heat exchanger
Setpoint 2
TC
Fumes
Fuel
Steam

Figure 4.2: Tested SOFC system flowsheet.

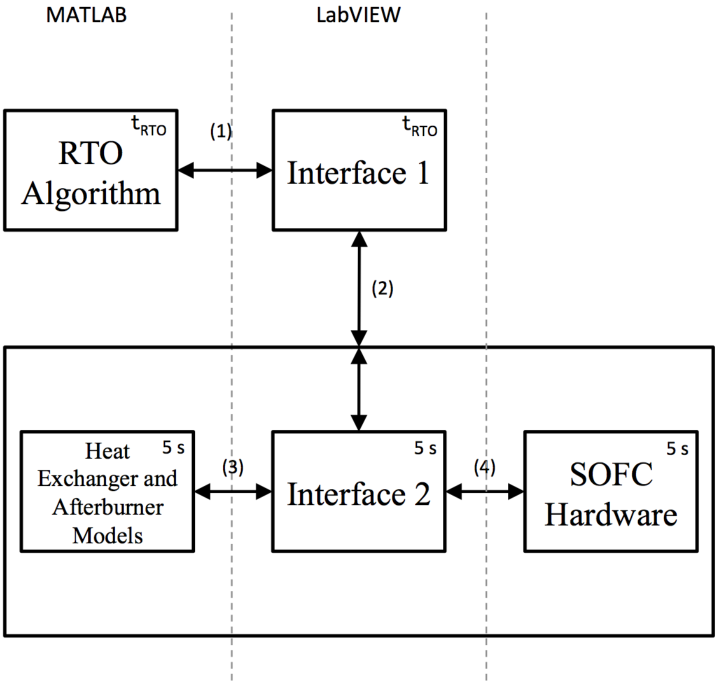
MATLAB
LabVIEW
RTO Algorithm
t_{RTO}
(1)
Interface 1
t_{RTO}
(2)
Heat Exchanger and Afterburner Models
5 s
(3)
Interface 2
5 s
(4)
SOFC Hardware
5 s

Figure 4.3: Interface structure of the system optimization. Each box corresponds to a process, whose execution period is specified in the upper-hand corner. The largest rectangle comprises the inner-loop (loop performed in a higher frequency) blocks, while the *RTO* and the *Interface 1* blocks correspond to the outer-loop (loop performed in a lower frequency) blocks. Each arrow correspond to data exchange between processes: (1) RTO inputs and constraint measurements; (2) RTO inputs and constraint measurements, communication between inner- and outer-loops; (3) electrical heater setpoints and measurements; (4) all system temperature and cell voltage measurements, and inputs.

- **RTO:** This block runs in MATLAB and provides the optimal inputs computed by the selected RTO method to the *Interface 1* block. It also acquires constraint measurements that are used to compute the zeroth-order modifiers. The frequency at which this block is executed depends on the chosen RTO period. However, the execution frequency of this block is always lower than the inner-loop blocks.
- **Interface 1:** This block is implemented in LabVIEW and is used to verify the inputs provided by the RTO algorithm. A warning window pops up every τ_{RTO} min with the input values to be applied to the system and the user must '*comply*' in order for the data to be sent to the next block. *Interface 1* is important as it allows modifying the inputs in case MATLAB crashes or RTO provides unreasonable values.
- **Heat Exchanger and Afterburner Models:** This block contains the models of the heat exchanger and the afterburner described in Section 2.3. The measured temperature of the air heated by the electrical heater is sent to this block via *Interface 2* and used as initial conditions for the model. The model is integrated every 5 s in order to compute the heat exchanger and afterburner temperature predictions. These temperatures are then sent back to the *Interface 2* block.
- **Interface 2:** This block corresponds to the communication between the inner and outer loops. It acquires and sends verified RTO optimal inputs and constraint measurements. This procedure is performed according to the specified RTO period. In addition, this block is the bridge between the *Heat Exchanger and Afterburner Models* block and the *SOFC Hardware* block. The communication between these two blocks happens every 5 s. The heat exchanger and afterburner temperature predictions are input to the SOFC hardware as setpoints to the PI controllers of the heat exchanger temperatures. Then, after 5 s the heat exchanger temperatures are once again sent to *Interface 2* .

4.3 Real-Time Optimization of the SOFC System

4.3.1 Dynamic Model

Each component of the model utilized for the RTO scheme is described in Section 2.3. Note that two different models are used: (1) the heat exchanger and afterburner models for the 'hardware-in-the-loop' operation, and (2) the model of the entire system used in the RTO scheme. Here, we refer to the latter. Figure 3.3 depicts the flowsheet of the model utilized for the optimization.

4.3.2 Experimental Results

This section describes the implementation of steady-state constraint-adaptation (CA_ss) and constraint adaptation using transient measurements and a dynamic model (CA_dyn) to the experimental SOFC system. The methods are presented in Section 2.2.1 and Section 3.2.2, respectively. The problem formulation is described in Section 3.3.2. The following experiments are performed:

- **Experiment 1:** *CA_ss,* K_f *= 0.6.*
- **Experiment 2:** *CA_dyn,* K_f *= 0.6 and* τ_{RTO} *= 10 min.*
- **Experiment 3:** *CA_dyn,* K_f *= 0.6 and* τ_{RTO} *= 3 min.*

As indicated by the simulation results obtained in the previous chapter, the filter gain does not significantly affect the convergence speed of CA_dyn. Hence, we will only analyze the effect of the RTO period.

The SOFC system is initially at steady state with an electric power of 100 W and an efficiency of about 55%. We will first try to maximize the efficiency at that power demand and then follow the electrical power setpoint profile given in (3.3.5).

As seen in Figures 4.4 to 4.10, the measurements and the quantities computed from these measurements can be noisy. Hence, we average the last minute of acquired data to compute mean values. The blue and red lines in these figures represent the measurements after applying a moving-average filter offline [86].

CA using Steady-State Measurements

We apply CA_ss according to Section 2.2.1 and Figure 2.1. The plant is initially at steady state with an electric power of 100 W. The plant and the model are subjected to the same inputs, and the corresponding outputs are used to compute the modifiers according to (2.2.3). The inputs for the next RTO period are computed by solving the modified RTO Problem (2.2.4). These optimal inputs are filtered as per (2.2.5) with $K_f = 0.6$ and then fed to the plant and the model. This procedure is repeated every 30 min until convergence. The performance of CA_ss applied to the experimental SOFC system is described next.

Experiment 1, CA_ss, K_f = 0.6: Figures 4.4 and 4.5 show the performance of CA_ss. Initially, the plant takes 3 to 4 iterations (90 to 120 min) to converge to the plant optimum, thereby increasing efficiency from 55% to about 62% for the same power demand. Then, a single iteration (30 min) is sufficient to converge to a new steady state following a step change in power demand.

CA using Transient Measurements and a Dynamic Model

We apply next CA_dyn as per Section 3.2.1 and Figure 3.2. We perform two experiments with RTO periods of 3 and 10 min, respectively. The measurements are taken during the transient phase as the experimental SOFC system does not reach steady state for any of the investigated cases.

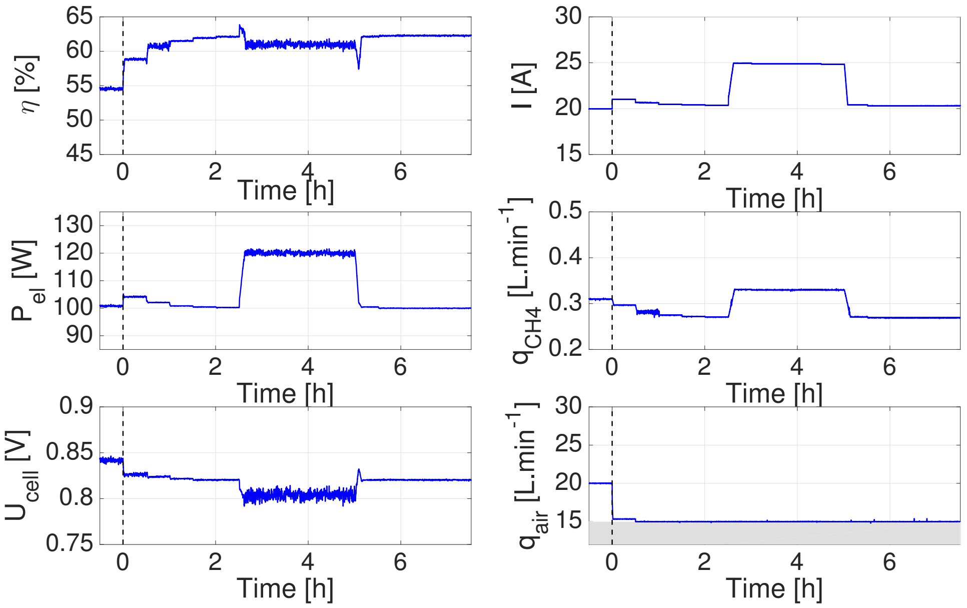

Figure 4.4: *Experiment 1*: Efficiency, current, electrical power, methane flowrate, cell voltage, and air flowrate vs. time.

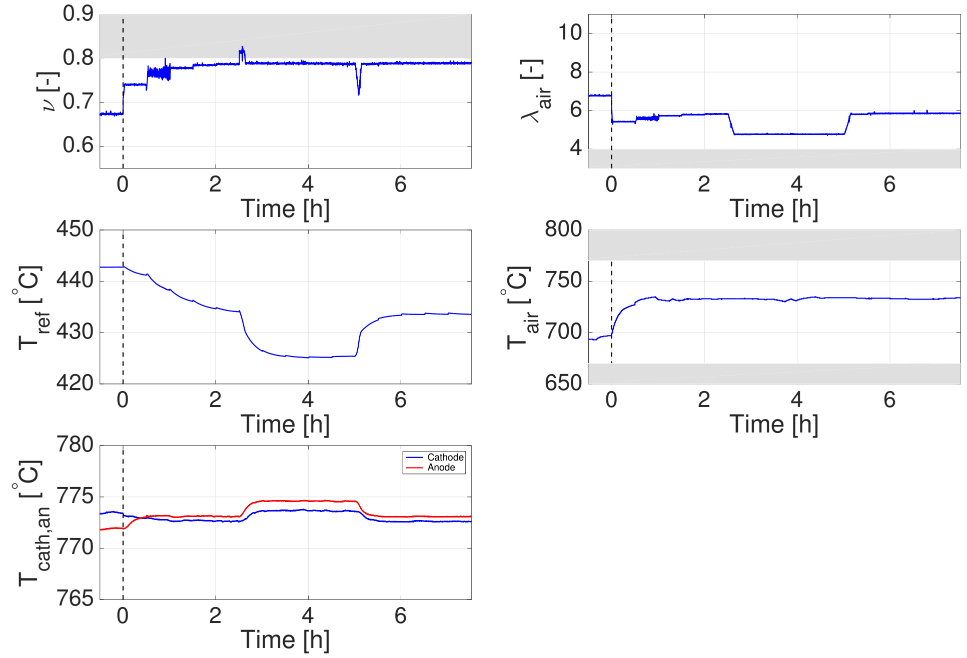

Figure 4.5: *Experiment 1*: Fuel utilization, air excess ratio, pre-reformer temperature, inlet air temperature, cathode and anode temperatures vs. time.

The plant is initially at steady state with an electric power of 100 W. The plant and the model are subjected to the same inputs, the dynamic SOFC model is integrated, and the corresponding outputs are used to compute the modifiers according to (3.2.7). The inputs for the next RTO period are computed by solving the modified RTO Problem (3.2.1). These optimal inputs are filtered as per (3.2.3) with $K_f = 0.6$ and then fed to the plant and the model. This procedure is repeated every 3 or 10 min until convergence. The effect of the RTO period on the performance of CA_dyn is described next.

Effect of RTO Period

Experiment 2, CA_dyn, K_f = 0.6 and τ_{RTO} = 10 min: Figures 4.6 and 4.7 show the performance of CA_dyn with a RTO period of 10 min. Initially, the plant takes 4 to 5 iterations (40 to 50 min) to converge to the plant optimum, which is considerably faster than in *Experiment 1*. Then, a single iteration (10 min) is sufficient to converge to a new steady state following a step change in power demand.

There are spikes on the efficiency, cell voltage, and fuel utilization when the power setpoint is changed. This is due to the fact that the inputs are updated at different rates. Indeed, the rates of change of the inputs are set by the operator, with the rate of change of the current being larger than that of the methane flowrate. Hence, spikes are seen on the fuel utilization plot as it is a function of the inputs only. The cell voltage and the efficiency are affected as well since they are functions of the fuel utilization.

Experiment 3, CA_dyn, K_f = 0.6 and τ_{RTO} = 3 min: Figures 4.8 and 4.9 show the performance of CA_dyn with a RTO period of 3 min. Initially, the plant takes 6 to 7 iterations (18 to 21 min) to converge to the plant optimum, which is considerably faster than in *Experiments 1* and *2*. Then, the plant takes only 1 to 2 iterations (3 to 6 min) to converge to a new steady state following a step change in power demand.

As in *Experiment 2*, one can see spikes on the efficiency, cell voltage, and fuel utilization when the power setpoint is changed for the reasons explained previously. One also sees a spike after 2.5 h when the electric power is set to 120 W, which can be explain by the "sudden" input change with this small RTO period. This behavior could be avoided by increasing the amount of input filtering (lower K_f).

Figure 4.10 compares the performance (in terms of efficiency and electric power) of CA_ss with τ_{RTO} = 30 min and CA_dyn with τ_{RTO} = 3 min. One clearly sees a major improvement in response speed through the use of CA_dyn. Table 4.1 lists the settling times necessary to reach the power setpoint, more specifically the interval of ±2% around the setpoint.

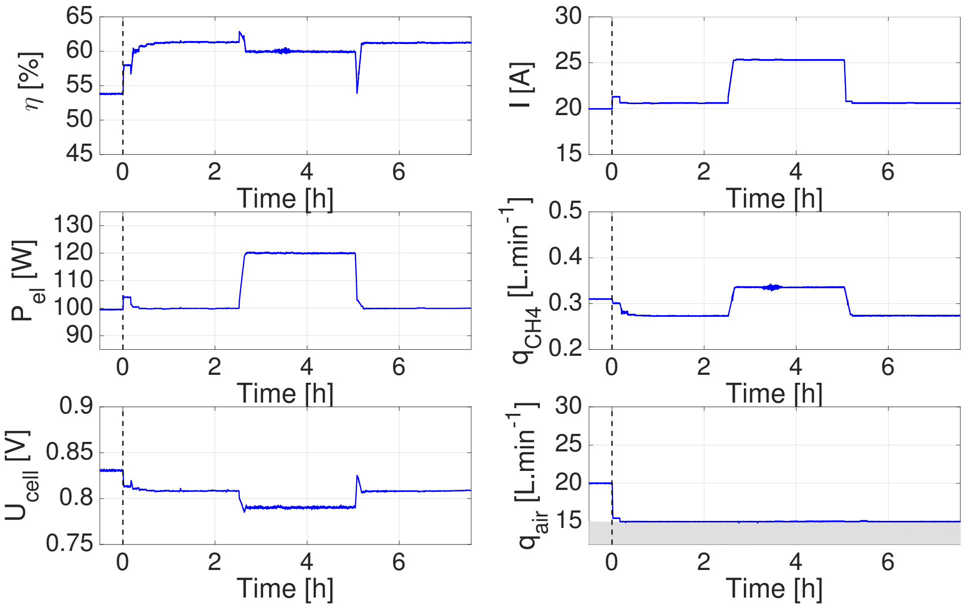

Figure 4.6: *Experiment 2*: Efficiency, current, electrical power, methane flowrate, cell voltage, and air flowrate vs. time.

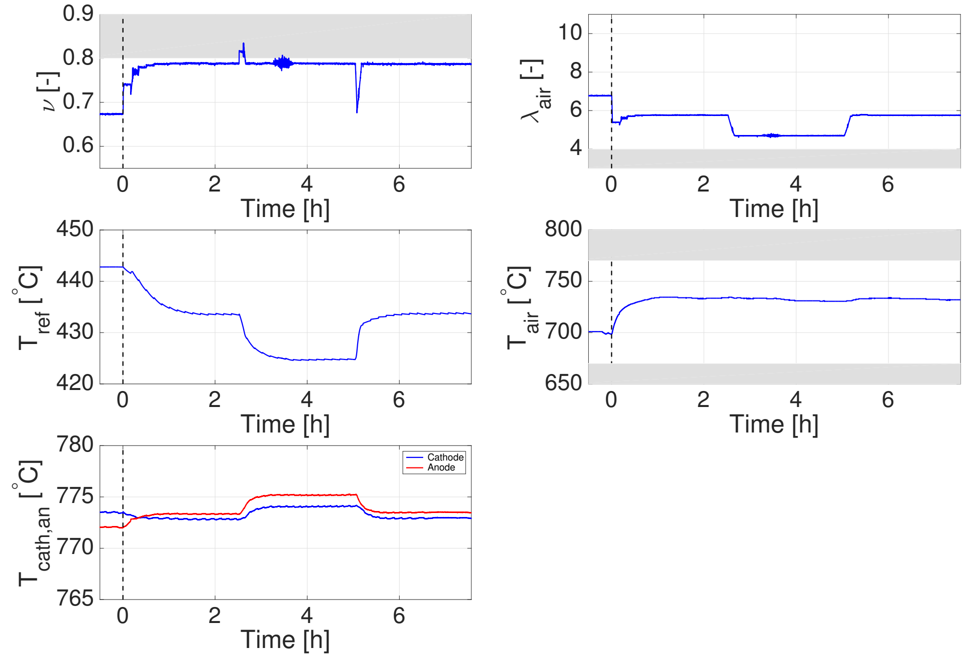

Figure 4.7: *Experiment 2*: Fuel utilization, air excess ratio, pre-reformer temperature, inlet air temperature, cathode and anode temperatures vs. time.

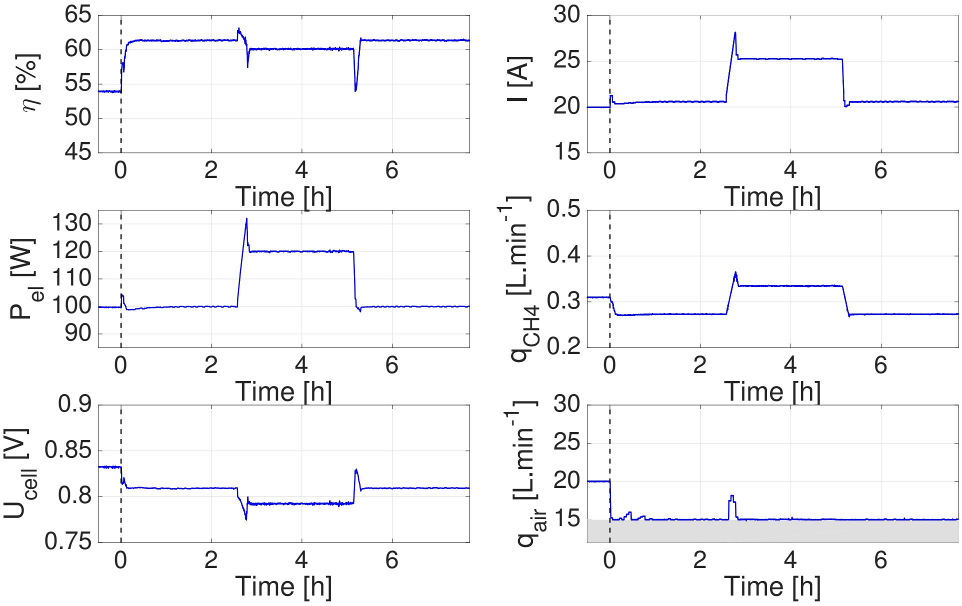

Figure 4.8: *Experiment 3*: Efficiency, current, electrical power, methane flowrate, cell voltage, and air flowrate vs. time.

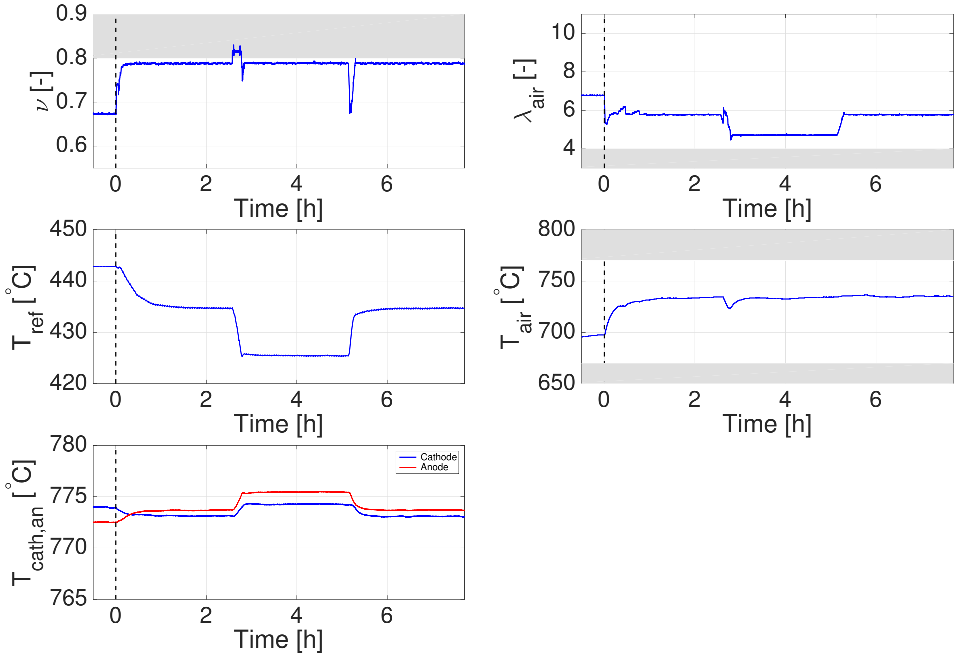

Figure 4.9: *Experiment 3*: Fuel utilization, air excess ratio, pre-reformer temperature, inlet air temperature, cathode and anode temperatures vs. time.

Table 4.1: Settling time to reach the power setpoint (±2%).

Experiment	Method	τ_{RTO} (min)	Settling time (min)
1	CA_ss	30	30-120
2	CA_dyn	10	10-50
3	CA_dyn	3	3-21

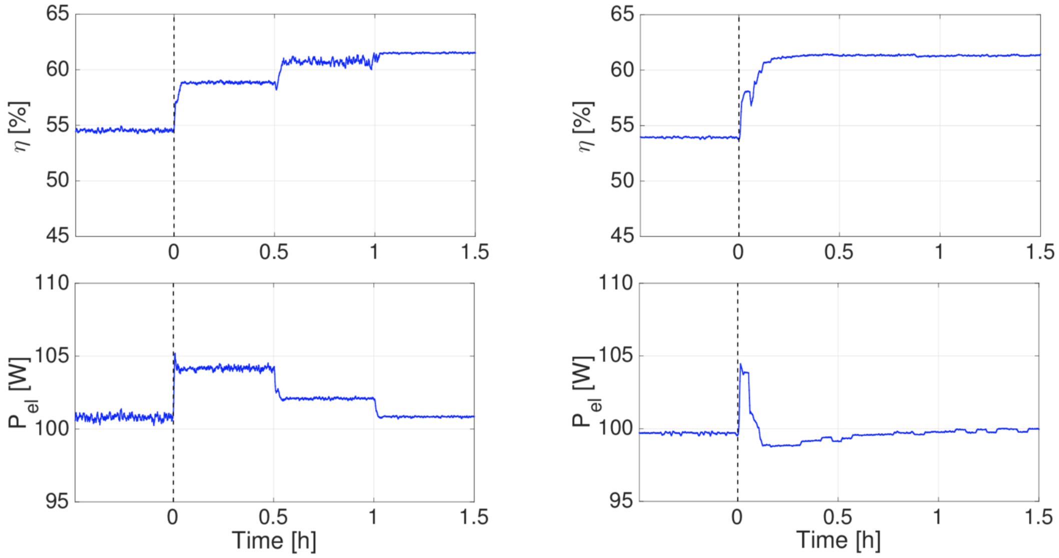

(a) Experiment 1: CA_ss, τ_{RTO} = 30 min. (b) Experiment 3: CA_dyn, τ_{RTO} = 3 min.

Figure 4.10: Performance (in terms of efficiency and electric power) of CA_ss with $\tau_{RTO} = 30$ min and CA_dyn with $\tau_{RTO} = 3$ min.

4.4 Conclusions

In the performed experiments, the plant efficiency was increased from 55% to 62% through application of real-time optimization. SOFC systems are characterized by the presence of different time scales. The use of a dynamic model allows reducing significantly the RTO period. This way, convergence speed can be increased and the RTO scheme does not suffer from the impact of different plant time scales. Although SOFC systems have slow thermal dynamics that may take a few hours to settle to steady state, it has been possible to reduce the time necessary to reach the power setpoint from 1 h to about 5 min. This experimental work has shown that it is possible, not only to control the SOFC system at the desired operating point, but also to operate it near optimality despite changes in power demand.

This chapter has described the experimental implementation of real-time optimization to an

SOFC system. The proposed approach consists in utilizing either steady-state measurements or transient measurements together with a dynamic model to implement constraint adaptation. In spite of significant plant-model mismatch and uncertainty, it was shown that the approach is able to efficiently steer the SOFC system to near optimality, while always meeting the power demand and respecting the operational constraints. This opens up nice industrial perspectives, in particular with respect to dealing with system degradation.

The results are very encouraging and offer the possibility to rapidly and adequately optimize the operation of complete large-scale industrial SOFC systems without compromising on safety and lifetime. This will be illustrated in the next chapter.

5 Real-Time Optimization of a Commercial SOFC System

This chapter discusses the experimental implementation of the fast RTO approach proposed in Chapter 3 to a commercial SOFC system. It is based on the following publication [87]

T. de Avila Ferreira, Z. Wuillemin, T. Faulwasser, C. Salzmann, J. Van Herle, and D. Bonvin. Enforcing Operational Efficiency in SOFC Micro-CHPs. *Energy*, *Submitted*, 2018.

5.1 Introduction

In this chapter, we consider high-temperature solid-oxide fuel-cell (SOFC) systems that electrochemically oxidize fuels (hydrogen and/or methane) to generate electricity. SOFC systems are mostly considered for stationary applications such as combined heat and power (CHP) generation for households, whereby the thermal integration of fuel-cell stack, reformer and heat exchangers is key to achieve commercially competitive efficiency levels above 55% [3, 33].

As previously mentioned, SOFC systems are operated continuously for long periods of time (several years). Therefore, certain technical constraints must be guaranteed for safe and reliable operation. However, slow drifts of system parameters (due to degradation, thermal inertia, etc.) make achieving optimal efficiency under all circumstances difficult. Moreover, disturbances and frequent changes in electrical power demand are additional operational challenges. Hence, the question of how to continuously enforce optimal operation of a SOFC system is of considerable interest.

The outcomes of an experimental case study on a commercial micro-CHP built around a SOFC stack is presented in this chapter. Specifically, we consider the BlueGEN system [33], which comprises a fuel-cell stack, a pre-reformer, an afterburner and several heat exchangers. To the best of the author's knowledge, none of the reported investigations deal with a complete commercial SOFC system. Specifically, we suggest improving the operational efficiency of such systems online, that is at run time, by means of real-time optimization (RTO).

The conceptual foundation of the previous RTO approach proposed is a time-scale separation [7], that is, the fact that the fuel cell is characterized by two time scales (a fast time scale associated with the electrochemical reactions and a much slower time scale associated with the thermal processes). Since constraint adaptation fails when a time-scale separation is absent, we propose to use the approach described in Chapter 3. This RTO approach uses transient measurements in combination with a dynamic model, thereby overcoming the time-scale separation issue in constraint adaptation. In general, it can be shown that constraint adaptation reaches a feasible operating point upon convergence, that is, an operating point that satisfies the considered constraints [17]. In contrast, guaranteeing optimality upon convergence requires first-order corrections [22].

In this chapter, we apply constraint adaptation using transient measurements combined with a dynamic model to a complete SOFC system that includes a pre-reformer, an afterburner and several heat exchangers. Note that the experimental setup in the previous chapter considered an experimental SOFC stack without the physical presence of the afterburner and the heat exchangers (the effects of these elements were simulated and implemented via electrical heaters). Here, we consider a complete commercial BlueGEN system. Our experimental results indicate that the RTO scheme drives the system toward optimal efficiency regardless of the requested power demand and the constraints imposed on the system. In addition, we provide a posteriori analysis that supports the fact that optimality was indeed reached.

This work is a collaborative project between Group of Energy Materials – EPFL, Automatic Control Laboratory – EPFL and SOLIDPower SA. A data exchange interface was built to establish a communication between the optimization algorithm implemented in MATLAB and the BlueGEN system controlled via LabVIEW. Although the BlueGEN SOFC system was located at SOLIDpower SA in Yverdon-les-Bains, Switzerland, all experiments were performed remotely from EPFL Lausanne.

The remainder of the chapter is organized as follows. A system description and the considered tendency model are provided in Section 5.2. Section 5.3 briefly discusses the RTO techniques used in this study. Section 5.4 analyzes the experimental results obtained with BlueGEN. Then, analysis and assessment of optimal operation is given in Section 5.5, while Section 5.6 concludes the paper.

5.2 BlueGEN System

The demand for CHP or co-generation technology has substantially increased due to the need for decarbonization of energy supply and the steadily increasing demand for electricity. Several commercial CHP systems are available. While many CHP systems, such as those provided by 2G Energy AG [88], ETW Energietechnik [89], SenerTec Center NRW-Süd GmbH [90], rely on internal combustion engines or gas/steam turbines in conjunction with a generator, the BlueGEN system developed by SOLIDpower SA is based on a micro power SOFC [33]. Subsequently, we describe the main features of the BlueGEN system, the tendency model used for control, and the formulation of the optimization problem.

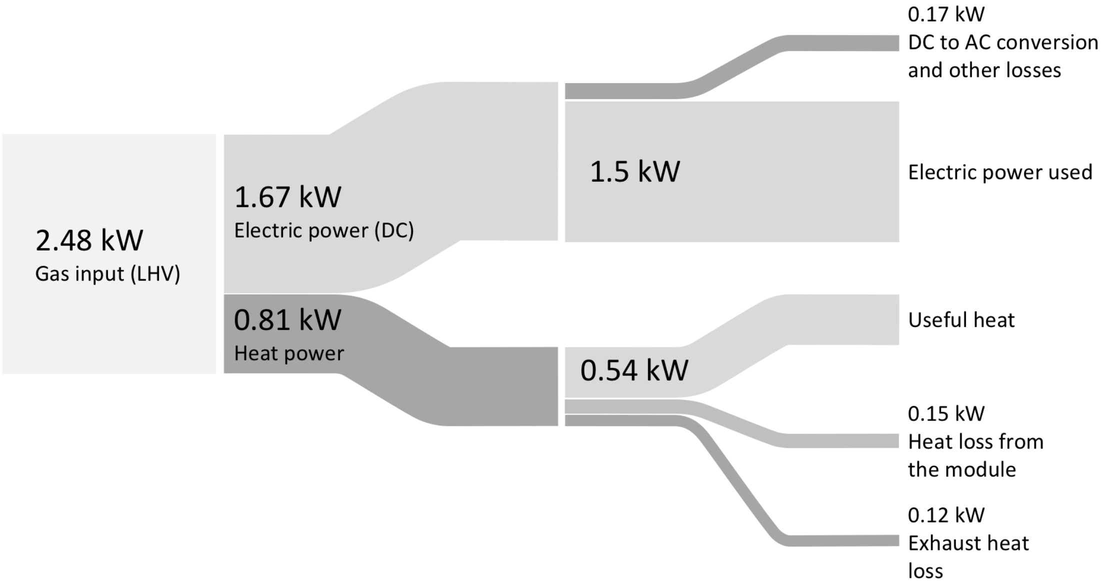
0.17 kW
DC to AC conversion and other losses
1.5 kW
Electric power used
2.48 kW
Gas input (LHV)
1.67 kW
Electric power (DC)
0.81 kW
Heat power
0.54 kW
Useful heat
0.15 kW
Heat loss from the module
0.12 kW
Exhaust heat loss

Figure 5.1: Power balance of the BlueGEN system [33].

5.2.1 System Description

BlueGEN is a commercial micro-CHP system targeted to small businesses, private households and public buildings. The BlueGEN system can deliver about 13'000 kWh of electricity a year. Currently, the system is able to run with AC electrical efficiency of about 60% at 1.5 kW, producing electricity 50% cheaper than current market prices [33].

BlueGEN is a fully integrated SOFC fuel-cell module that converts fuel into electrical energy. The heat produced by the system can be used to heat water. BlueGEN weighs 195 kg and has a size of 1010 x 600 x 660 mm in height, width and depth. Natural gas or biomethane can be used as the source of energy. At the electrical power of 1.5 kW and AC electrical efficiency of about 60%, the fuel consumption is about 2.5 kW. In addition, about 0.55 kW can be used as energy to external heating systems. Figure 5.1 depicts BlueGEN power balance at the electrical power of 1.5 kW.

The BlueGEN system consists of a pre-reformer, a stack, several heat exchangers and an afterburner. The system consists of 70 planar anode-supported cells with an active area of 80 cm^2. The cells are pressed between gas-diffusion layers and metallic interconnector plates. The anodes consist of standard nickel/yttrium-stabilized-zirconia (Ni-YSZ) cermet, and thin electrolyte, which is made of dense YSZ and a CGO (ceria-gadolinia) barrier layer. The cathodes consist of screen-printed (La, Sr)(Co, Fe)O_3 that allows operating at temperatures between 650°C and 850°C. The system is connected to a station that provides air and fuel, while the delivered current is set by an active load.

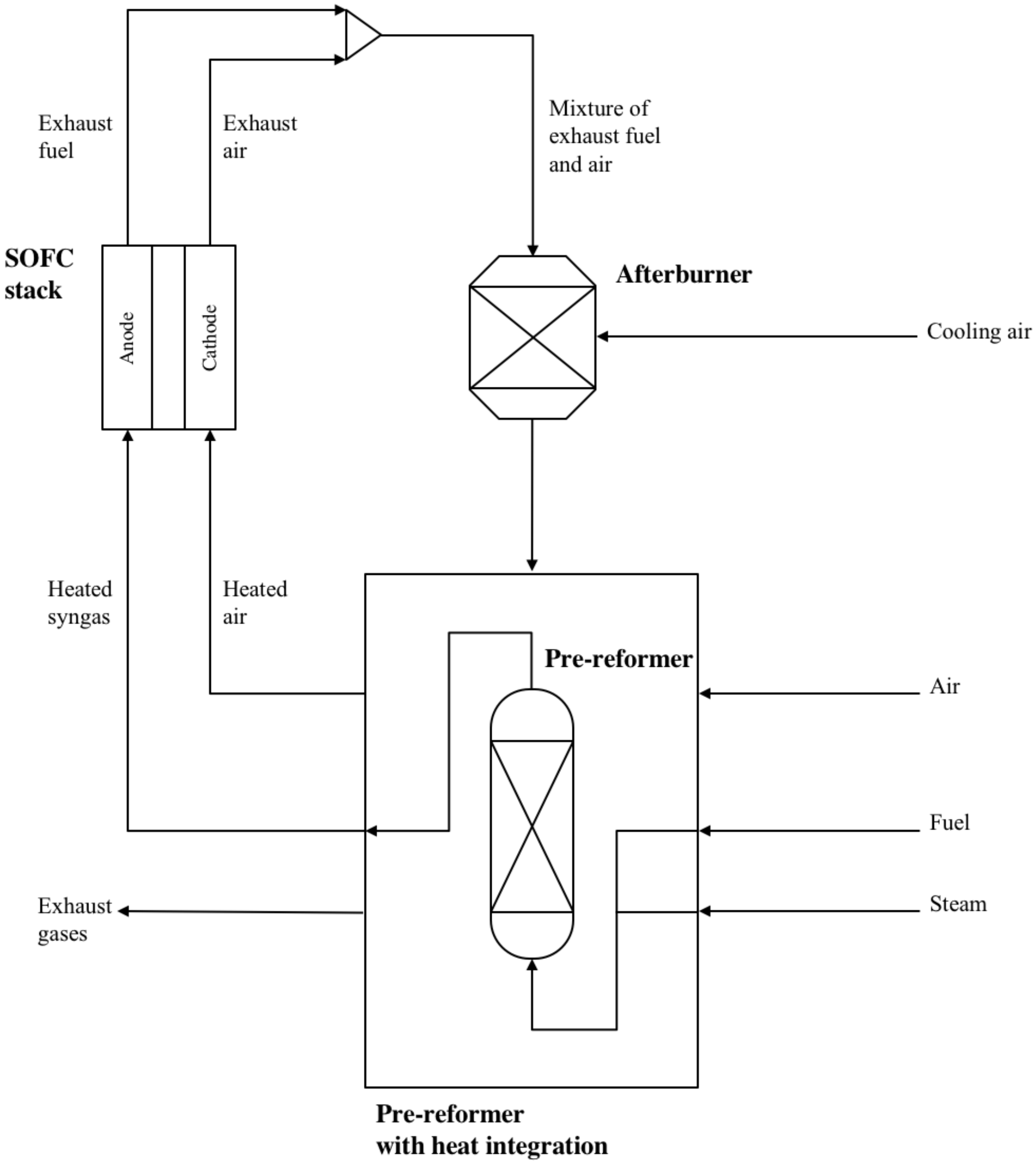
Exhaust fuel
Exhaust air
Mixture of exhaust fuel and air
SOFC stack
Anode
Cathode
Afterburner
Cooling air
Heated syngas
Heated air
Pre-reformer
Air
Fuel
Steam
Exhaust gases
Pre-reformer with heat integration

Figure 5.2: BlueGEN system flowsheet.

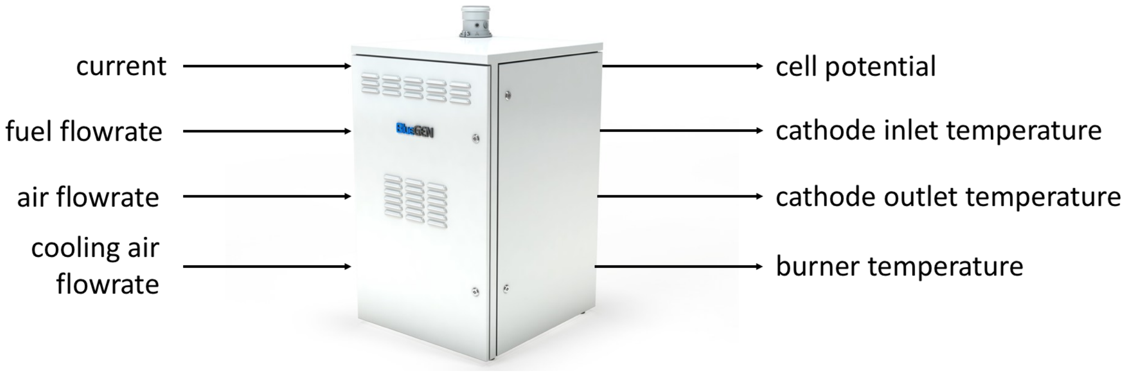

Figure 5.3: Input-output representation of the BlueGEN system.

The BlueGEN flowsheet is given in Figure 5.2. The electrical current and the flows of air, fuel and cooling air are the manipulated variables. These variables are regulated by PI controllers. The measured outputs are the cathode inlet and outlet temperatures of the stack, the burner temperature, and the electrical potential of the stack. The electrical power, system efficiency, fuel utilization and air-excess ratio are computed based on the manipulated and output variables. Figure 5.3 depicts a simplified input-output representation of the BlueGEN system.

5.2.2 Tendency Model

Next, we turn to the mathematical model used for RTO. As will be discussed later, the RTO scheme used in this study does not require an accurate model since correction terms based on measurements will be added to the predicted values of the constraints. To reflect this aspect, we say here that we use a *tendency model* (in practice, we use the best available model, which, however, does not need to be very accurate). In particular, we will use a lumped model as this will be sufficient to capture the fundamental aspects of the SOFC system, while allowing for fast computation and reasonable accuracy. The components of the tendency model used are described in Section 2.3. The connections of each of the model component is done according to the plant flowsheet in Figure 5.2. Note that four available inputs are used to control the system, namely, the current and the flowrates of fuel, air and cooling air, which gives $\mathbf{u} = [\ I, q_{CH_4},\ q_{air},\ q_{cool}]^{\mathrm{T}}$.

Dynamic Behavior

The dynamic behavior of a SOFC stack alone was studied in [91]. This behavior is characterized by a fast response of the cell voltage when a step change is imposed to the current density, followed by a relaxation process that is considerably slower. This relaxation time depends on the cell size and configuration, the thermal properties and the operating conditions.

The BlueGEN system has several components, with each component being characterized by its own dynamics. Moreover, the system has a thermal recycle, which increases its dynamic complexity. Hence, the system is expected to have (i) fast dynamics associated with the electrochemical reactions, (ii) slow dynamics associated with the thermal inertia of the individual components, and (iii) still slower dynamics associated with the thermal recycle. It is also important to mention the relative large thermal inertia of the burner, which affects the system dynamics.

5.2.3 Operational Constraints

The operational constraints present in the BlueGEN system are summarized in Table 5.1. The constraint that most limits efficiency is the fuel utilization ν. BlueGEN can have different values of fuel utilization for the same electrical power. System efficiency is mainly driven by high fuel utilization. However, too high values of fuel utilization can damage the stack through re-oxidation of the anode and fuel starvation [7, 92]. Hence, in this study, we set a relative conservative upper bound (80%) on fuel utilization.

BlueGEN is designed to operate at high values of the cell voltage U_{cell}. We set a conservative lower bound on U_{cell} to avoid accelerated cell degradation that occur at low cell potentials.

The stack operating temperature varies depending on the cathode material [92]. In this study, we maintain the cathode outlet temperature $T_{cath,out}$ between certain bounds to avoid damage of the cathode material. To prevent elevated temperatures, we set an upper bound on the burner temperature T_{burner}. Large thermal gradients between the cathode inlet and outlet temperatures would impact the temperature profile inside the cell, which affects the potential losses and consequently may shorten the system life-time due to degradation [93]. Hence, lower and upper bounds on the cathode inlet temperature are also taken into account.

In addition, to avoid strong thermal gradients in the stack, we set a lower limit on the air-excess ratio λ_{air}, which is defined as the ratio of the amount of oxygen in-take to the stoichiometric amount of oxygen needed to react with the fuel. Moreover, the air inlet flowrate q_{air} is constrained between lower and upper values based on device specifications. The fuel flowrate q_{CH4} has a lower bound to avoid fuel starvation and an upper bound based on device specifications. Since cooling air is used to regulate the burner temperature, an upper bound is set on the cooling air flowrate q_{cool} to avoid too low system temperatures.

Finally, an upper bound on the current I is set to limit degradation.

5.2.4 Formulation of the Optimization Problem

In operating the BlueGEN micro-CHP, it is of vital interest to improve the overall system efficiency for varying demands of electrical power. In addition, operating constraints as per Section 5.2.3 are included to guarantee safe operation. Based on the aforementioned tendency model, the optimization problem can be formulated as the following nonlinear program (NLP):

Table 5.1: Operational constraints in the BlueGEN system.

Constraint	Lower bound	Upper bound
U_{cell} $[V]$	0.76	-
ν [-]	-	0.8
λ_{air} [-]	3	-
$T_{cath,in}$ [°C]	650	750
$T_{cath,out}$ [°C]	650	790
T_{burner} [°C]	-	890
q_{CH4} $[L.min^{-1}]$	1	7
q_{air} $[L.min^{-1}]$	85	200
I $[A]$	0	50
q_{cool} $[L.min^{-1}]$	0	40

$$\begin{aligned} \max_{\mathbf{u}} \quad & \eta_{sys}(\mathbf{u}) = \frac{P_{el}}{q_{CH_4}\ LHV_{CH_4}} - \delta_{air} q_{air}^2 - \delta_{cool} q_{cool}^2 \\ \text{s.t.} \quad & \text{steady-state model equations (2.3.2)-(2.3.15)} \\ & \text{constraints in Table 5.1} \\ & P_{el}(\mathbf{u}) = P_{el}^S \ [W], \end{aligned} \tag{5.2.1}$$

where η_{sys} represents the cost function (related to system efficiency) to be maximized, P_{el} denotes the electrical power demand and P_{el}^S its setpoint, LHV_{CH_4} is the lower heating value of the fuel. Note that the flowrates of air and cooling air are included in the cost function to force the system to use small amounts of air and cooling air in an effort to reduce the operational costs, with $\delta_{air} = 1 \times 10^{-5}$ and $\delta_{cool} = 1 \times 10^{-4}$ the corresponding weights. Note that, in contrast to the DC electrical efficiency η, the cost function η_{sys} includes terms to account for parasitic blower consumption.

5.3 Real-Time Optimization Approach

If the tendency model used in this work were an exact representation of the true system behavior, it would be straightforward to achieve optimal system operation by means of numerical optimization [3, 7, 8, 94]. However, in practice, models are never exact. Hence, we now turn to a family of methods known as real-time optimization (RTO) that can handle inexact models.

We refer to the previous chapters to review the RTO approaches used here, see Section 2.2.1 for steady-state constraint-adaptation scheme, and see Section 3.2.2 for constraint adaptation using transient measurements and a dynamic model.

Table 5.2 emphasizes the differences between the steady-state CA scheme and its fast counterpart implemented in this work. Note that the use of transient measurements allows reducing

Table 5.2: Two CA schemes.

Algorithm	Measurements	Optimization problem	Modifiers (bias update rule)	RTO period
Steady-state CA	At steady state	(2.2.4)	(2.2.3)	90 min
Fast CA	During transient	(3.2.1)	(3.2.7)	5 min

the sampling interval from 90 to 5 min, which speeds up convergence considerably. With both schemes, the converged solution is guaranteed to be feasible. However, without plant-specific analysis, it is in general not possible to infer optimality upon convergence. Hence, we will discuss optimality issues in Section 5.5, after presentation of the experimental results in the next section.

5.4 Experimental Results with the BlueGEN System

This section describes the experimental results obtained upon applying RTO to the BlueGEN system. The experiments were performed considering three distinct operating points corresponding to electrical power demands of 1, 1.25 and 1.5 kW. Note that the electrical power acts as an unknown disturbance. These scenarios were chosen to (i) assess the performance of the proposed approach, (ii) demonstrate the change in active constraints, and (iii) show the effect of the different time scales.

- **Steady-state CA:** A 72-h experiment with steady-state CA.
- **Fast CA:** A 6-h experiment with fast CA.

The fuel-cell system is controlled using a LabVIEW interface, in which the optimization algorithm is implemented via a MATLAB Script function. The results of the experiments are detailed next.

5.4.1 Steady-State CA

We first performed a 72-h experiment solving Problem (2.2.4) using a steady-state model and steady-state measurements, that is, computing the modifiers as per (2.2.3). The model used is the steady-state version of the tendency model described in Section 5.2.2.

The filter matrix **K** in (2.2.5) is the diagonal matrix $K_f\,\mathbf{I}$, where K_f is a scalar and $\mathbf{I} \in \mathbb{R}^{n_u \times n_u}$ is the identity matrix. K_f is set to 0.4 to prevent large moves between RTO iterations and reduce the effect of measurement noise.

To explore the range of power demand that the system can provide, the power setpoint P_{el}^S is changed every 24 h as follows:

$$P_{el}^{S}(t) = \begin{cases} 1000\ [W], & \text{t} \leq 24\text{ h} \\ 1250\ [W], & 24\text{ h} < \text{t} \leq 48\text{ h} \\ 1500\ [W], & \text{t} > 48\text{ h.} \end{cases} \tag{5.4.1}$$

At the start, BlueGEN is set at the relative conservative operating condition of 55% DC efficiency at 1 kW. Next, the control algorithm is applied to drive the system to optimal efficiency. The modifiers are computed as per (2.2.3). Problem (2.2.4) is solved to compute the next inputs, which are filtered according to (2.2.5). With the RTO period of 1.5 h, the procedure is repeated until convergence. Figures 5.4 and 5.5 depict the performance of steady-state CA. All lines represent measurements after application of an offline moving-average filter [86].

The DC electrical efficiency increases to about 62% in the first 5 h. However, since the system is not at thermal equilibrium yet, the efficiency decreases slightly with temperature to eventually reach 61%. The system takes about 20 h to reach steady state. Note that, although the electrical power is kept constant, the efficiency increases by 11% with respect to its initial value.

After 24 h, the power setpoint is changed to 1.25 kW. It takes the system five iterations, or 7.5 h, to reach the new power setpoint. However, since the temperatures are slower and take about 16-20 h to reach steady state (Figure 5.5), the system efficiency is not at steady state after 7.5 h. The temperatures keep increasing, and the DC electrical efficiency eventually settles at about 63.5%.

After 48 h, the electrical power setpoint is increased again to 1.5 kW. The system reaches the new power setpoint in about seven iterations, or 10.5 h. Here, the temperatures do not change much as the cathode outlet temperature was already close to its upper bound. Hence, the efficiency reaches steady state faster, as it is not affected by the slow thermal changes. It reaches about 62.5% after two iterations.

Note that the RTO scheme minimizes the cooling air flowrate for all operating points. This is not surprising since (i) this input is used to control the burner temperature and prevent it from getting too high, and (ii) in this experiment, the burner temperature is below 860 °C and thus no control action is needed.

5.4.2 Fast CA

This section describes a shorter 6-h experiment performed to assess the performance of fast CA, that is, steady-state CA that uses transient measurements and a dynamic model to estimate the plant steady state.

Problem (3.2.1) is solved using the modifiers (3.2.7). The dynamic model is the tendency model described in Section 5.2.2. A diagonal filter matrix, with $K_f = 0.4$, is used.

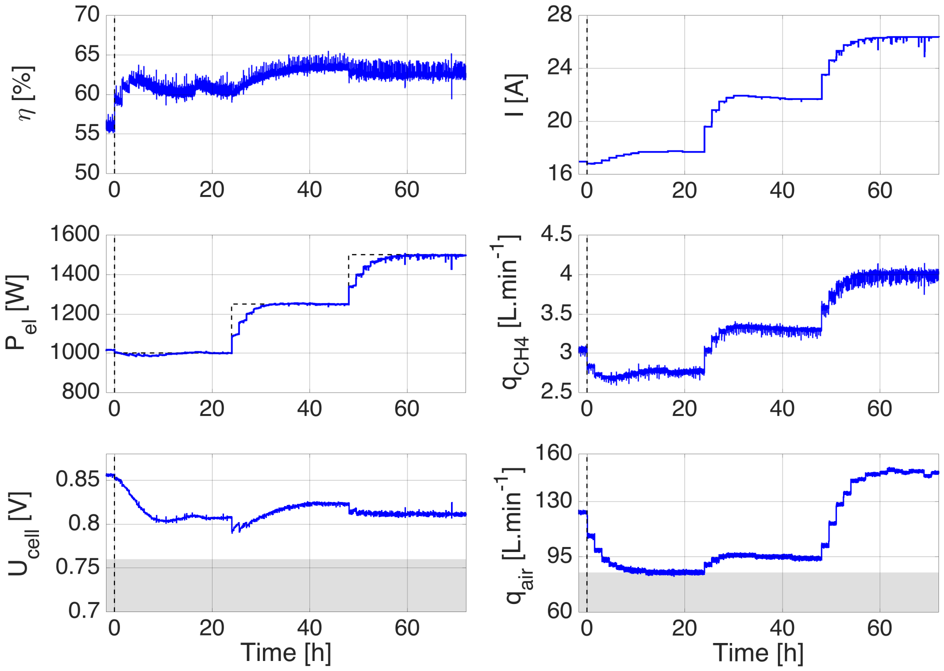

Figure 5.4: *Steady-state CA*: Efficiency, current, electrical power, methane flowrate, cell voltage, and air flowrate vs. time.

The power setpoint P_{el}^{S} is changed every 2 h as follows:

$$P_{el}^{S}(t) = \begin{cases} 1000\ [W], & \mathrm{t} \leq 2\ \mathrm{h} \\ 1250\ [W], & 2\ \mathrm{h} < \mathrm{t} \leq 4\ \mathrm{h} \\ 1500\ [W], & \mathrm{t} > 4\ \mathrm{h}. \end{cases} \tag{5.4.2}$$

The BlueGEN system starts again at steady state with an electrical power of 1 kW and about 55% DC efficiency. The procedure is repeated with the RTO period of 5 min until convergence. Figures 5.6 and 5.7 depict the performance of fast CA. The lines represent measurements after application of an offline moving-average filter [86].

The DC electrical efficiency increases to about 64.5% in the first 30 min. However, since the system is not at thermal equilibrium, the efficiency decreases slightly with temperature to eventually reach 64% after 2 h. The DC electrical efficiency is thus increased by about 16% with respect to its initial value for the same electrical power.

Next, the power setpoint is changed to 1.25 kW after 2 h. It takes the system about 15 min to reach 96% of the new power setpoint and 45 min to completely reach it. The cell potential and the temperatures keep increasing, with the electrical efficiency reaching 62% at this point.

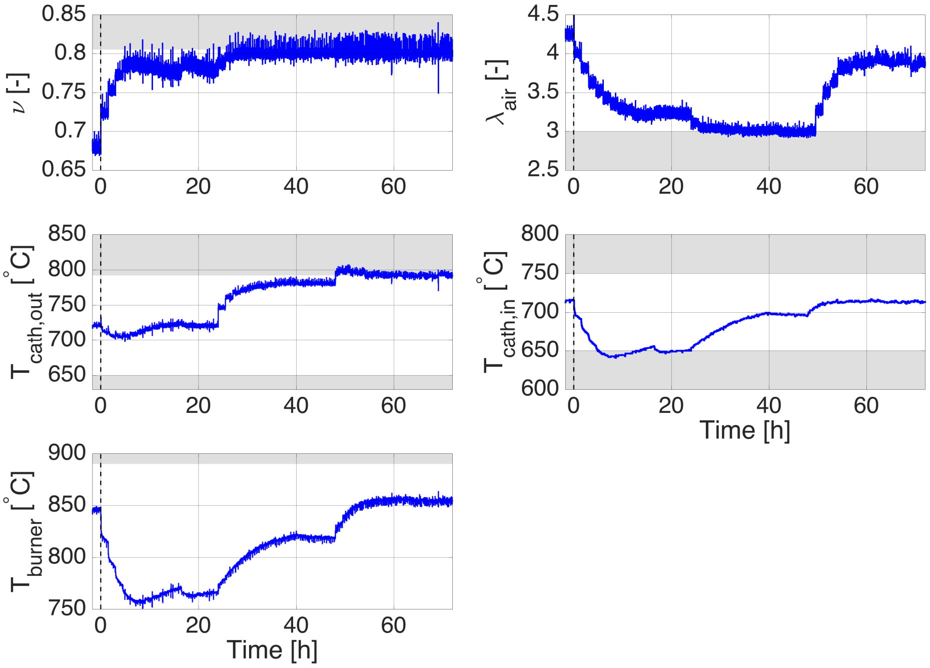

Figure 5.5: *Steady-state CA*: Fuel utilization, air-excess ratio, cathode outlet and inlet temperatures, and burner temperature vs. time.

Finally, after 4 h, the electrical power setpoint is changed to 1.5 kW. The system takes about 11 min to complete 95% of the change and 40 min to fully complete it. The DC electrical efficiency reaches about 61% after 2 h.

Table 5.3 summarizes the range of efficiencies that the BlueGEN system is able to reach for each electrical power tested when either steady-state CA or fast CA is applied.

5.4.3 Change in Active Constraints for Different Power Levels

For all tested electrical powers and upon convergence, the optimal operation of BlueGEN system is determined by active constraints (Figures 5.4 - 5.7). This feature makes the proposed RTO scheme attractive. At steady state, for the power setpoint of 1 kW, the following four constraints are active: the electrical power, the cathode inlet temperature, the air flowrate and the cooling air flowrate. At the power of 1.25 kW, another set of four constraints are active, namely, the electrical power, the fuel utilization, the air-excess ratio and the cooling air flowrate. Finally, at the power of 1.5 kW, the active constraints are the electrical power, the fuel utilization, the cathode outlet temperature and the cooling air flowrate.

Note that, when fast CA is applied, the system can exhibit a set of active constraints that differs from the corresponding set obtained with steady-state CA for the same power setpoint. For

Table 5.3: Range of DC efficiencies for each electrical power tested, where SS CA stands for standard steady-state constraint adaptation and Fast CA stands for constraint adaptation using transient measurements combined with a dynamic model.

	Electrical Power [kW]					
	1		1.25		1.5	
RTO scheme	SS CA	Fast CA	SS CA	Fast CA	SS CA	Fast CA
Efficiency [%]	61	64	62	63.5	61	62.5

example, at the power of 1 kW, the electrical power, the fuel utilization, the air flowrate and the cooling air flowrate are active with fast CA. However, as the system settles to steady state, the lower bound of the cathode inlet temperature becomes active, thereby freeing the fuel utilization. This is caused by the slow thermal transients, with the cathode inlet temperature reaching its lower bound very slowly. Fuel utilization is not at its upper bound at steady state because this would result in a lower burner temperature and thus also to a lower cathode inlet temperature, which is not possible because the lower bound is already active.

5.4.4 Transient vs. Steady-State Performance

A comparison of the results obtained with steady-state CA and fast CA in Figures 5.4 to 5.7 is clearly to the advantage of fast CA. Indeed, in addition to the ability of reaching a new setpoint much quicker, fast CA also seems to be able to generate, at least temporarily, higher efficiency values. A closer look indicates that this is probably linked to the fact that the cathode can be kept at higher temperatures, which is linked to the fact that the higher the fuel utilization, the higher the system efficiency. At 1 kW, fuel utilization can be at its maximum if the cathode inlet temperature is not at its lower bound.

Hence, an additional experiment, shown in Figure 5.8, was performed to evaluate the performance when the system is forced to remain in transient mode in such a way that the lower bound on $T_{cath,in}$ is not reached. Initially, the system is at steady state at 1 kW with a DC efficiency of about 55%. The modifiers are computed as per (3.2.7). Problem (3.2.1) is solved to compute the next inputs, which are then filtered according to (3.2.3). The RTO period is 5 min, as with fast CA. Every 50 min, the system is pushed back to the initial state and kept there 10 min by resetting manually the values of the inputs. This procedure is repeated several times so as to keep the fuel-cell system in a transient operating mode.

As shown in Figure 5.8, the electrical power is kept at 1 kW throughout this experiment. Due to the periodic excitation, the system undergoes cyclic operation. Once a limit cycle is reached, the system exhibits maximal efficiency of about 62%, with an average efficiency of about 60%. Although the average efficiency is slightly lower than the corresponding steady-state value, the plateau at maximal efficiency is higher than the steady-state value. No attempt was made to determine the parameter values that would optimize such a limit cycle. However, this experiment suggests the possibility of optimizing system performance by appropriate cycling,

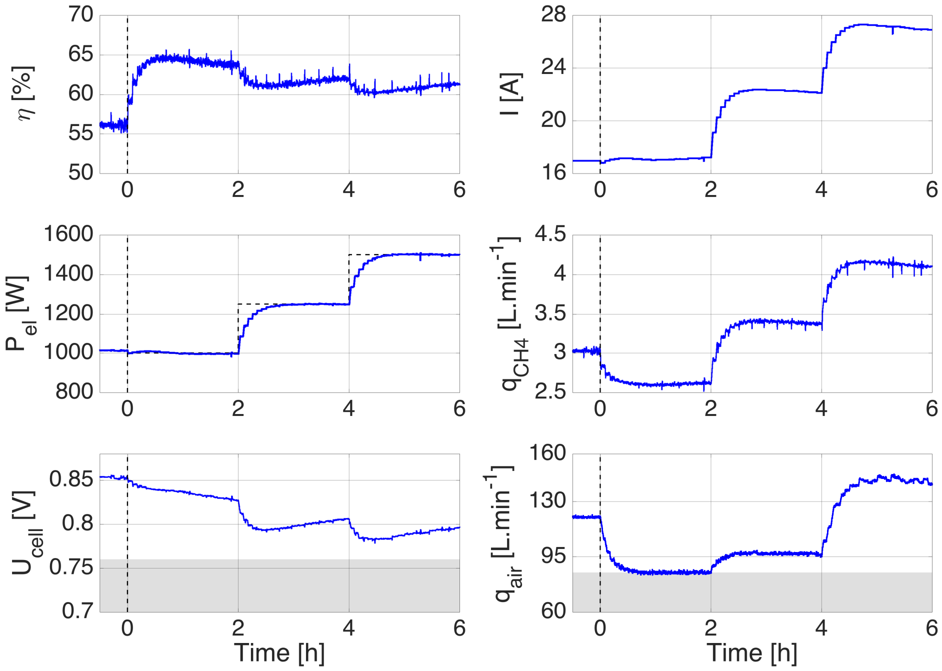

Figure 5.6: *Fast CA*: Efficiency, current, electrical power, methane flowrate, cell voltage, and air flowrate vs. time.

particularly in applications where cycles appear naturally, such as in daily power demands. It also shows that the BlueGEN system copes well with frequent load cycling, which is positive for its application as residential micro-CHP. This, however, is beyond the scope of this work.

5.5 Discussion and Analysis of Experimental Results

This section discusses and analyzes the results obtained in the previous section, in particular (i) the effect for optimization of the presence of different times scales, (ii) the effect of constraints on operability and performance, and (iii) an a posteriori assessment of optimality.

5.5.1 Effect of Different Time Scales

As already mentioned, the BlueGEN system is characterized by the presence of several time scales. One can observe three time scales that are associated with the electrochemical process, the burner and the thermal recycle, respectively. As seen by the rather quick response to changes in power setpoint, the efficiency responds almost instantaneous to input changes. This is due to the fact that efficiency is mostly affected by the electrochemical time scale. In contrast, the cell potential keeps changing even when the inputs do not change much as seen in Figures 5.4 and 5.6. Since the cell potential is also a function of temperatures,

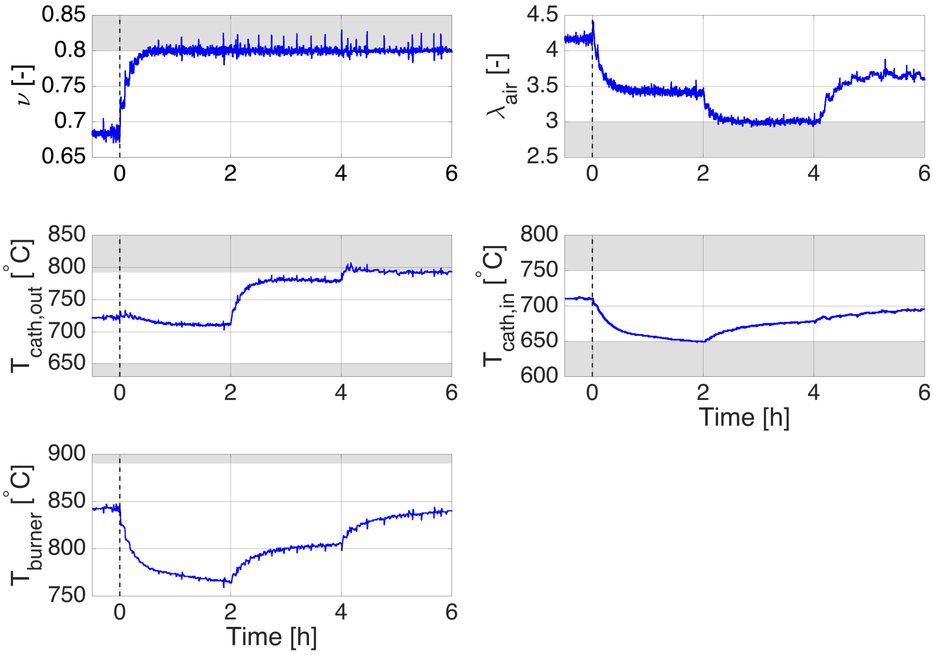

Figure 5.7: *Fast CA*: Fuel utilization, air-excess ratio, cathode outlet and inlet temperatures, and burner temperature vs. time.

these slow changes are related to the slow thermal time scale. The burner, due to its large thermal inertia, has a much larger time constant compared to the electrochemical effects. Furthermore, the time constant associated with the thermal recycle is rather large and the one that ultimately governs the system steady state. This appears to be the reason for the change in active constraints between the transient and steady-state phases of operation at 1 kW. During transient operation, as the temperatures decrease slowly and the cathode inlet temperature has not reached its lower bound yet, fuel utilization is temporarily at its upper bound. Note that the fuel utilization decreases when the cathode inlet temperature reaches its lower bound.

These results are very promising. Indeed, due to this large difference in time scales, the proposed approach can reach the electrical power setpoint much faster than the time it takes for the system to settle to thermal steady state. This way, the optimizer is quick at finding and tracking the active constraints, thus implementing optimal operation quickly.

5.5.2 Effect of Constraints on Operability and Performance

Different sets of active constraints have been observed at the plant optimum for the three investigated electrical power loads.

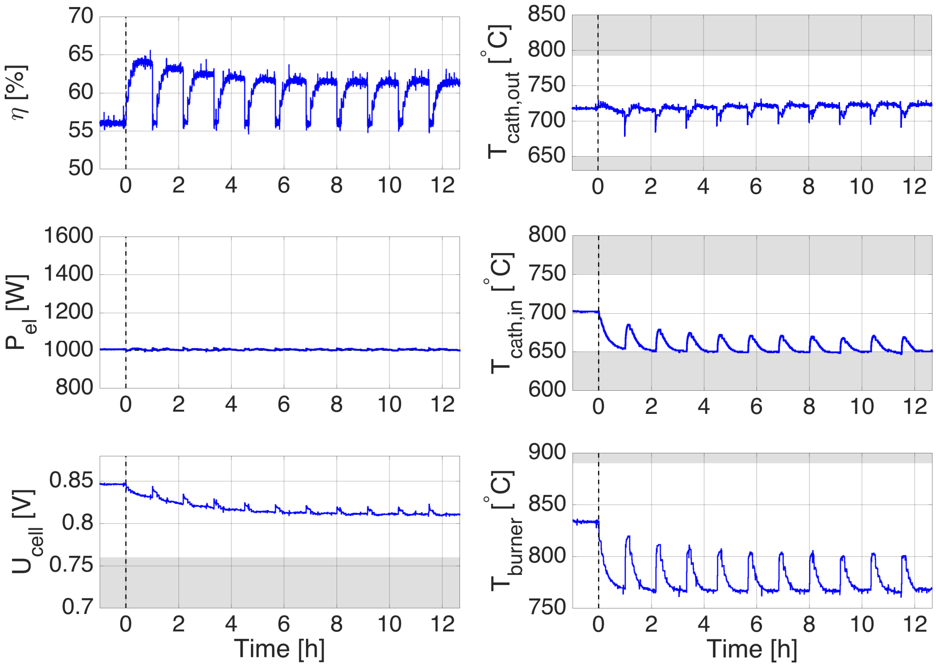

Figure 5.8: *Cycling experiment*: Efficiency, cathode outlet temperature, electrical power, cathode inlet temperature, cell potential, and burner temperature vs. time.

At 1 kW, the most restrictive constraint appears to be that on the cathode inlet temperature, which is at its lower bound. A performance comparison between steady-state CA and fast CA shows that the electrical efficiency can reach higher values (up 64.5%) when the constraint on fuel utilization is active. Since the cathode inlet temperature constraint is active at steady state, fuel utilization cannot be at its upper bound, which causes a decrease in system performance.

At 1.5 kW, the most restrictive constraint seems to be that on the cathode outlet temperature, which is at its upper bound. In this case, a relatively large air flowrate is used to regulate the cathode outlet temperature. Unfortunately, the larger the air flowrate, the lower the efficiency.

At the intermediate power value of 1.25 kW, constraints that are only functions of inputs are active. This means that system performance relies more on the electrochemical dynamics than on the slow thermal dynamics. Consequently, the system reaches the power setpoint quickly. This suggests that there is an electrical power range between 1 and 1.5 kW, where the electrochemical time scale plays the dominant role. Note that this information is of high practical value.

5.5.3 A Posteriori Assessment of Optimality

Without an exact plant model, it is not possible to certify optimality for RTO schemes.[1] In the case of CA, optimality guarantees would required to know the correct set of active constraints beforehand. Because of this difficulty, we conduct next an a posteriori analysis that supports the claim of local optimality.

The BlueGEN system has four inputs. The current, which has a limited impact on temperatures, is used to regulate the electrical power. The flowrate of cooling air is available to keep the burner temperature below its upper bound. The remaining inputs, namely, the fuel and air flowrates, are available to push efficiency, while respecting all other constraints. An intuitive way of pushing system efficiency is to increase fuel utilization to its upper bound.

Let us consider BlueGEN's operation at various power demands and assess qualitatively whether performance could be improved.

- At 1 kW, both the cathode inlet temperature and the air flowrate are at their lower bounds.

  Fuel utilization can be increased by reducing the fuel flowrate. However, this would eventually decrease the cathode inlet temperature and thus violate its lower bound. An increase in current would also lead to an increase in fuel utilization, but this would make the electrical power deviate from its setpoint. Alternatively, one could consider increasing the current and decreasing simultaneously the fuel flowrate so as to keep the electrical power at 1 kW. However, this would violate the cathode inlet temperature as the current has less effect on temperatures.

  The air flowrate is at its lower bound, and any increase would lead to a decrease in system temperatures, thus violating the constraint on the cathode inlet temperature. In addition, the system efficiency would decrease.

  The cooling air flowrate is also at its lower bound. An increase of this input would decrease the temperatures, thus violating the constraint on the cathode inlet temperature and reducing the efficiency.

  These qualitative arguments suggest that optimality is reached at the electrical power of 1 kW as no input change would lead to better efficiency while remaining feasible. In other words, small (i.e. local) changes of the inputs will very likely not improve efficiency.

- At 1.25 kW, no temperature constraint is active. Fuel utilization is at its upper bound, which implies that a change in fuel flowrate would not improve the efficiency. The air flowrate cannot be decreased as the air-excess ratio is at its lower bound. Note that an increase of the air flowrate would reduce efficiency. Since the cooling air flow is also at its lower bound, any change of this variable would lead to suboptimal performance as mentioned previously. All these reasons suggest that, for the power of 1.25 kW, the system is also locally optimal.

---

[1] Even RTO schemes providing nominal certificates of optimality upon convergence require certain assumption, for example the availability of exact plant gradients for modifier adaptation [22]. In general, the fact that the plant optimum is unknown makes the generic certification of optimal operation impossible.

- For 1.5 kW, fuel utilization is also at its upper bound, which indicates that no change in fuel flowrate or current would result in better performance. Furthermore, the air flowrate can neither be decreased as this would violate the constraint on the cathode outlet temperature, nor increased as this would reduce efficiency. The cooling air flow is at its lower bound and cannot be increased without compromising the system performance as previously mentioned. This also suggests that the system is at a local optimum at 1.5 kW.

5.5.4 Operational Guidelines

Supported by the results presented in this paper, one can state operational guidelines to help operate BlueGEN efficiently in the electrical power range between 0.6 and 1.7 kW:

- For electrical powers between 1 and 1.5 kW, two operational constraints must be active besides the electrical power and the cooling air flowrate: (i) the fuel utilization needs to be at its upper bound to maximize efficiency, and (ii) the air flowrate (or the air-excess ratio if it becomes active first) needs to be minimal since smaller amounts of air lead to higher efficiency.
- For electrical powers lower than 1 kW, the constraint on the cathode inlet temperature is always active. Hence, one could relax this constraint to increase fuel utilization and improve efficiency. Typically, the air flowrate is also active at this power range. However, the air-excess ratio may become active depending on the fuel utilization.
- For electrical power values higher than 1.5 kW, the cathode outlet temperature is at its upper bound. This constraint could be relaxed to decrease the amount of air in-take, which would improve performance. The fuel utilization needs to be active to guarantee high efficiency. At electrical power values close to 1.7 kW, the burner temperature and the cathode inlet temperature might become active. These variables can be controlled via the flowrates of air and cooling air. However, it may be of interest to find a trade-off between these two flowrates that maximizes performance.

5.6 Conclusions

Real-time optimization via constraint adaptation has been applied to a commercial SOFC system. The approach is based on updating the model constraints using either steady-state measurements or transient measurements combined with a dynamic model. It has been shown that the set of active constraints that determine plant optimality changes with the power demand. Despite the presence of significant plant-model mismatch, the proposed RTO scheme is able to drive the SOFC system to optimality and maintain it there despite changing power loads and the presence of disturbances such as slow drifts.

In addition, this chapter has analyzed the system operability with respect to constraints and provided a qualitative assessment of optimal performance. The proposed strategy can implement a change in electrical power demand in about 15 min, that is, well before the thermal dynamics have settled to steady state. Thermal inertia is a slow process that makes the system drift "somewhere" after a change in load/demand/operation. The proposed approach drives and maintains the system at optimal efficiency despite the ongoing drift.

Furthermore, it has been shown that this iterative RTO scheme acts as a self-optimizing controller that is able to push the operational efficiency to its limits and make the SOFC micro-CHP work in dynamic mode, thereby responding to load changes in real time.

Finally, note that this investigation has considered a rather conservative upper bound of 80% on fuel utilization. In practice, fuel utilization values of 85% or even 90% are possible, which would drive efficiency even higher.

6 Conclusions

This thesis has demonstrated that the incorporation of measurements in the optimization framework helps to improve the performance of industrial processes, in particular when the available models are of limited accuracy. Modeling often requires significant time and effort and is thereby associated with significant costs. In practice, we use the best model available as long as the optimization routines can be performed within the selected RTO period. Hence, we utilized a model that captures the fundamental behavior of the SOFC system while providing a good trade-off between accuracy and fast computation.

We have proposed a novel RTO approach in order to deal with the slow convergence of RTO approaches applied to systems that possess slow dynamics such as SOFC systems. The proposed approach allows reducing the RTO period even in the absence of time-scale separation. Multiple time scales may lead to oscillatory behavior and even prevent convergence. Avoiding these adverse effects was achieved by applying a variant of constraint adaptation that uses transient measurements combined with a dynamic model. This way, static RTO was applied during transient operation with the aim of reaching optimality in a single transition to steady state. The main contributions of the proposed approach include a different manner of predicting plant steady state by using transient measurements and a demonstration that the use of dynamic models decreases the negative effects of different time scales, thereby helping reach plant optimality.

We performed experiments on SOFC systems to validate the proposed methodology. In the small-scale experimental SOFC system, we implemented and operated a 6-cell SOFC system that contained a few simulated units in the loop. The experimental results showed that convergence speed was significantly increased and the performance of the system improved. We demonstrated that the proposed approach can achieve the desired electrical power despite the setpoint changes. The time necessary to reach the power setpoint was reduced from 1 h to about 5 min in spite of the fact that the systems is characterized by slow thermal dynamics, which take a few hours to settle to steady state. In addition, it was observed experimentally that the adverse effect of different time scales could be significantly reduced by the use of a dynamic model. These results are quite important as the experiments showed that it is possible to act rapidly and optimize the operation of SOFC systems. These experimental results are very encouraging to apply this methodology to a complete and larger industrial SOFC system.

The proposed RTO approach was also implemented on a commercial micro-CHP system, the BlueGEN system that consists of a 70-cell SOFC stack, a pre-reformer, an afterburner and a heat-exchanger network. This means that the BlueGEN system has a much slower dynamics compared to the aforementioned small-scale SOFC system. Through the experiments, we have shown that the proposed RTO approach steers the BlueGEN system to optimal efficiency despite changes in electrical power demand. Also, we performed a qualitative analysis to assess plant optimality. In addition, we analyzed how the set of active constraint changes with the electrical power and provided guidelines for optimal operation. The most significant contribution of these experimental results was the fact that fast RTO can drive the BlueGEN system to optimal efficiency and keep it there far before the thermal variables settle to steady state. This opens up new perspectives related to how to deal with slow drift disturbances, in particular concerning the dire effects of degradation. However, it would require performing long-term experiments to assess whether the proposed RTO approach can deal with it.

6.1 Summary

Next, we summarize the main conclusions of each chapter:

Chapter 3: Fast Real-Time Optimization Using Transient Measurements. This chapter has extended the RTO scheme, labeled constraint adaptation, to the cases where transient measurements are available. We have shown that the proposed fast RTO approach allows speeding up plant convergence significantly. Fast CA consist in processing transient measurements through a dynamic model. This way, the estimation of plant constraints is improved as the approach accounts for transient behaviors when the system is not at steady state. It follows that steady-state CA can be applied during transient operation, with the aim of reaching plant optimality in a single transient transition to steady state. The proposed methodology exhibits the same basic features as standard CA, that is, the plant is guaranteed to reach a feasible operating point upon convergence. In addition, provided model-adequacy conditions are fulfilled, fast CA has the ability to deal with changing active constraints. This is possible because fast CA has the advantage of being an explicit RTO method, that is, it repeatedly solves the optimization problem. Moreover, as the RTO frequency can be much higher than with standard CA, more plant information is acquired and quicker actions are taken, thereby preventing the plant from large constraint violations. Finally, the use of a dynamic model circumvents the need to have time-scale separation in order to apply RTO using transient measurements.

Chapter 4: Real-Time Optimization of a Small-Scale Experimental SOFC System. This chapter has discussed the experimental RTO implementation to an SOFC system with 6 cells that consists of both hardware and software components. We applied the RTO approach described in Chapter 3, where CA was implemented using both steady-state measurements and transient measurements combined with a dynamic model. The experimental results show that the proposed approach allows reaching plant optimality, while meeting the electric power demand and respecting all the imposed operational constraints. In addition, the results have shown that the use of measurements can overcome the difficulties related to plant-model mismatch and uncertainty. Moreover, it is shown that fast CA is able to increase plant efficiency up to 62%. The presented experimental results agree with the methodology presented in Chapter 3. Indeed, the use of a dynamic model permits to significantly reduce the RTO period, which both increases the convergence speed and allows dealing with a SOFC system with multiple time scales. Finally, it has been shown that the time needed to reach the electric power setpoint was reduced from 1 h to about 5 min despite the slow thermal dynamic effects of the tested SOFC system.

Chapter 5: Real-Time Optimization of a Commercial SOFC System. This chapter has presented an RTO experiment applied to a complete commercial SOFC system that consists of 70 cells. We have implemented steady-state and fast CA approaches to the BlueGEN system. The experimental results have shown that the set of active constraints that determine the optimal operating point change according to the power setpoint. In addition, the results have demonstrated that fast RTO can operate optimally while delivering the demanded electric power even when the system is being affected by slow drifts such as thermal inertia. This shows that the proposed approach is capable of dealing with other slow drift disturbances such as degradation that often compromise the performance of SOFC systems. Furthermore, we have shown that fast RTO significantly speed up convergence compared to steady-state RTO. The time to reach the power setpoint was reduced to about 15 min even though the system was still in a transient phase. Finally, we have analyzed the BlueGEN system in terms of its constraints, time scales, transient and steady-state performance, and provided an ex-post analysis of its optimal operating conditions.

6.2 Perspectives

At the end, we propose some suggestions related to the optimization of SOFC systems and RTO methodology.

6.2.1 Optimization of SOFC Systems

Solid-oxide fuel cells are fuel-cell systems that are mostly used for stationary applications. Combined heat and power generation for households, businesses or public buildings is promising as electric and thermal energy generation technology are produced simultaneously. This thesis has shown how to operate SOFC systems safely and optimally. However, the optimization problem has been formulated with the aim of maximizing electrical efficiency. One could explore the idea of combining thermal and electrical efficiency in the optimization problem. In addition, one could split this problem into two optimization problems: with *electrical efficiency* as the objective function when the electrical energy consumption is at its peak, and with *thermal efficiency* as the objective function when the thermal consumption is at its peak. Moreover, SOFC systems release on average 50% less CO_2 compared to carbon-based energy systems, which means to save up to 4 tons of CO_2 emissions per year [33]. Although SOFC systems are considered environmentally friendly, one could also re-formulate the optimization problem in order to prevent the system from producing CO_2 outside of a certain range, mainly when the system is on *thermal efficiency* mode. Furthermore, the optimization problem could be formulated as a sum of all operational costs that are associated with the consumption of natural gas, water and air.

As previously mentioned, thermal gradients between stack inlet and outlet temperatures may affect the life time of the system due to degradation. Hence, one could include additional constraints or a penalty function which would restrict the temperature difference to a certain maximal value. The main disadvantage of adding those additional constraints is the fact that they may compromise the system performance as either the fuel utilization or the air-excess ratio would have to be modified in order to reduce this temperature difference. Another possibility is to use a one-dimensional stack model in order to predict the spatial distribution of temperature, gas composition and overpotentials along the gas flow direction. Although more complex, this approach would allow having more flexibility and the temperature constraints would not only be restricted between inlet and outlet.

The electrical power setpoints have been changed as step functions. Another possibility would be to set the power setpoints as ramp functions. This would enable smoother temperature profiles, and slower fuel utilization and air-excess ratio changes. This would allow operating the SOFC system in a safer manner and also increasing the fuel-cell life span by reducing the adverse effect of degradation. In addition, as shown in the previous chapter, fuel-cell performance could be increased with cyclic operation. In order to solve this problem, one could formulate it as an optimal control problem, which can be solved in cycle-to-cycle fashion in the context of RTO.

As part of this thesis, but not reported in this document, we compared output MA approach with standard MA, which is available in [95]. We have demonstrated that this approach, labeled output modifier adaptation (MAy), provides additional corrections to the Hessian of the cost and constraint functions compared to MA. This is possible because the cost and constraint functions are nonlinear functions of the inputs and outputs. MAy allows the plant to converge to its optimum in a single iteration in the case when the output functions can be expressed as linear functions of the inputs, whereas MA may take several iterations to converge and, in some cases, depending on the plant-model mismatch, may not converge. Moreover, it has been shown that MAy generally provides a better approximation of the plant curvature. Since plant knowledge is assumed to be unavailable, it is not possible to tell in advance which method will have a better performance. However, taking into account the presented examples, MAy is likely to present better performance than MA for the cases where the cost and constraint functions are nonlinear function of inputs and outputs. This opens up nice perspectives in the context of SOFC systems as these types of systems have many variables that can be measured and used to perform the output corrections made by MAy.

6.2.2 RTO Methodologies

The CA approach has been experimentally applied to SOFC systems and reported in this thesis. The main drawback of the CA scheme is the fact that it requires prior knowledge of the correct set of active constraints. It may be a problem in the case where the input dimension is large. One way to overcome this is to estimate the cost and constraint plant gradients. Modifier adaptation utilizes this information in order to update the cost and constraint functions. The technique most used to estimate plant gradients is finite differences. However, it may become impractical if the plant settling time is large as convergence speed would be significantly reduced. Estimation of plant gradients during transient operation represents a possible solution to this problem. The use of plant gradients obtained during transient operation in the context of RTO has already been reported [27]. Nevertheless, the proposed approach works only for parametric plant-model mismatches. One could use transient data to fit a given function—e.g. regression via Gaussian processes or polynomial regression—to estimate functions while the plant is on transient phase. This is particularly interesting for fuel-cell systems, since before implementing any control technique, the system is subject to test and input-output data are collected. Preliminary results regarding combination of RTO schemes with Gaussian processes have been proposed as part of this thesis and are reported in [96].

This thesis has applied static RTO with both steady-state measurements and transient measurements combined with a dynamic model. An alternative to static RTO would be to utilize dynamic RTO in the context of modifier adaptation. This way, the dynamic effects of the process would be taken into account not only by the transient measurements that are used to compute the modifiers but also by the ODEs that are solved in the optimization problem. This could result in better estimates of plant outputs during transient, which could lead to better performance. Hence, transient quantities such as constraint and cost functions would be updated with transient corrections, which could result in fewer constraint violations and better estimates of the cost and constraint gradients. A first step towards this proposition has been investigated in [97]. Therein, the authors have proposed to combine the modifier-adaptation approach with offset-free economic MPC, and highlighted that this combination avoids failure of MPC in achieving plant optimum in closed loop. Although only parametric plant-model mismatch case is considered, the results are promising as a new viewpoint concerning the combination of MPC and RTO is considered.

Finally, MA requires plant measurements and a system model to compute the plant optimum at each RTO iteration. Although the model used can support a significant level of approximation, it must satisfy the following two requirements: (i) a model adequacy condition related to the second-order optimality conditions must be valid at the plant optimum, and (ii) the model must have the same input variables as the plant. As part of this thesis, we have considered a case where (ii) is not verified because only a partial or incomplete model is available in [98]. We have proposed to approximate the unmodeled part of the system by a linear model that is identified using the same excitation that is used in modifier adaptation for gradient estimation. In the context of SOFC systems, this may be applied in the case when a part of the plant is not modeled because of modeling difficulties. This linear approximation could replace a component of the SOFC system such as a reformer or even recycle streams.

Bibliography

[1] Swiss Federal Office of Energy SFOE. http://www.bfe.admin.ch/. Accessed: 2018-02-11.

[2] Deployment Strategy. European Hydrogen and Fuel Cell Technology Platform. http://www.fch.europa.eu/. Accessed: 2018-03-25.

[3] A. Choudhury, H. Chandra, and A. Arora. Application of solid oxide fuel cell technology for power generation – A review. *Renewable and Sustainable Energy Reviews*, 20:430–442, 2013.

[4] L. Liu. *Solid Oxide Fuel Cell Reliability and Performance Modeling and Fabrication by Spray Pyrolysis*. PhD thesis, Iowa State University, 2011.

[5] J. Golbert and D. R. Lewin. Model-based control of fuel cells: (1) Regulatory control. *J. Power Sources*, 135:135–151, 2004.

[6] P. Aguiar, C. S. Adjiman, and N. P. Brandon. Anode-supported intermediate-temperature direct internal reforming solid oxide fuel cell: II. Model-based dynamic performance and control. *J. Power Sources*, 147(1):136 –147, 2005.

[7] G. A. Bunin, Z. Wuillemin, G. François, A. Nakajo, L. Tsikonis, and D. Bonvin. Experimental real-time optimization of a solid oxide fuel cell stack via constraint adaptation. *Energy*, 39(1):54–62, 2012.

[8] T. de Avila Ferreira, Z. Wuillemin, A. G. Marchetti, C. Salzmann, J. Van Herle, and D. Bonvin. Real-time optimization of an experimental SOFC system. *J. Power Sources, Submitted*, 2018.

[9] M. L. Darby, M. Nikolaou, J. Jones, and D. Nicholson. RTO: An overview and assessment of current practice. *J. Process Contr.*, 21:874–884, 2011.

[10] C. R. Cutler and R. T. Perry. Real time optimization with multivariable control is required to maximize profits. *Comp. Chem. Eng.*, 7(5):663–667, 1983.

[11] T. E. Marlin and A. N. Hrymak. Real-time operations optimization of continuous processes. In *AIChE Symposium Series - CPC-V*, volume 93, pages 156–164, 1997.

[12] R. E. Young. Petroleum refining process control and real-time optimization. *IEEE Contr. Syst. Mag.*, 26(6):73–83, 2006.

[13] A. Marchetti, B. Chachuat, and D. Bonvin. Batch process optimization via run-to-run constraints adaptation. In *ECC*, Kos, Greece, 2007.

[14] B. Chachuat, B. Srinivasan, and D. Bonvin. Adaptation strategies for real-time optimization. *Comp. Chem. Eng.*, 33:1557–1567, 2009.

[15] A. Marchetti. *Modifier-Adaptation Methodology for Real-Time Optimization (No. 4449)*. PhD thesis, Ecole Polytechnique Fédérale de Lausanne, 2009.

[16] J. F. Forbes and T. E. Marlin. Model accuracy for economic optimizing controllers: the bias update case. *Ind. Eng. Chem. Res.*, 33:1919–1929, 1994.

[17] B. Chachuat, A. Marchetti, and D. Bonvin. Process optimization via constraints adaptation. *J. Process Contr.*, 18:244–257, 2008.

[18] P. D. Roberts. An algorithm for steady-state system optimization and parameter estimation. *J. System Science*, 10:719–734, 1979.

[19] A. Marchetti, B. Chachuat, and D. Bonvin. Modifier-adaptation methodology for real-time optimization. *Ind. Eng. Chem. Res.*, 48(13):6022–6033, 2009.

[20] G. François, B. Srinivasan, and D. Bonvin. Use of measurements for enforcing the necessary conditions of optimality in the presence of constraints and uncertainty. *J. Process Contr.*, 15(6):701–712, 2005.

[21] P. D. Roberts. Coping with model-reality differences in industrial process optimisation - a review of integrated system optimisation and parameter estimation (ISOPE). *Computers in Industry*, 26:281–290, 1995.

[22] A. Marchetti, T. Faulwasser, and D. Bonvin. A feasible-side globally convergent modifier-adaptation scheme. *J. Process Contr.*, 54:38–46, 2017.

[23] K. B. Ariyur and M. Krstic. *Real-Time Optimization by Extremum-Seeking Control*. John Wiley & Sons, 2003.

[24] B. Srinivasan and D. Bonvin. Interplay between identification and optimization in run-to-run optimization schemes. In *American Control Conference*, pages 2174–2179, Anchorage, AK, 2002.

[25] P. D. Roberts and T. W. Williams. On an algorithm for combined system optimisation and parameter estimation. *Automatica*, 17(1):199–209, 1981.

[26] M. Krstic and H. H. Wang. Stability of extremum seeking feedback for general nonlinear dynamic systems. *Automatica*, 36:595–601, 2000.

[27] G. François and D. Bonvin. Use of transient measurements for the optimization of steady-state performance via modifier adaptation. *Ind. Eng. Chem. Res.*, 53(13):5148–5159, 2014.

[28] C. Y. Chen and B. Joseph. On-line optimization using a two-phase approach: An application study. *Ind. Eng. Chem. Res.*, 26:1924–1930, 1987.

[29] A. D. Quelhas, N. J. Castro de Jesus, and J. C. Pinto. Common vulnerabilities of RTO implementations in real chemical processes. *The Canadian J. Chem. Eng.*, 91:652–668, 2013.

[30] J. F. Forbes, T. E. Marlin, and J. F. MacGregor. Model adequacy requirements for optimizing plant operations. *Comp. Chem. Eng.*, 18(6):497–510, 1994.

[31] E. Baur and H. Preis. Über Brennstoffketten mit Festleitern. *Zeitschrift für Elektrochemie und angewandte physikalische Chemie*, 43(9):727–732, 1937.

[32] T. Suzuki, Md. Z. Hasan, T. Yamaguchi, Y. Fujishiro, M. Awano, Y. Funahashi, and N. Sammes. Use of hydrocarbon fuel for micro tubular SOFCs. *Advances in Solid Oxide Fuel Cells VI: Ceramic Engineering and Science Proceedings*, 31:107–112, 2010.

[33] Solid Power. https://www.solidpower.com/en/. Accessed: 2017-05-17.

[34] E. Entchev. Residential fuel cell energy systems performance optimization using "soft computing" techniques. *J. Power Sources*, 118(1-2):212–217, 2003.

[35] F. Ramadhani, M. A. Hussain, H. Mokhlis, and S. Hajimolana. Optimization strategies for solid oxide fuel cell (SOFC) application: A literature survey. *Renewable and Sustainable Energy Reviews*, 76:460–484, 2017.

[36] A. Arce, A. J. del Real, C. Bordons, and D.R. Ramírez. Real-time implementation of a constrained MPC for efficient airflow control in a PEM fuel cell. *IEEE Trans. on Industrial Electronics*, 57(6):1892–1905, 2010.

[37] P. Rodatz, G. Paganelli, A. Sciarretta, and L. Guzzella. Optimal power management of an experimental fuel cell/supercapacitor-powered hybrid vehicle. *Control Eng. Practice*, 13: 41–53, 2005.

[38] Y. P. Yang, F. C. Wang, H. P. Chang, Y. W. Ma, and B. J. Weng. Low power proton exchange membrane fuel cell system identification and adaptive control. *J. Power Sources*, 164: 761–771, 2007.

[39] E. Riensche, U. Stimming, and G. Unverzagt. Optimization of a 200 kW SOFC cogeneration power plant: Part I: Variation of process parameters. *J. Power Sources*, 73(2):251–256, 1998.

[40] A. Arsalis. Thermoeconomic modeling and parametric study of hybrid SOFC–gas turbine–steam turbine power plants ranging from 1.5 to 10MWe. *J. Power Sources*, 181(2):313–326, 2008.

[41] L. Zhang, J. Jiang, H. Cheng, Z. Deng, and X. Li. Control strategy for power management, efficiency-optimization and operating-safety of a 5-kW solid oxide fuel cell system. *Electrochim. Acta*, 177:237–249, 2015.

[42] N. Perdikaris, K. D. Panopoulos, Ph. Hofmann, S. Spyrakis, and E. Kakaras. Design and exergetic analysis of a novel carbon free tri-generation system for hydrogen, power and heat production from natural gas, based on combined solid oxide fuel and electrolyser cells. *Int. J. Hydrogen Energy*, 35(6):2446–2456, 2010.

[43] A. Goyal, U. Diwekar, and R. Geisbrecht. Multi-objective optimization for hybrid fuel cells power system design. In *AIChE 2001 Annual Meeting, Reno, Nevada*, 2001.

[44] R. Roshandel and T. Parhizkar. Degradation based optimization framework for long term applications of energy systems, case study: Solid oxide fuel cell stacks. *Energy*, 107: 172–181, 2016.

[45] A. Odukoya, J. A. Carretero, and B. V. Reddy. Thermodynamic optimization of solid oxide fuel cell-based combined cycle cogeneration plant. *Int. J. of Energy Res.*, 35(15): 1399–1411, 2011.

[46] N. Autissier, F. Palazzi, F. Maréchal, J. Van Herle, and D. Favrat. Thermo-economic optimization of a solid oxide fuel cell, gas turbine hybrid system. *J. Fuel Cell Sci. Technol.*, 4(2):123–129, 2007.

[47] K. H. Lee. *Configuration and Operating Condition Design Analysis of SOFC Systems for Building Applications.* PhD thesis, University of Illinois at Urbana-Champaign, 2008.

[48] I. Tikiz and I. Taymaz. An experimental investigation of solid oxide fuel cell performance at variable operating conditions. *Thermal Science*, 20(5):1421–1433, 2016.

[49] B. Huang, Y. Qi, and M. Murshed. Solid oxide fuel cell: Perspective of dynamic modeling and control. *J. Process Contr.*, 21(10):1426–1437, 2011.

[50] X. Song, A. R. Diaz, A. Benard, and J. D. Nicholas. A 2D model for shape optimization of solid oxide fuel cell cathodes. *Struct. Multidiscip. Optim.*, 47(3):453–464, 2013.

[51] A. Faes, J. M. Fuerbringer, D. Mohamedi, A. Hessler-Wyser, G. Caboche, and J. Van Herle. Design of experiment approach applied to reducing and oxidizing tolerance of anode supported solid oxide fuel cell. Part I: Microstructure optimization. *J. Power Sources*, 196 (17):7058–7069, 2011.

[52] X. Wang, B. Huang, and T. Chen. Data-driven predictive control for solid oxide fuel cells. *J. Process Contr.*, 17(2):103–114, 2007. ISSN 0959–1524.

[53] M. J. Kupilik and T. L. Vincent. Control of a solid oxide fuel cell system with sensitivity to carbon formation. *J. Power Sources*, 222:267–276, 2013.

[54] A. Pohjoranta, M. Halinen, J. Pennanen, and J. Kiviaho. Model predictive control of the solid oxide fuel cell stack temperature with models based on experimental data. *J. Power Sources*, 277:239–250, 2015.

[55] T. Das and S. Snyder. Adaptive control of a solid oxide fuel cell ultra-capacitor hybrid system. *IEEE Trans. Autom. Contr.*, 21(2):372–383, 2013.

[56] R. Zhang, A. Xue, and S. Wang. Dynamic modeling and nonlinear predictive control based on partitioned model and nonlinear optimization. *Ind. Eng. Chem. Res.*, 50(13): 8110–8121, 2011.

[57] A. Marchetti, A. Gopalakrishnan, L. Tsikonis, A. Nakajo, Z. Wuillemin, B. Chachuat, J. Van herle, and D. Bonvin. Robust real-time optimization of a solid oxide fuel cell stack. *J. Fuel Cell Sci. Technol.*, 8:051001, 2011.

[58] S. Pushpavanam. *Control and Optimisation of Process Systems*, volume 43. Academic Press, 2013.

[59] S. Boyd and L. Vandenberghe. *Convex optimization*. Cambridge university press, 2004.

[60] O. Rotava and A. C. Zanin. Multivariable control and real-time optimization – An industrial practical view. *Hydrocarbon Process.*, 84(6):61–71, 2005.

[61] B. Srinivasan, D. Bonvin, E. Visser, and S. Palanki. Dynamic optimization of batch processes: II. Role of measurements in handling uncertainty. *Comp. Chem. Eng.*, 27: 27–44, 2003.

[62] M. Brdyś and P. Tatjewski. *Iterative Algorithms for Multilayer Optimizing Control*. Imperial College Press, London UK, 2005.

[63] L. T. Biegler, I. E. Grossmann, and A. W. Westerberg. A note on approximation techniques used for process optimization. *Comp. Chem. Eng.*, 9(2):201–206, 1985.

[64] J. E. Ellis, C. Kambhampati, G. Sheng, and P. D. Roberts. Approaches to the optimizing control problem. *Int. J. Systems Sci.*, 19(10):1969–1985, 1988.

[65] B. Srinivasan, C. J. Primus, D. Bonvin, and N. L. Ricker. Run-to-run optimization via control of generalized constraints. *Control Engineering Practice*, 9(8):911–919, 2001.

[66] S. Skogestad. Self-optimizing control: The missing link between steady-state optimization and control. *Comp. Chem. Eng.*, 24:569–575, 2000.

[67] M. S. Govatsmark and S. Skogestad. Selection of controlled variables and robust setpoints. *Ind. Eng. Chem. Res.*, 44(7):2207–2217, 2005.

[68] B. Srinivasan and D. Bonvin. Real-time optimization of batch processes via tracking the necessary conditions of optimality. *Ind. Eng. Chem. Res.*, 46(2):492–504, 2007.

[69] G. A. Bunin, G. François, and D. Bonvin. Sufficient conditions for feasibility and optimality of real-time optimization schemes - I. Theoretical foundations. *ArXiv:1308.2620*, 2013.

[70] G. A. Bunin, G. François, and D. Bonvin. Sufficient conditions for feasibility and optimality of real-time optimization schemes - II. Implementation issues. *ArXiv:1308.2625*, 2013.

[71] W. Gao and S. Engell. Iterative set-point optimization of batch chromatography. *Comp. Chem. Eng.*, 29:1401–1409, 2005.

[72] A. Marchetti, B. Chachuat, and D. Bonvin. A dual modifier-adaptation approach for real-time optimization. *J. Process Contr.*, 20:1027–1037, 2010.

[73] E. Rodger. *Dual Modifier Adaptation Methodology for the On-line Optimization of Uncertain Processes.* Master's thesis, McMaster University, 2010.

[74] E. A. Rodger and B. Chachuat. Design methodology of modifier adaptation for on-line optimization of uncertain processes. *IFAC Proceedings Volumes*, 44(1):4113–4118, 2011.

[75] G. François and D. Bonvin. Measurement-based real-time optimization of chemical processes. In *Advances in Chemical Engineering*, volume 43, pages 1–50. Elsevier, 2013.

[76] J. F. Forbes and T. E. Marlin. Design cost: A systematic approach to technology selection for model-based real-time optimization systems. *Comp. Chem. Eng.*, 20:717–734, 1996.

[77] G. François and D. Bonvin. Use of convex model approximations for real-time optimization via modifier adaptation. *Ind. Eng. Chem. Res.*, 52:11614–11625, 2013.

[78] A. G. Marchetti, T. Faulwasser, and D. Bonvin. A feasible-side globally convergent modifier-adaptation scheme. *J. Process Contr.*, 54:38–46, 2017.

[79] T. Faulwasser and D. Bonvin. On the use of second-order modifiers for real-time optimization. *IFAC Proceedings Volumes*, 47(3):7622–7628, 2014.

[80] G. A. Bunin. On the equivalence between the modifier-adaptation and trust-region frameworks. *Comp. Chem. Eng.*, 71:154–157, 2014.

[81] AKM. M. Murshed, B. Huang, and K. Nandakumar. Control relevant modeling of planer solid oxide fuel cell system. *J. Power Sources*, 163:830–845, 2006.

[82] J. Xu and F. G. Froment. Methane steam reforming, methanation and water-gas shift: I. Intrinsic kinetics. *AIChE J.*, 35:88–96, 1989.

[83] J. Gut and J. Pinto. Modeling of plate heat exchanger with generalized configurations. *Int. J. Heat Mass Transf.*, 46:2571–2585, 2003.

[84] T. de Avila Ferreira, G. François, A. G. Marchetti, and D. Bonvin. Use of transient measurements for static real-time optimization. *IFAC-PapersOnLine*, 50(1):5737–5742, 2017.

[85] MathWorks Documentation. Read and write data to an OPC data access server. https://www.mathworks.com, . Accessed: 2016-01-23.

[86] MathWorks Documentation. Filter data. https://www.mathworks.com, . Accessed: 2016-03-13.

[87] T. de Avila Ferreira, Z. Wuillemin, T. Faulwasser, C. Salzmann, J. Van Herle, and D. Bonvin. Enforcing Operational Efficiency in SOFC Micro-CHPs. *Energy, Submitted*, 2018.

[88] 2G Energy AG. https://www.2-g.com/de/, 2017. Accessed: 2018-05-17.

[89] ETW Energietechnik. https://etw-energie.de/en/. Accessed: 2018-05-19.

[90] SenerTec Center NRW-Süd GmbH. https://senertec-center-nrw-sued.de/. Accessed: 2018-05-14.

[91] E. Achenbach. Response of a solid oxide fuel cell to load change. *J. Power Sources*, 57(1): 105–109, 1995.

[92] Z. Wuillemin. *Experimental and Modeling Investigations on Local Performance and Local Degradation in Solid Oxide Fuel Cells.* PhD thesis, Ecole Polytechnique Fédérale de Lausanne, 2009.

[93] A. Nakajo, P. Tanasini, S. Diethelm, J. Van Herle, and D. Favrat. Electrochemical model of solid oxide fuel cell for simulation at the stack scale ii: Implementation of degradation processes. *J. Electrochem. Soc.*, 158(9):B1102–B1118, 2011.

[94] F. J. Serralunga, M. C. Mussati, and P. A. Aguirre. Model adaptation for real-time optimization in energy systems. *Industrial & Engineering Chemistry Research*, 52(47):16795–16810, 2013.

[95] A. Papasavvas, T. de Avila Ferreira, M. A. Marchetti, and D. Bonvin. Analysis of output modifier adaptation for real-time optimization. *Comp. Chem. Eng.*, 121:285–293, 2018.

[96] T. de Avila Ferreira, H. A. Shukla, T. Faulwasser, C. N. Jones, and D. Bonvin. Real-time optimization of uncertain process systems using machine learning via gaussian processes. *European Control Conference (ECC)*, 2018.

[97] M. Vaccari and G. Pannocchia. A modifier-adaptation strategy towards offset-free economic MPC. *Processes*, 5(1):2, 2016.

[98] A. Papasavvas, T. de Avila Ferreira, A.G. Marchetti, and D. Bonvin. Real-time optimization via modifier adaptation using partial plant models. *IFAC-PapersOnLine*, 50(1):4666–4671, 2017.

Ch. de Boston 16
1004 Lausanne VD
Switzerland
+41 78 812 27 08
tafarel.deavilaferreira@epfl.ch
Date of birth: 21.07.1988
Nationality: Brazilian

Tafarel de Avila Ferreira

Education

2014–present: **PhD**, *École Polytechnique Fédéral de Lausanne (EPFL)*, Lausanne.
Real-Time Optimization of Solid-Oxide Fuel-Cell Systems – Methodology and Implementation

2011–2012: **M.Sc. in Chemical Engineering**, *Alberto Luiz Coimbra Institute for Graduate Studies and Research in Engineering (COPPE/UFRJ)*, Rio de Janeiro.
Master's thesis in the field of Process Control & Chemical Engineering: Optimal Control of a Bioreactor for Production of Poly((R))-3-hydroxy-butyrate) from *Bacillus sp.*

2006–2010: **B.Ch.E. in Chemical Engineering**, Federal University of Rio Grande. (FURG), Rio Grande.
Bachelor dissertation in the field of Chemical Engineering: Biogas Production from Municipal Solid Waste.

Experience

2014–present: **École Polytechnique Fédéral de Lausanne (EPFL)**, *Lausanne*.
- Teaching assistant in classes related process control
- Supervision of student projects

2013–2016: **École Polytechnique Fédéral de Lausanne (EPFL)**, *Lausanne*.
- Scholarship holder of the Swiss Government Excellence Scholarships for Foreign Scholars and Artists

2010: **Federal University of Rio Grande (FURG)**, *Rio Grande*.
- Scholarship for the project Biofilm Production from the Seafood Industry Waste

2009: **Federal University of Rio Grande (FURG)**, *Rio Grande*.
- Teaching assistant of the course Instrumental Analysis

Presentations

T. de Avila Ferreira, A. G. Marchetti, T. Faulwasser, Z. Wuillemin, S. F. Au, A. Nakajo, J. Van Herle and D. Bonvin. Real-time optimization of a SOFC system with reformer. *Symposium on Modeling & Experimental Validation of Fuel Cells, Batteries & Electrolysers (MODVAL)*, 2016.

A. Papasavvas, T. de Avila Ferreira, A. G. Marchetti, and D. Bonvin. Real-time optimization via modifier adaptation – On updating the model outputs. *AIChE Annual Meeting*, 2017.

T. de Avila Ferreira, Z. Wuillemin, A. G. Marchetti, J. Van Herle and D. Bonvin. Optimal operation of an experimental SOFC system via constraint activation. *European SOFC & SOE Forum (EFCF)*, *Poster Presentation*, 2018.

Publications

T. de Avila Ferreira, G. François, A. G. Marchetti, and D. Bonvin. Use of transient measurements for static real-time optimization. *IFAC-PapersOnLine*, 50(1):5737–5742, 2017.

A. Papasavvas, T. de Avila Ferreira, A. G. Marchetti, and D. Bonvin. Real-time optimization via modifier adaptation using partial plant models. *IFAC-PapersOnLine*, 50(1):4666–4671, 2017.

T. de Avila Ferreira, H. A. Shukla, T. Faulwasser, C. N. Jones, and D. Bonvin. Real-time optimization of uncertain process systems using machine learning via gaussian processes. *European Control Conference (ECC)*, 2018.

T. de Avila Ferreira, Z. Wuillemin, T. Faulwasser, C. Salzmann, J. Van Herle, and D. Bonvin. Enforcing operational efficiency in SOFC micro-CHPs. *Energy, Submitted*, 2018.

T. de Avila Ferreira, Z. Wuillemin, A. G. Marchetti, C. Salzmann, J. Van Herle, and D. Bonvin. Real-time optimization of an experimental SOFC system. *J. Power Sources, Submitted*, 2018.

A. Papasavvas, T. de Avila Ferreira, M. A. Marchetti, and D. Bonvin. Analysis of output modifier adaptation for real-time optimization. *Comp. Chem. Eng.*, 121:285–293, 2018.

T. de Avila Ferreira, Z. Wuillemin, M. A. Marchetti, and D. Bonvin. RTO applied to a commercial SOFC system. *IFAC Symposium on Dynamics and Control of Process Systems, Including Biosystems (DYCOPS), Submitted*, 2019.

Ce document a été imprimé au Centre d’impression EPFL,
imprimerie climatiquement neutre, certifiée myClimate.